

Hexagonal Perovskites as Quantum Materials

Loi T. Nguyen and R.J. Cava

Department of Chemistry, Princeton University, Princeton New Jersey 08544

ABSTRACT: Hexagonal oxide perovskites, in contrast to the more familiar perovskites, allow for face-sharing of metal-oxygen octahedra or trigonal prisms within their structural frameworks. This results in dimers, trimers, tetramers, or longer fragments of chains of face-sharing octahedra in the crystal structures, and consequently in much shorter metal-metal distances and lower metal-oxygen-metal bond angles than are seen in the more familiar perovskites. The presence of the face-sharing octahedra can have a dramatic impact on magnetic properties of these compounds, and dimer-based materials, in particular, have been the subjects of many quantum-materials-directed studies in materials physics. Hexagonal oxide perovskites are of contemporary interest due to their potential for geometrical frustration of the ordering of magnetic moments or orbital occupancies at low temperatures, which is especially relevant to their significance as quantum materials. As such, several hexagonal oxide perovskites have been identified as potential candidates for hosting the quantum spin liquid state at low temperatures. In our view, hexagonal oxide perovskites are fertile ground for finding new quantum materials. This review briefly describes the solid state chemistry of many of these materials.

1. Introduction

CONTENTS

1. Introduction	1
2. Mixtures of cubic plus hexagonal packing	3
3. Dimers and trimers. Relation to classic double perovskites.	4
3.1. <i>Dimer-based hexagonal perovskites</i>	4
3.2. <i>Trimer-based hexagonal perovskites</i>	9
3.3. <i>A structure based on both trimers and dimers</i> 12	
3.4. <i>12R structures based on trimers</i>	12
3.5. <i>A_{4-n}A_nMM'₂O₁₂: Missing an octahedron in a trimer</i> 13	
3.6. <i>Tetramers</i>	14
4. Materials with MO ₄ tetrahedra in the framework 14	
5. Oxygen deficiency: vacancies both random and ordered.....	17
6. Polymorphism.....	19
7. Summary of some of the complex variations in stacking	19
8. Hexagonal Perovskites with Ba-Cl or Ba-Br layers in addition to Ba-O layers.....	19
9. Chains.....	20
10. Some unusual derivatives of hexagonal perovskites 22	
11. Conclusions.....	25
12. Author contributions.....	25
13. Notes.....	25
14. Biographies.....	25
15. References.....	25

Halide perovskites have recently been widely studied by chemical researchers. They can be processed under relatively mild conditions compared to oxides and, as semiconductors, can sometimes have favorable optical and charge transport properties, making them suitable for study as materials with the potential for solar energy conversion. They are not currently widely studied in the materials physics community as quantum materials. These materials are variants of the familiar perovskite AMX₃ formula, where the A atom or molecule (e.g. Cs or CH₃NH₃) is in the large cavity in the classic perovskite structure, and the MX₆ octahedra, made from main group M ions, share corner X ions (here Cl, Br, or I) in a three-dimensional framework. Such materials obey the familiar radius rules known for derivatives of cubic perovskites, with some potential refinements¹⁻⁹. Many reviews of this type of perovskite can be found in the chemical literature, including in this journal¹⁰. They are not the subject of this review.

The classic oxide perovskites, with formulas AMO₃, (where A = a larger ion, typically monovalent, divalent or trivalent, and M is a smaller metal ion) are well known in the solid state chemistry and materials physics communities and have been intensively studied for many decades¹¹. This is due to their interesting structural chemistry and often forefront magnetic and electronic properties. The interest in oxide perovskites as quantum materials often arises from the fact that the M ions can be members of the transition metal series, which can result in properties that can best be understood as quantum mechanical in nature.

The familiar oxide perovskites are typically made from electropositive (non-molecular) A ions (e.g. Alkali, alkaline earth or rare earth ions) that reside somewhere in a perovskite cavity where they are ideally 12 coordinated to the surrounding oxygens, and MO₆ octahedra sharing corners with each other to create a MO₃ framework structure. The *d* orbitals on

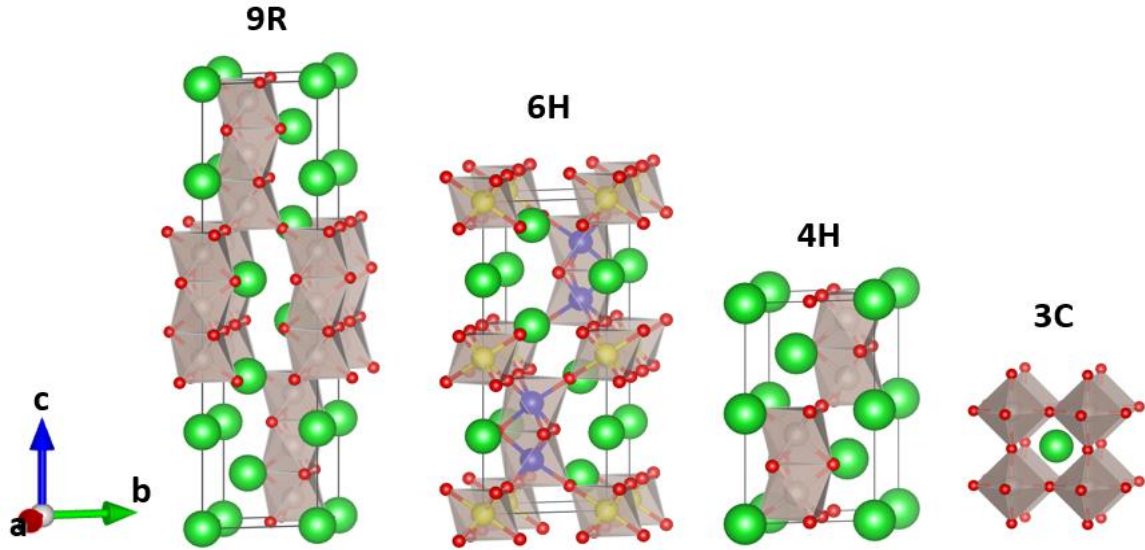


Figure 1. The different polymorphs of BaRuO₃. Color: Ba (green), Ru (gray octahedra) and O (red). In the 6H drawing, the two kinds of Ru – blue in the dimers and yellow in the perovskite-like layers – are shown. BaRuO₃ at ambient pressure is found in the 9R or 4H structure types, SrRuO₃ is found in a distortion of the 3C structure type, as is BaRuO₃ prepared at high pressures.

the M ions hybridize in different degrees with the oxygen *p* orbitals. The quantum-like properties can arise for *dⁿ* ions (where the *d* states are partly filled, and *n* is between 1 and 9) and even for *d⁰* or *d¹⁰* ions (e.g. Ti⁴⁺ or Pb⁴⁺) in the octahedra in the MO₃ framework.

Structurally, the octahedra are often considered as rigid entities that tilt around their shared corners to accommodate different size A site ions and an overall cell size that is also determined by temperature or pressure. A rich set of symmetry variants is possible due to the tilting, and too many interesting combinations of atoms, physical properties and structural distortions have been studied to even list generally^{12,13}. The tilting, from a chemical and quantum materials perspective, changes the degree of overlap between the oxygen *p* and metal *d* orbitals at the connections between the corner-sharing MO₆ octahedra in the perovskite framework, with a significant impact on the electronic and magnetic properties displayed. Even a relatively simple oxide perovskite like SrTiO₃ can display profound quantum mechanical properties such as superconductivity at sub-Kelvin temperatures when doped with a very small number of electrons^{14–16}. Even though the tilt system in classical perovskites can sometimes yield a rhombohedral symmetry crystal structure, such materials are in general not the subjects of this review. Ruddlesden Popper and Dion Jacobsen series materials are celebrated layered oxide perovskites where different ratios and relative sizes of A to B site ions result in the break-up of the MO₃ perovskite network into layers of different thicknesses. Electrons and magnetic moments, when confined to layers, or largely confined to layers, can display quite unexpected quantum-derived properties, such as superconductivity^{17–19}. The structural break-up of the normally three-dimensional MO₃ array into layers can lead to dramatically different physical properties for some of these materials, which have also been the subjects of many reviews. Double perovskites in oxides are also well known and have been the subjects of research in halide perovskites as well^{6,7,20–26}. Perovskites are a well for research that never seems to run dry.

This review, however, is about a currently lesser known class of oxide perovskite quantum materials, based on hexagonal symmetry rather than cubic symmetry. These materials are also based on AMO₃ stoichiometries but, in contrast to the more familiar perovskites, admit for face sharing of MO₆ octahedra or A- or M- centered trigonal prisms in the structural framework rather than the corner-sharing geometries found in the framework of conventional perovskites. This can result in dimers, trimers, tetramers or longer fragments of chains of face-sharing octahedra in the structure. The face sharing of the octahedra within the dimers trimers tetramers and chains leads to much shorter metal-metal distances and lower metal-oxygen-metal bond angles than are seen in more familiar perovskites. It has been argued that hexagonal perovskites can best happen for selected A site ions in oxides because their ionic radii and that of oxygen are such that it is possible for them to mix in an ordered arrangement to form a closest-packed plane. Ba²⁺ and O²⁻ seem to be a perfect pair for engendering this kind of structural stability. A Ba²⁺ ion replacing one of the oxygen ions in a close packed oxygen plane appears to be happily surrounded by the 6 near neighbor O²⁻ ions that it acquires in the plane. The fact that face sharing is present has a dramatic impact on the transition metal oxygen *d* orbital oxygen *p* orbital overlap and the direct *d-d* overlap of the transition metals, and, consequently on the quantum properties.

Symmetry matters when it comes to physical properties, and the 3 or 6 fold rotational symmetries of the structural components in the hexagonal perovskites are of contemporary interest due to the potential that such geometries have to engender the geometrical frustration of the ordering of the magnetic moments or orbital occupancies of the framework ions into a single lowest energy state at low temperatures. Thus such materials are good candidates for the quantum-spin-liquid state, as described briefly here. (In quantum spin liquids, the spin state of the magnetic ions continues to fluctuate down to very low temperatures compared to the strength of the magnetic interactions as measured by the Curie-Weiss temperature.)

Further, their properties frequently challenge our current understanding of when a chemistry (i.e. an orbital based) vs. a physics (i.e., a Fermi Surface based) description is most appropriate for interpretation and prediction of the properties of a material, which is good fun²⁷⁻²⁹ (see e.g. the review by D. Khomskii and S.V. Streltsov in this issue). Many hexagonal oxide perovskites based on face-sharing of magnetic octahedra have been studied due to their potential for hosting the quantum spin liquid state at low temperature.

As is found in the more familiar cubic-symmetry-based AMO_3 perovskites, structural distortions, chemical disorder, and non- AMO_3 stoichiometries are also found in the hexagonal perovskites. Structurally layered variants are also known. The basic crystal structures and, in some cases, the known structural complexities are the focus of this review. Although metallic, semiconducting, and dielectric hexagonal perovskites are known, the physical properties of this class of materials have so far not turned out to be of as wide interest in the materials physics community as those of their cubic-symmetry-based cousins. The properties of the materials whose chemistry and structure are the primary focus of this review are also generally summarized here when known.

This organization of this review is based on the solid state chemistry of the hexagonal perovskites, and is based primarily on their crystal structures. A reader particularly interested in the crystal structures of such materials can find alternative presentations in books on perovskites¹¹⁻¹³. Our intention is to present a structural description of as many of them as we can, although some interesting materials may be omitted by accident. On the other hand, occasionally we may describe variants that are be considered by some researchers to be “not-really-hexagonal-perovskites”, or better classified in a different way, and we apologize to people whose views are stricter than ours if our classification appears to include too many materials; we do not mean to exclude other classifications for such materials. In our view, hexagonal perovskites are fertile ground for finding interesting quantum materials and we hope that the descriptions presented in this review will be accessible to a wide range of scientists who may be interested in such things.

2. Mixtures of cubic plus hexagonal packing

Let’s start with the SrRuO_3 - BaRuO_3 perovskites as our initial example. SrRuO_3 is a slightly distorted conventional cubic perovskite due to a small tilt of the RuO_6 octahedra in the RuO_3 framework, while, at conventional pressures, the Ba^{2+} ion is not a good fit for the cubic perovskite cavity. It is a better fit when inserted into a close packed plane of oxygen, however, and thus, the crystal structures of the ambient pressure BaRuO_3 polymorphs are hexagonal perovskites.

For A site ions of size between Sr and Ba, the resulting crystal structure is an ordered mixture of cubic perovskite plus hexagonal perovskite. There is no electropositive divalent ion with a size intermediate between Sr and Ba, but as is often found in solid state chemistry, such an ion can be simulated by mixing Sr and Ba together. Although any individual position in one unit cell is occupied by either Ba or Sr, their average radius is what impacts the long range average crystal structure observed. The (111) plane of conventional cubic perovskites has three fold rotational symmetry. When used as a building block

a small section of the (111) plane is a layer of isolated MO_6 octahedra lying on their faces in a triangular array. The A ions are found between these layers. When the (111) layers are included in a structure, the octahedra share corners with others. When this layer is used as a structural building block in the creation of a new material and mixed with hexagonal symmetry AMO_3 layers that consist of face-shared octahedra, then materials with overall hexagonal symmetry are the result.

The compounds in the SrRuO_3 - BaRuO_3 system allow us to introduce the simple short-hand nomenclature that is used to describe hexagonal perovskites. In this nomenclature, a number is first, which indicates the number of structural layers within a unit cell. The designation then ends with a letter, an R, an H or a C, which indicates whether the material is based on rhombohedral, hexagonal or cubic layer stacking (like in all perovskites, small distortions are possible, typically due to octahedral tilting) Using this nomenclature, classic cubic-symmetry-based SrRuO_3 has a 3C structure (three cubic layers per cell stacked along (111) and BaRuO_3 has three polymorphs, one with a 4H structure, one with a 6H structure and one with a 9R structure³⁰ (**Figure 1**). (In rhombohedral symmetry hexagonal perovskite crystal structures the number of layers is always a multiple of 3). At high pressures, BaRuO_3 is stable in a different crystal structure, transforming to a conventional 3C perovskite (**Figure 1**). This cubic BaRuO_3 perovskite is metallic and shows a ferromagnetic transition at $T_c = 60$ K, significantly lower than the $T_c = 160$ K of SrRuO_3 , as shown in **Figure 2**. A related designation is when a layer of MO_6 octahedra is connected by corner sharing to the next layer, as is found in cubic perovskites, then that connection is designated by a lowercase c, when the octahedra are connected by sharing faces then that kind of connection has 3 or 6 fold symmetry and is designated by a lowercase h. Thus the structure of many 9-layer hexagonal perovskites may be designated as 9R or (chh)₃.

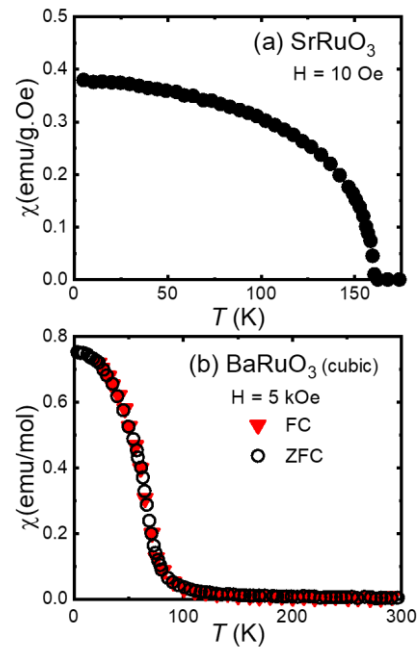


Figure 2. The ferromagnetic transitions in (a) orthorhombic SrRuO_3 ³¹ and (b) cubic BaRuO_3 conventional perovskites³⁰.

In the case of the $\text{Ba}_{1-x}\text{Sr}_x\text{RuO}_3$ solid solution, the resulting crystal structure is clearly determined by the average radius of the A site ions; an on-average-smaller A site ion yields a crystal structure with a larger fraction of cubic-like perovskite character, while a larger A site ion yields a hexagonal-like perovskite structure³²⁻³⁴. The same may be the case for other $(\text{Ba}_{1-x}\text{Sr}_x)\text{MO}_3$ perovskites where the Ba end member ($x=0$) is a hexagonal perovskite and the Sr end member ($x=1$) is a cubic perovskite. In solid solutions of the type $\text{Ba}_{1-x}\text{Sr}_x\text{RuO}_3$, when increasing the values of x , the nine-layer structure with stacking sequence $(\text{chh})_3$ (9R) transforms to the four-layer structure $(\text{ch})_2$ (4H) and finally to the classical perovskite type structure $(\text{c})_3$ (3C) at x is about 1/6 and 1/3, respectively³³. The 4H and 9R forms of BaRuO_3 have substantially different electronic properties³⁵, and even the $\text{Sr}_{1-x}\text{Ca}_x\text{RuO}_3$ perovskites in the more familiar cubic perovskite structure types are famously enigmatic quantum materials³⁶⁻³⁸. In the event that readers are not familiar with magnetism we point out that the A ions in perovskites, with the exceptions of the rare earths, are not magnetic (i.e. Ba^{2+} , Sr^{2+} and Ca^{2+}) nor are the oxygen ions.

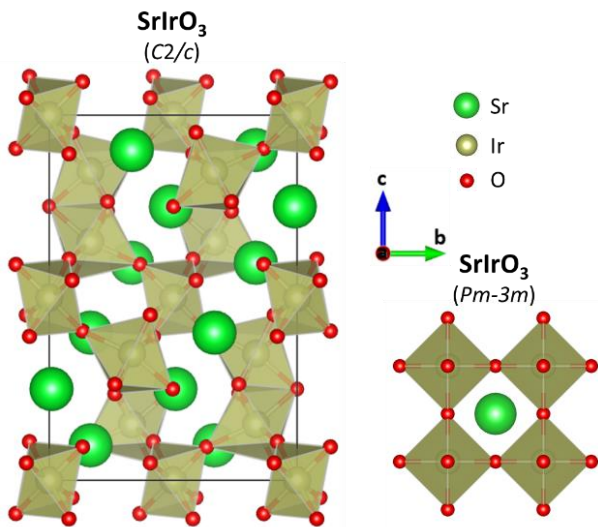


Figure 3. The crystal structures of distorted monoclinic SrIrO_3 (left), the ambient pressure phase, and cubic SrIrO_3 , a stable high pressure phase (right). The former is a distorted variation of a 6H hexagonal perovskite.

Iridium oxides are of special interest in the study of quantum materials because, for these materials, spin-orbit-coupling can have a dramatic effect on the energies of the valence electrons associated with the M ions and consequently the materials' electronic and magnetic properties. The strong influence of spin-orbit-coupling can explain some of the properties of iridates such as their widely insulating behavior. SrIrO_3 and BaIrO_3 are quantum materials closely related to the ruthenate perovskites. In this series, however, SrIrO_3 and BaIrO_3 are both monoclinic $C2/c$ distortions of the 6H- BaTiO_3 hexagonal $(\text{hc})_2$ structure^{39,40} (former: $a = 5.604 \text{ \AA}$, $b = 9.618 \text{ \AA}$, $c = 14.17 \text{ \AA}$, $\beta = 93.26^\circ$). These structural distortions have not yet been theoretically modeled to our knowledge, but they may well be related to the influence of the strong spin orbit coupling in Ir, which is widely known to be influential in determining the magnetic and electrical properties of iridium oxide based quantum materials⁴¹⁻⁴⁷. The monoclinic and cubic crystal structures

of SrIrO_3 are shown in **Figure 3**. Both SrIrO_3 and BaIrO_3 are non-magnetic electrical insulators^{39,48,49} and adopt the ideal cubic $Pm-3m$ perovskite structure at high pressure. A substitution of Zn or Li for Ir in the 6H- SrIrO_3 polymorph destabilizes the face-sharing octahedra, and hence $\text{SrIr}_{1-x}\text{Zn}_x\text{O}_3$ is found to be an orthorhombic distortion of the classical cubic perovskite for $0.25 \leq x \leq 0.33$ and $\text{SrIr}_{1-x}\text{Li}_x\text{O}_3$ has that type of crystal structure for $x = 0.25$ only⁵⁰. The reason for the destabilization of the hexagonal perovskite structure for Zn and Li substitutions has not been proven theoretically.

3. Dimers and trimers. Relation to classic double perovskites.

In classical double perovskites, there are two different "M type" ions in an ordered array or a partially ordered array within the MO_3 framework. Double perovskites can be written in the form $\text{A}_2\text{MM}'\text{O}_6$, where M and M' can be different ions such as in Sr_2FeWO_6 , a material that has a particularly high magnetoresistance⁵¹ or even the same M metal with different oxidation states, such as is seen in BaBiO_3 ($\text{Ba}_2\text{Bi}^{3+}\text{Bi}^{5+}\text{O}_6$ formally)⁵²⁻⁵⁷, the basis for superconductivity in several perovskite oxides^{58,59}. Disordered and partially ordered M-M' double perovskites are known. "Double perovskites" are also known for ratios of M to M' that are not 1:1, for example also 2:1, where the formula is $\text{A}_2\text{M}_{4/3}\text{M}'_{2/3}\text{O}_6$ i.e. $\text{A}_2[\text{M}[\text{M}'_{1/3}\text{M}_{2/3}]]\text{O}_6$, with M and M' selected to yield charge neutrality. An example of this kind of double perovskite is $\text{Ca}_4\text{Nb}_2\text{O}_9$ ^{60,61}. Of further interest are oxide double perovskites where one of the ions does not display octahedral coordination^{52,62}.

Double hexagonal perovskites are also known – when there is more than one chemically distinct type of M site ion present. The materials can have ordered M-M' or disordered M-M' structures. Many ordered materials and disordered materials are known and briefly described in this review. Consider the 6H structure shown in **Figure 1** as the basis. There are two distinctly different octahedral sites for the M ions present. One (yellow in the figure) shares only corners with other octahedra, making a separate triangular plane (seen in the figure at levels 0, $\frac{1}{2}$, and 1 along the crystallographic c axis, and the other shares corners with one set of $(\text{M},\text{M}')\text{O}_6$ octahedra but a face with another set (blue in the figure). When there are two octahedra in the face sharing sub-structure, the basic formula is $\text{A}_3\text{MM}'_2\text{O}_9$. Occasionally M and M' can be the same ion (as in some of the polymorphs of BaRuO_3) but much more frequently they are two distinctly different ions. While the M ions form triangular planar lattices of potentially isolated MO_6 octahedra, the M' ions form a dimer array on a triangular lattice. When either M or M' has unpaired electrons, the magnetism can make these quite interesting quantum materials due to the triangular lattice and the localized vs. delocalized character of unpaired electrons in the dimers⁴⁷. For consistency with more complex structures, we refer to these materials simply as dimer-based hexagonal perovskites.

3.1. Dimer-based hexagonal perovskites

Dimer-based hexagonal oxide perovskites are by far the most frequently studied quantum materials in this family. The most common dimer-based hexagonal double perovskite family of quantum materials is found when the M'-site is occupied by Ru or Ir, making the formula $\text{Ba}_3\text{MRu}_2\text{O}_9$ or $\text{Ba}_3\text{Mlr}_2\text{O}_9$. For

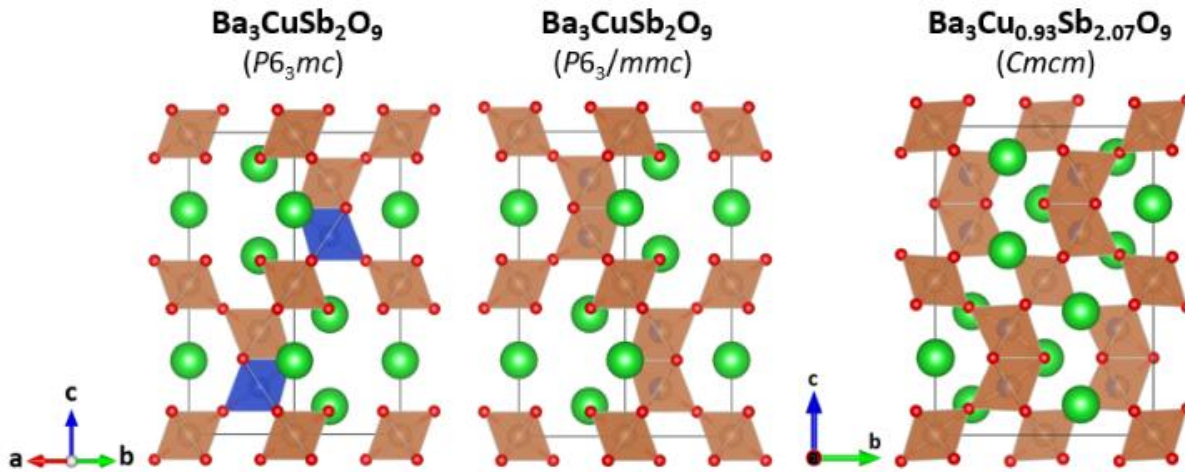


Figure 4. The reported crystal structures of “ $\text{Ba}_3\text{CuSb}_2\text{O}_9$ ”.

purposes of organization in this group, which consists of many frequently studied materials, we consider the generic formula to be $\text{Ba}_3\text{MM}'_2\text{O}_9$, and we classify the materials into subgroups that differ in the total number of electrons on the $\text{M}'_2\text{O}_9$ dimer. The formal oxidation state of M can range from 1+ to 4+ - as the formal charge on the M site ion increases, to maintain neutrality, the formal oxidation state of the M' ion, and thus the total number of electrons on the $\text{M}'_2\text{O}_9$ dimer, decreases. (For formal electron counts, the electropositive Ba ion is always taken to be Ba^{2+} and the oxygen ion is taken to be O^{2-} .) As in many quantum materials, determination of the physical properties is not related in a trivial way to the formal electron count, as how the electrons are distributed on the $\text{M}'_2\text{O}_9$ dimers depends on some important chemical characteristics of how the orbitals on M' and oxygen overlap, discussed in the review by Khomskii and Streltsov in this issue.

In $\text{Ba}_3\text{MRu}_2\text{O}_9$, when M is a non-magnetic monovalent cation (eg. Li or Na), the total number of electrons donated by the Ru to the oxygens in a Ru_2O_9 dimer is 11⁶³⁻⁶⁵. (The Ru can be considered formally as a 1:1 mixture of Ru^{5+} and Ru^{6+} , but “where’s the charge, really?” is a good question that has been asked by some for decades for such highly charged transition metal ions in oxides.) Both of these compounds crystallize in the hexagonal space group $P6_3/mmc$. While the hexagonal structure of $\text{Ba}_3\text{LiRu}_2\text{O}_9$ remains stable down to 100 K, $\text{Ba}_3\text{NaRu}_2\text{O}_9$ undergoes a structural transition at 225 K to a lower symmetry space group, $Cmcm$, a simple dimensional distortion of the hexagonal perovskite. This has been attributed to a well-known phenomenon in materials physics and solid state chemistry known as charge ordering; in this case where the Ru^{5+} ions are said to occupy one of the sites in the dimer and the Ru^{6+} ions to occupy the other site in the dimer, in an ordered array. $\text{Ba}_3\text{NaRu}_2\text{O}_9$, which, in contrast has not been shown to undergo charge ordering transition, has a negative Curie-Weiss temperature, indicating antiferromagnetic interactions between the Ru spins, but remains paramagnetic down to 1.7 K. Its magnetic effective moment is calculated to be about $0.91\mu\text{B}/\text{mol-f.u.}$, and the conductivity activation gap is about 0.1 eV. Why the Li^{1+} material behaves so differently from the Na^{1+} material is a potentially interesting puzzle to address in future research. These are excellent examples of quantum materials.

When M is clearly a divalent cation in $\text{Ba}_3\text{MRu}_2\text{O}_9$, the hexagonal 6H crystal structure that we have been discussing has been reported for in the cases of Ni^{2+} , Ca^{2+} , Mg^{2+} , and Zn^{2+} . For these materials there would be 10 electrons donated to the Ru_2O_9 dimer by its constituent metal atoms, for a formal charge on both Ru of 5+. For the cases above when M is a transition metal (i.e. Ni^{2+} , which is an $S=1$ ion), there must be an internal equilibrium within the compound between the formal valence of the M ion and the formal valence of the Ru in the dimers. Thus dimer-based hexagonal perovskites such as $\text{Ba}_3\text{CoRu}_2\text{O}_9$ and $\text{Ba}_3\text{FeRu}_2\text{O}_9$ would be interesting if studied in this context because Fe^{3+} or Co^{3+} may more likely be in equilibrium with a formally Ru^{4+} - Ru^{5+} mixture than a Co^{2+} or Fe^{2+} mixture would be with Ru^{5+} . Some of the divalent ions listed above are non-magnetic (i.e. Ca, Mg and Zn), an important characteristic for M ions that results in the magnetism, and the resulting quantum properties, arising from transition metal ions in the dimers and their orbital overlap with the oxygens.

Sb is a common 5+ ion in octahedral coordination in oxides and is an important constituent in some hexagonal perovskites. It is non-magnetic, so when it is present, the magnetism arises from the other ions present. The dimer-based hexagonal perovskite which mixes Cu and Sb as the M and M' ions is both important and unusual. An ordered 6H hexagonal perovskite crystal structure for $\text{Ba}_3\text{CuSb}_2\text{O}_9$ was reported in 1978⁶⁶. This structure consists of ordered face-sharing of SbO_6 octahedra and isolated CuO_6 octahedra, in a normal hexagonal perovskite type structure as shown in **Figure 4**. If this is the crystal structure of the phase, then the Cu^{2+} spin $\frac{1}{2}$ ions are in triangular layers, a nice ordered triangular plane spin $\frac{1}{2}$ configuration, the canonical arrangement for a quantum material⁶⁷⁻⁶⁹. Recent powder and single crystal XRD structural analysis conforms that the material is hexagonal (the senior author wonders what happened to the Jahn-Teller distortion virtually always seen for Cu^{2+} in octahedral coordination), but that it is something more like an inverse spinel than an ordered 6H perovskite, with the Cu and Sb randomly occupying positions in the dimers and Sb found on the individual octahedral layers (**Figure 4**), a $\text{Ba}_3(\text{Sb})(\text{SbCu})\text{O}_9$ configuration in spite of the fact that the formula suggests otherwise. In this structure, the magnetic spin $\frac{1}{2}$ Cu^{2+} ion is disordered in the dimers with a nonmagnetic ion,

Sb⁵⁺. This material has been proposed to be a quantum spin liquid candidate with an $S = \frac{1}{2}$ triangular lattice, tested by magnetic susceptibility and neutron scattering experiments down to 0.2 K. There is no magnetic ordering observed, while the Curie-Weiss temperature is calculated to be -55 K. The specific heat shows a T-linear dependence, and a relatively large Sommerfeld constant was found, 43.4 mJ/mol-K² below 1.4 K⁷⁰, although the material is insulating (which should lead to a Sommerfeld constant near 0). A study of Ba₃CuSb₂O₉ single crystals, which also have disordered Cu and Sb in the dimers, showed that the hexagonal symmetry and the presence of dynamical Jahn-Teller distortions remain down to 3.5 K. There is a very big investment in the “quantum materials” properties of this material by the materials physics community, a community that does not appear to be disturbed by the extensive Cu/Sb disorder present in the dimers. When the Sb/Cu ratio is slightly different from 2/1, a distorted orthorhombic structure is observed. Further, the stoichiometry and symmetry of the phase appear to be dependent on the synthesis temperature⁷¹. A particularly interesting set of materials of this type are the Ba₃CuOs₂O₉ double hexagonal perovskites, for which both the structural symmetry and the magnetic properties depend profoundly on whether the material is prepared with an ordered M'M₂ array or one where an inverse hexagonal perovskite of the type Ba₃(Os)(CuOs)O₉ is made⁷².

In the same structural vein, we also have Ba₃CoSb₂O₉, another dimer-based quantum material that crystallizes in the hexagonal space group P6₃/mmc. That is, it is another classical dimer hexagonal perovskite, with the lattice parameters $a = 5.857 \text{ \AA}$ and $c = 14.459 \text{ \AA}$ ⁷³⁻⁷⁷. This material, nominally consisting of Co²⁺ and Sb⁵⁺ in an ordered array is an ideal effective spin $= \frac{1}{2}$ (that is, when the orbital and spin contributions to the moment are both considered, the effective spin of the Co²⁺ turns out to be $\frac{1}{2}$, Co is unique among the 3d transition metals in that the orbital contribution to the magnetic moment is not quenched) triangular lattice antiferromagnet. The extensive continuum of available energies seen for the spin system above the spin wave excitations by neutron scattering, is claimed to be clear evidence that Ba₃CoSb₂O₉ is close to the proximity of a quantum spin liquid state in a 2D triangular lattice system⁷³⁻⁸². As for Ba₃CuSb₂O₉, there is a big investment in this material by the materials physics community.

Much more obscure, but none-the-less chemically interesting, with substantially different magnetic properties, are Ba₃MoCr₂O₉ and Ba₃WCr₂O₉⁸³. These materials are fun from a chemical perspective because Cr, Mo and W are in the same column in the periodic table and yet Cr is in a nominally 3+ state, while Mo and W are formally in a 6+ (d⁰) state. (Cr³⁺ is arguably the mother of all strongly Hund's rule coupled ions, and is therefore quite stable, but when combined with Ba and O, Cr can be in more highly oxidized valence states. These materials appear to require an extremely reducing ambient for synthesis). The crystal structures are classical dimerized hexagonal perovskites like we have been describing here, and while the W variant is argued to be chemically ordered with Cr in the dimers, displaying a “dimer like” magnetic susceptibility, the Mo variant is said to be disordered, with Cr in an oxidation state greater than 3+, displaying a classical Curie-Weiss magnetic behavior. Further work on the chemistry, structures and properties of these materials would be of interest.

We now consider the group of compounds where the isolated M octahedra are occupied by 3+ ions. The only distorted hexagonal perovskite having the M formal valence = 3 in the 6H family of ruthenates is monoclinic Ba₃ScRu₂O₉. (Sc is an electropositive, non-magnetic, 3+ ion in oxides.) Some structures can also be stabilized in the orthorhombic space group *Cmcm*, such as Ba₃CuRu₂O₉ or the low temperature phase of Ba₃CoRu₂O₉⁸⁴⁻⁸⁹, but the most studied 6H hexagonal perovskites are those where M is a rare earth element. Chemically, this is presumably because they are relatively easy to make, but from the point of view of magnetic properties they are interesting because the rare earth ions are found in a triangular planar lattice, and all the rare earths behave magnetically differently due to their *f* electron count. The crystal structures adopt the usual hexagonal space group *P6₃/mmc* for all compounds in the series (M = Y, La to Lu). The magnetic ordering temperatures are summarized in **Table 1**.

In the M = M³⁺ group, M = In³⁺ Ba₃InRu₂O₉ is reported to be hexagonal. For this material, researchers claim that due to the strong hybridization of Ru and O orbitals, the Ru₂O₉ dimers are better explained as being molecular units, where an $s = \frac{1}{2}$ moment is delocalized in the dimers. This kind of consideration - whether the face sharing units are best considered as “molecules” with distinct molecular orbitals, or simply should be thought of as the sum of the electron configurations of the transition metals that often occupy them - is one of the fundamental interesting aspects of the hexagonal perovskites. A spin glass transition was observed at 3.5 K, which can either be due to geometric frustration or disorder on the magnetic lattice (i.e. some so-far undetected structural mixing of In and Ru the hexagonal perovskite M+M' sites). In addition, the static magnetic “ground state” (Theoretically a T = 0 Kelvin state but from a practical perspective materials physicists mean the lowest temperature state that they can attain in their measurements.) in this material, studied by μ SR, has been said by the researchers involved to indicate that Ba₃InRu₂O₉ is more complicated than a conventional spin glass⁹⁰⁻⁹².

In the case of M⁴⁺ cations, there are several reported compounds, such as Ba₃BiRu₂O₉, Ba₃TiRu₂O₉ and Ba₃ZrRu₂O₉. Ba₃BiRu₂O₉ is particularly unusual, in that although the average formal valence of Bi is claimed to be 4+, charge disproportionation of 2Bi⁴⁺ to Bi³⁺ + Bi⁵⁺ is said to be present, similar to what is seen in BaBiO₃. The evidence for this exotic state (said to be a “negative U” state in materials physics) is Bi L₃-edge X-ray absorption near-edge (XANES) spectroscopy. This compound also undergoes a spin gap opening at T* = 176 K, meaning that above 176 K, Ba₃BiRu₂O₉ is a S=1 magnetic dimer system, and a spin gap state (in other words that there is a distinct energy range of forbidden spin excitations, which are usually continuously available through “magnons”) emerges below 176 K. The effect on magnetoelastic transitions in Ba₃BiRu₂O₉ by external physical or internal chemical pressure has also been studied. It is claimed to reduce the spin gap opening temperature^{93,94}. Moreover, a small amount of La-doping (~10%) on the Bi-site suppresses the spin gap and also eliminates the sharp structural and magnetic transitions that accompany it, suggesting that the spin-gap behavior is strongly associated with the unstable charge of Bi⁴⁺ in this material^{95,96}. (Ba₃BiLr₂O₉ also shows the opening of a spin gap, at 74 K. Magnetoelastic transitions induced by external physical or internal chemical pressure reduce the gap opening temperature^{93,94}). More conventional in this group is Ba₃TiRu₂O₉, which shows structural

disorder between Ti and Ru in both the corner-sharing octahedra and face-sharing dimers^{97,98}. The system is magnetically disturbed by a substantial amount of Ti/Ru chemical disorder, with the Curie-Weiss temperature of -29.5 K and the effective magnetic moment of $1.82 \mu\text{B}/\text{f.u.}$ A bifurcation of the zero field cooled and field cooled magnetic susceptibility is observed below 4.7 K, which, along with the structural disorder, indicates that $\text{Ba}_3\text{TiRu}_2\text{O}_9$ is a compositionally-disordered spin-glass system. The material is a semiconductor with an activation energy for charge transport of approximately 0.14 eV ⁹⁸.

6H hexagonal oxide perovskites are not the only $\text{Ba}_3\text{MM}'_2\text{O}_9$ materials known in this family. Materials with dimers can also have rhombohedral (9R) rather than hexagonal (6H) stacking along c . $\text{Ba}_3\text{MnRu}_2\text{O}_9$ (Mn has the formal valence of Mn^{2+} , apparently) adopts a 9R structure while the majority of the $\text{Ba}_3\text{MRu}_2\text{O}_9$ phases form the 6H structure. When the A site ion is too small, hexagonal perovskites are not stable, and $\text{Ca}_3\text{MnRu}_2\text{O}_9$ for example adopts the standard $Pbnm$ space group seen often for orthorhombically distorted conventional perovskites. In this material, Mn and Ru are randomly distributed over the M-sites. $\text{Ba}_3\text{MnRu}_2\text{O}_9$, unsurprisingly due to its magnetic disorder, shows a short range spin glass transition at 30 K while for the orthorhombically distorted conventional perovskite $\text{Ca}_3\text{MnRu}_2\text{O}_9$ a glass transition is seen at 150 K⁹⁹ also a likely indication of Mn-Ru disorder. Similarly, $\text{Sr}_3\text{CaRu}_2\text{O}_9$ and $\text{Sr}_3\text{CaIr}_2\text{O}_9$ have monoclinic structures, distortions of the conventional perovskite structure, with space group $P2_1/c$ ^{100,101}.

Moving now to iridates, of particular interest as quantum materials due to the fact that Ir is a $5d$ ion and therefore its orbital energies are known to be influenced spin orbit coupling, the materials and crystal structures are similar to what is seen in the $\text{Ba}_3\text{MRu}_2\text{O}_9$ system. Again, the oxidation state of M in the $\text{Ba}_3\text{Mlr}_2\text{O}_9$ series of dimer-based hexagonal perovskites can range from $1+$ to $4+$, resulting in the total number of electrons donated by Ir to the Ir_2O_9 dimer ranging from 11 to 8 , respectively. For monovalent M ions, both $\text{Ba}_3\text{NaIr}_2\text{O}_9$ and $\text{Ba}_3\text{LiIr}_2\text{O}_9$ compounds crystallize in the hexagonal space group $P6_3/mmc$, however, only $\text{Ba}_3\text{NaIr}_2\text{O}_9$ undergoes a structural transition to a monoclinic of a hexagonal perovskite, space group $C2/c$, below 100 K. For divalent M ions, hexagonal structures are stabilized when $M = \text{Mg}, \text{Zn}$ and Ni , and distorted monoclinic structures are observed in the cases of $M = \text{Ca}$ and Sr . While all rare earth M elements result in structures in the hexagonal space group $P6_3/mmc$ in the $\text{Ba}_3\text{MRu}_2\text{O}_9$ ruthenates, the structural trends in the $\text{Ba}_3\text{Mlr}_2\text{O}_9$ system are quite different, in that the small rare earth ions ($M = \text{Sm-Lu}$) result in hexagonal structures, while the larger rare earth ions (eg. La and Nd) lead to structures in the distorted monoclinic space group $C2/c$. Finally, analogous to $\text{Ba}_3\text{BiRu}_2\text{O}_9$, $\text{Ba}_3\text{BiIr}_2\text{O}_9$ also adopts a monoclinic structure. This material displays a spin gap opening at a lower temperature of 74 K, as described briefly above.

In the Ir_2O_9 dimers, pure Ir^{5+} is expected to have a non-magnetic ground state. For Ir^{4+} dimers, small the observed effective moments in a localized spin picture can be taken to indicate the presence of strong AFM interactions between the Ir^{4+} ions within the dimers. For the case of the mix between Ir^{4+} and Ir^{5+} , magnetic ordering of Ir^{4+} is reported to occur at 10 K in $\text{Ba}_3\text{ScIr}_2\text{O}_9$ and $\text{Ba}_3\text{InIr}_2\text{O}_9$ ¹⁰². $\text{Ba}_3\text{Mlr}_2\text{O}_9$ compounds with $M = \text{Rare Earth (RE)}$ adopt the usual ordered hexagonal perovskite $P6_3/mmc$ space group, except for RE= La and Nd (which have

the monoclinically distorted $C2/c$ space group) as demonstrated in **Figure 5**. $\text{Ba}_3\text{Mlr}_2\text{O}_9$ shows antiferromagnetic ordering at 4 K for $M = \text{Y}$, at 5.1 K for $M = \text{Lu}$ and 2.0 K for $M = \text{Tb}$ ¹⁰³. The fact that the 6H iridates are studied less frequently in the materials physics community than the 6H ruthenates are is very likely due to the difficulty in growing single crystals of easily accessible size for iridates.

The $\text{Ba}_3\text{InIr}_2\text{O}_9$ hexagonal perovskite has been proposed to be a quantum spin liquid, where the unpaired electrons are localized on a mixed valence state between Ir^{4+} and Ir^{5+} within the Ir_2O_9 dimers. The gapless ground state and persistent spin dynamics that remain active down to 20 mK, probed by magnetic susceptibility, heat capacity, neutron diffraction, NMR and μSR , are cited as evidence. As shown in **Figure 6**, no long range magnetic ordering or spin freezing down to 20mK is seen in this $S = 1/2$ dimer Ir_2O_9 compound¹⁰⁴.

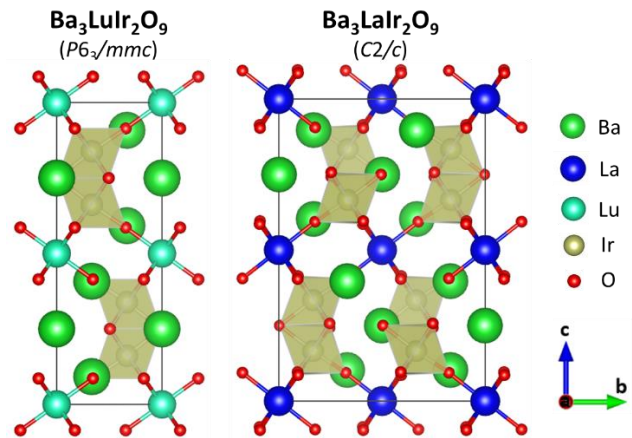


Figure 5. The crystal structures of the $\text{Ba}_3\text{LuIr}_2\text{O}_9$ and monoclinic $\text{Ba}_3\text{LaIr}_2\text{O}_9$ “hexagonal perovskites”. The Ir_2O_9 dimers are shaded. The rare earth ions are shown by teal or blue balls.

$\text{Ba}_3\text{IrTi}_2\text{O}_9$, where the magnetism comes from Ir^{4+} , a spin $1/2$ ion, reportedly in the isolated triangular layers, (the Ti $4+$ is non-magnetic) crystallizes in the hexagonal space group $P6_3/mmc$, has been proposed to be an embodiment of the triangular Heisenberg-Kitaev model, and has been used to study the interplay between geometric and exchange frustration^{105,106}. Materials physicists argue that $\text{Ba}_3\text{IrTi}_2\text{O}_9$ is a spin $1/2$ Mott insulator¹⁰⁷ and that Kitaev exchange (Usually a weak kind of magnetic exchange that loses out to ordinary antiferromagnetic-exchange derived ordering. Materials physicists use the term Mott insulator to explain cases where the electrons are largely confined to their individual atomic orbitals, e.g. that they are localized in solids, rather freely from the perspective of the senior author of this paper, because such a classification seems to him to ignore the necessity for M-O-M orbital overlap extending through a whole network for the appearance of metallic conductivity. He would not classify many double perovskites that physicists believe to be Mott insulators, as actually being Mott insulators for example.) destabilizes the 120° ordering expected for Heisenberg spins on a triangular lattice, and thus leads to the formation of a Z2-vortex quantum spin liquid state, tested by spherical neutron polarimetry¹⁰⁶⁻¹⁰⁸. Magnetic susceptibility displays a very strong antiferromagnetic interaction with the Curie-Weiss temperature of -130 K, but according to the researchers involved, no magnetic ordering is observed

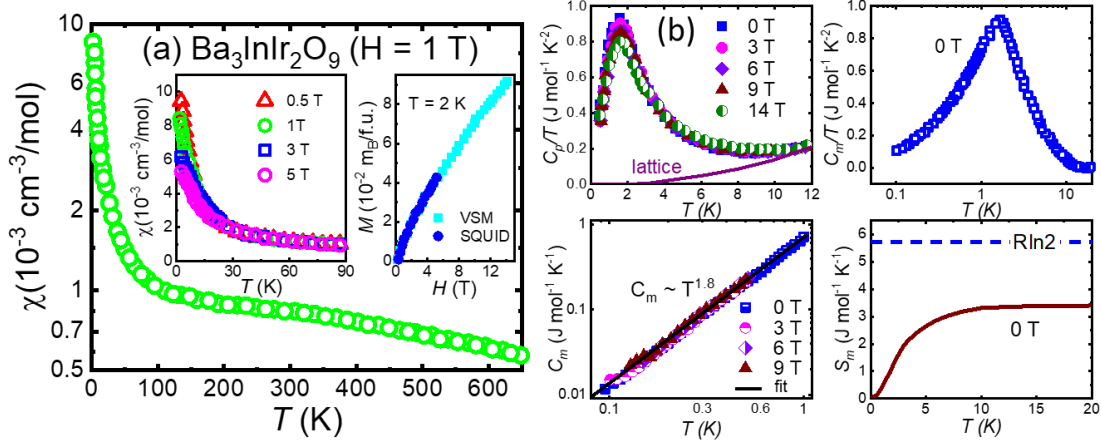


Figure 6. (a) Temperature-dependent magnetic susceptibility in the Quantum Spin Liquid candidate $\text{Ba}_3\text{InIr}_2\text{O}_9$ and (b) heat capacity measurements and magnetic entropy calculation in this $\text{Ba}_3\text{InIr}_2\text{O}_9$ material ¹⁰⁴.

down to 23 mK. The frustration index is ($= \Theta_{\text{CW}}/T_{\text{M}}$ where Θ_{CW} is the Curie Weiss theta and T_{M} is the temperature of the magnetic ordering. Materials are expected to magnetically order at a ratio between 1 and 10) therefore calculated to be larger than 5000, strongly implying the presence of a quantum spin liquid ground state^{105–107,109–111}. Although there may be Ir/Ti chemical disorder in both the MO_6 octahedra and the $\text{M}'_2\text{O}_9$ dimers, the researchers involved claim that the material is not a spin glass due to the absence of spin freezing in magnetic susceptibility measurements, heat capacity, and μSR measurements. Further, DFT calculation based researchers report that a Dirac-type nodal line should be present along the A-L direction in k -space (i.e. reciprocal space), and is “symmetry-protected”, meaning that it absolutely has to be there due to the material’s symmetry, suggesting the possible existence of emerging quantum phenomena^{108,112} (i.e. a novel spin-orbital singlet state). The senior author of this paper believes none of this by the way, because such predications in complex materials are always “within the model calculated” in his view, although he is happy to defer to the views of the large number of researchers involved in the study of this material.

The reader can easily see from what we summarize here that the dimer-based hexagonal perovskites are a mainstay of quantum materials research. Structural disorder is sometimes detected for these materials and sometimes not, and as frequently is the case in materials physics, disorder is not universally believed to be a bad thing when it comes to quantum materials. It is only considered significant when its influence on the quantum properties can be clearly detected through physics characterization^{113–115}.

We now briefly consider a few complex dimer-based hexagonal perovskites. The first of these is very highly structurally disordered, but in an interesting way. The complex disordered dimer material $\text{Ba}_3\text{Fe}_{1.56}\text{Ir}_{1.44}\text{O}_9$ ¹¹⁶ adopts the hexagonal space group $P3m1$, with the lattice parameters $a = 5.740 \text{ \AA}$ and $c = 14.160 \text{ \AA}$ as shown in **Figure 7**. Interestingly, the site disorder between the Fe and Ir occurs within the dimers, where the dimerized sites are said to be unequally occupied by Fe and Ir, and in one of the triangular layers of octahedra but not the other. This kind of crazy uneven occupancy is what reduces the symmetry from the usual space group for 6H perovskites. The

symmetry of this material is such that the complicated chemical disorder results in a non-centrosymmetric polar structure. The valence states of Fe^{3+} and Ir^{5+} were confirmed by X-ray absorption near edge spectroscopy (XANES). $\text{Ba}_3\text{Fe}_{1.56}\text{Ir}_{1.44}\text{O}_9$ is semiconducting and it has a near room temperature antiferromagnetic ordering transition of 270 K.

Table 1. The magnetic ordering temperatures (in degrees Kelvin) of the $\text{Ba}_3\text{MRu}_2\text{O}_9$ and $\text{Ba}_3\text{Mlr}_2\text{O}_9$ ($M = \text{Y, La-Lu}$) hexagonal perovskites. ^{47,84,117–121} PM: paramagnetic.

M ions	T_{C} or T_{N} of $\text{Ba}_3\text{MRu}_2\text{O}_9$	T_{C} or T_{N} of $\text{Ba}_3\text{Mlr}_2\text{O}_9$
Y	4.5	4
La	6.0	14.6
Ce	PM	PM
Pr	PM	PM
Nd	24.0	17.4
Sm	12.5	14.4
Eu	9.5	8.2
Gd	14.8	10.2
Tb	9.5	2.0
Dy	27.8	8.9
Ho	10.2	5.6
Er	6.0	6.0
Tm	8.3	5.5
Yb	4.5	5.3
Lu	9.5	5.1

The 6-layer hexagonal structure of $\text{Ba}_6\text{Rh}_{2.33}\text{Yb}_2\text{Al}_{1.67}\text{O}_{15}$ ¹²² is said to adopt the non-standard 6H space group $P-6m2$, with lattice parameters $a = 5.854 \text{ \AA}$ and $c = 14.660 \text{ \AA}$, as displayed in **Figure 8**. Unlike the “usual” 6H hexagonal

perovskites, this material has three different types of M-M' ions present. The crystal structure is slightly different from what is seen in the 6H-Ba₃MRu₂O₉ family, in that the face-sharing Rh₂O₉ dimers, which are reported to contain only Rh, while a second dimerized layer is said to be occupied by a disordered mix of Al plus Rh. The YbO₆ octahedra are confined to the isolated octahedra. To balance the charge, there appear to be oxygens missing in a random way in certain sites in the crystal structure. Given that some of the dimers are heavily Al-rich, the structure may be even more complex than this, with the missing oxygens associated with AlO₄ tetrahedra. This is definitely a challenging structural problem to figure out.

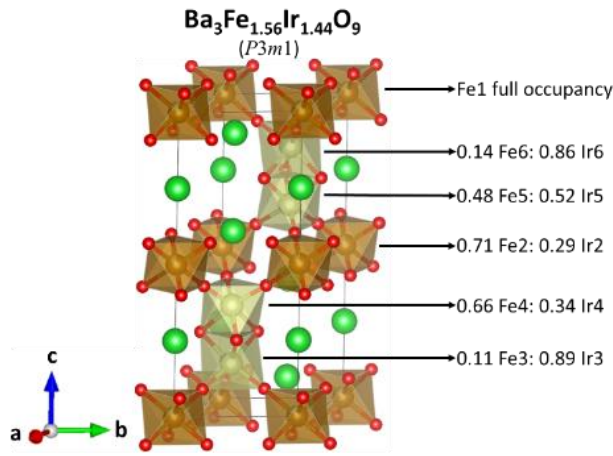


Figure 7. The crystal structure of Ba₃Fe_{1.56}Ir_{1.44}O₉

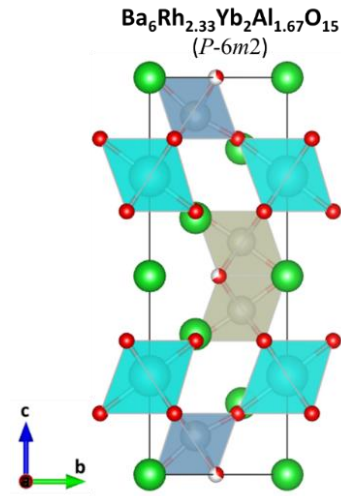


Figure 9. The crystal structure of Ba₆Rh_{2.33}Yb₂Al_{1.67}O_x. The Rh₂O₉ dimers are shown in light gray, the mixed (Al,Rh)₂O₉ dimers in dark gray and the YbO₆ octahedra shown in light blue. The oxygens are shown in Red, with partially occupied sites shown as mixtures of red and white spheres. The Ba ions are shown in green.

3.2. Trimer-based hexagonal perovskites

When the ratio of M to M' ions is 1:3 instead of 1:2 then variations of hexagonal double perovskites can form with formulas A₄MM'₃O₁₂. In these materials, there are three M'O₆ octahedra sharing faces with each other and corners with a triangular lattice of MO₆ octahedra. These trimer materials are much more rare than the hexagonal perovskite oxides based on dimers, and have been studied proportionally much less

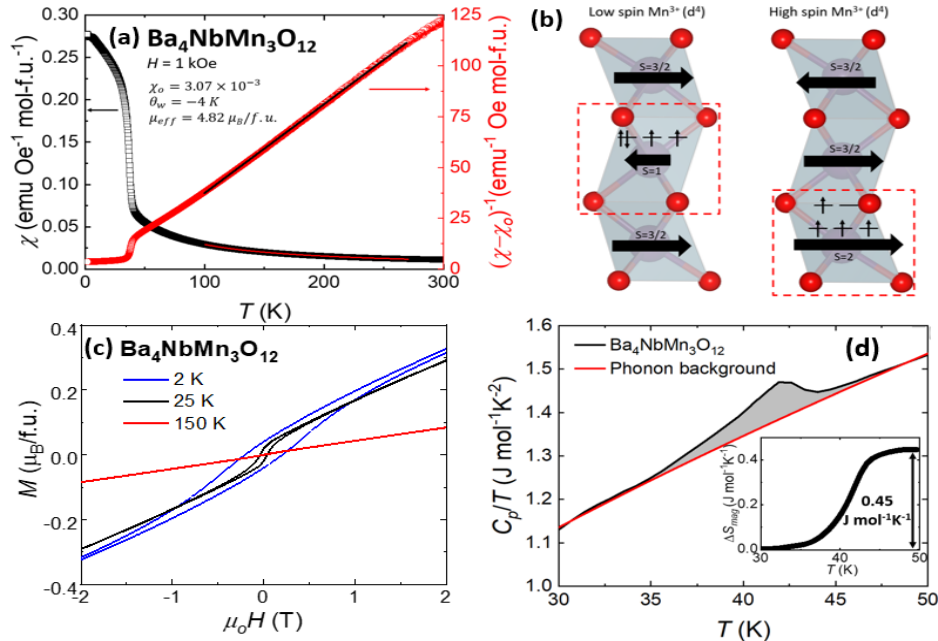


Figure 8. (a) Temperature-dependent magnetic susceptibility of Ba₄NbMn₃O₁₂, (b) The two magnetic models account for the observed magnetic moment of 4.82 μ_B/Mn₃O₁₂ per trimer, (c) Magnetic hysteresis loops above and below the ferrimagnetic transition temperature T ≈ 42 K, and (d) The heat capacity measurement that shows the partial entropy released at the ordering temperature at T ≈ 42 K¹²⁶.

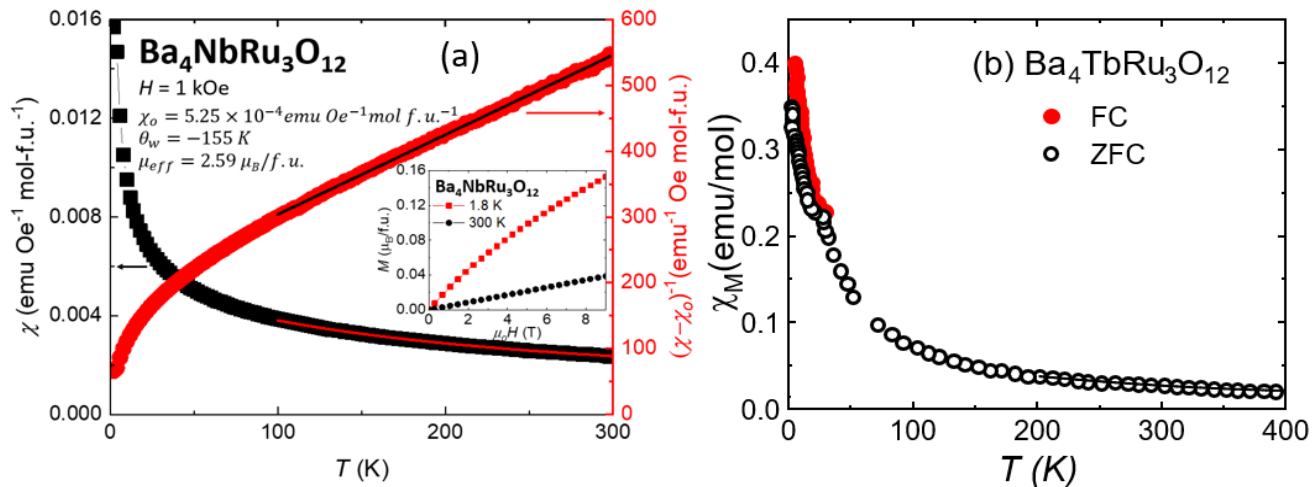


Figure 10. Temperature-dependent magnetic susceptibility of (a) $\text{Ba}_4\text{NbRu}_3\text{O}_{12}$ ¹²⁷ and (b) $\text{Ba}_4\text{TbRu}_3\text{O}_{12}$ ¹²⁹.

frequently. The site in the middle of the M' trimer is crystallographically distinct from that of the two outer octahedra (The central octahedron shares only faces with other octahedra while the two peripheral ones share a face on one side and corners on the other side). Thus it is occasionally noted that the central octahedron can have a different ion in it, described further below, making such materials hexagonal triple perovskites ($A_4MM'{}_2M''\text{O}_{12}$).

From a property perspective, the trimer-based materials can be interesting magnetically, as the electrons in the trimer are either localized on the ions, as they are when M' is a $3d$ element, or confused about whether they are localized or delocalized within the trimer, as has been proposed when M' is a $4d$ or a $5d$ element⁴⁷. This is particularly of interest to spectroscopists, who have most frequently studied this issue in dimers¹²³ and theorists (see the review by S.V. Streltsov and D. Khomskii in this journal). The “where are the electrons” question in these trimer perovskites can make them interesting as quantum materials.

In this section, we focus our attention mostly on the three trimer systems $\text{Ba}_4\text{MnRu}_3\text{O}_{12}$ ($M = \text{Mn, Ru, Ir}$), which have been investigated in the context of whether the unpaired electrons are localized or delocalized within the M_3O_{12} trimer clusters and whether spin orbit coupling can play an important role in the magnetism of face-sharing hexagonal perovskites. There are only three Mn_3O_{12} trimer compounds reported in the literature in this group so far, $\text{Ba}_4\text{MMn}_3\text{O}_{12}$ ($M = \text{Nb, Ce and Pr}$), all of which crystallize in the hexagonal space group $R\bar{3}m$. The latter two materials were only structurally reported without any magnetic analysis. This can be due to the multi-valent states of Ce and Pr, causing complicated magnetic properties, or that the phases are not pure enough for the magnetic study. Ce is $4+$ (with no d electrons and no f electrons) in the BaCeO_3 conventional perovskite, so there may be no interference of rare earth magnetism in that case, but Pr is a notorious nightmare to deal with in the more familiar oxide perovskites^{121,124,125}. Thus, we will discuss in detail the magnetic properties of $\text{Ba}_4\text{NbMn}_3\text{O}_{12}$ instead, where the Nb is $5+$ and non-magnetic¹²⁶. There are two Mn^{3+} and one Mn^{4+} present. As shown in **Figure 9a**, $\text{Ba}_4\text{NbMn}_3\text{O}_{12}$ shows an effective moment of $4.82 \mu\text{B}/\text{Mn}_3\text{O}_{12}$ trimer and competing antiferromagnetic and ferromagnetic

interactions between Mn ions are inferred from the Curie-Weiss temperature of -4 K and the ferrimagnetic ordering transition temperature of approximately 42 K. With the effective moment of $4.82 \mu\text{B}/\text{Mn}_3\text{O}_{12}$, two potential magnetic ordering schemes for this material are displayed in **Figure 9b**. Neutron diffraction is necessary in order to solve the magnetic structure and determine the actual magnetic spin configuration. From this magnetic picture, we can see that the magnetism of the Mn_3O_{12} trimer can be well explained by a localized electron model, meaning that the unpaired electrons reside locally at each ion site, instead of being delocalized within the Mn_3O_{12} trimer unit. The magnetic hysteresis loops above and below the transition temperature are shown in **Figure 9c**. Finally, the heat capacity measurement in **Figure 9d** demonstrates the presence of an entropy loss at the around 42 K, however, only a small amount of the total magnetic entropy expected for an $S = 2$ Heisenberg system is recovered. So, it is fair to ask, where is the missing entropy?

Moving to a $4d$ transition metal based material, the $\text{Ba}_4\text{MRu}_3\text{O}_{12}$ system for example, $\text{Ba}_4\text{NbRu}_3\text{O}_{12}$ and $\text{Ba}_4\text{TaRu}_3\text{O}_{12}$ are reported to adopt the hexagonal space group $R\bar{3}m$. The crystal structures consist of a trimer-based Ru_3O_{12} cluster. The exchange interaction between Ru^{3+} and Ru^{4+} is claimed to be the origin of the magnetic ground state^{127,128}. A few other compounds in this trimer family have been structurally reported, but the magnetic properties are not yet investigated. A comprehensive study of $\text{Ba}_4\text{LnRu}_3\text{O}_{12}$ - type materials has been reported, however. In the case of non-magnetic rare earth ions ($\text{Ln} = \text{Y, La, Lu}$), the magnetism comes purely from the magnetic Ru_3O_{12} trimers. But for other rare earth ions, the observed magnetic moments must arise from both the magnetic rare earth ions and the Ru_3O_{12} trimers. The magnetic ordering temperatures of the $\text{Ba}_4\text{LnRu}_3\text{O}_{12}$ series are summarized in **Table 2**. If the trimers could be made fully nonmagnetic, then these compounds would have nicely separated triangular layers of rare earth ions, and be good candidates for low temperature quantum magnets.

The magnetic properties of isolated Ru_3O_{12} trimers in $\text{Ba}_4\text{NbRu}_3\text{O}_{12}$ have been compared with the combined magnetic moments of the magnetic rare earth Tb^{4+} and the Ru_3O_{12} trimer in $\text{Ba}_4\text{TbRu}_3\text{O}_{12}$. The temperature-dependent magnetic

susceptibilities of both compounds are shown in **Figure 10**. The Curie-Weiss fitting of the data from 200-400 K in $\text{Ba}_4\text{TbRu}_3\text{O}_{12}$ results in a Curie-Weiss temperature of -57 K and an effective moment of $8.78 \mu\text{B}/\text{f.u.}$ This large magnetic moment has been attributed to the magnetic sum of Tb^{4+} ($7.94 \mu\text{B}$) plus three individual Ru^{4+} ($S = 1$, $\mu_{\text{eff}} = 2.83 \mu\text{B}$), which should be about $9.33 \mu\text{B}/\text{mol.f.u.}$ The observed moment is argued to be within experimental error of the expected moments from localized spins. From neutron diffraction, the magnetic structure of $\text{Ba}_4\text{TbRu}_3\text{O}_{12}$ was solved. It is displayed in **Figure 11**.

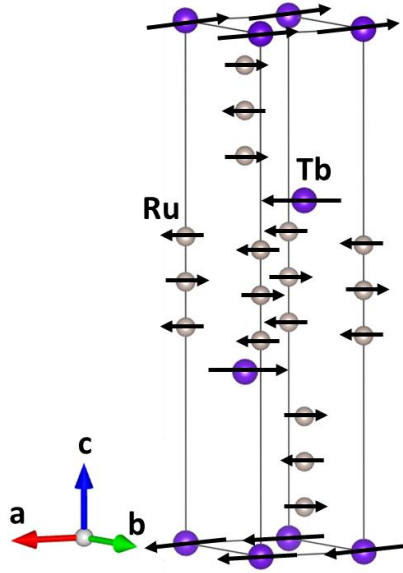


Figure 11. The magnetic structure of $\text{Ba}_4\text{TbRu}_3\text{O}_{12}$ at 2.5 K, solved from neutron diffraction¹²⁹. Arrows show the directions of the ordered magnetic spins at low temperatures.

Table 2. The summary of the magnetic ordering temperatures in $\text{Ba}_4\text{MRu}_3\text{O}_{12}$ and $\text{Ba}_4\text{MIR}_3\text{O}_{12}$ ¹²⁹⁻¹³¹ ($M = \text{Y, La-Lu}$) systems. DM: diamagnetic, CW: Curie-Weiss, VV: Van-Vleck.

M ions	T_C or T_N of $\text{Ba}_4\text{MRu}_3\text{O}_{12}$	T_C or T_N of $\text{Ba}_4\text{MIR}_3\text{O}_{12}$
La	6.0	DM
Ce^{4+}	CW	10.5
Pr^{4+}	2.4	35
Nd	11.5	CW
Sm	3.5	VV
Eu	4.0	VV
Gd	2.5	CW
Tb^{4+}	24	16
Dy	30	CW
Ho	8.5	CW
Er	8.0	CW
Tm	8.5	CW
Yb	13	CW
Lu	8.0	DM

In the case of $\text{Ba}_4\text{NbRu}_3\text{O}_{12}$, since Nb^{5+} is non-magnetic, the only magnetic moments come from the isolated Ru_3O_{12} trimer. Analysis of the magnetic susceptibility leads to a Curie-Weiss temperature of -155 K and an effective moment of $2.59 \mu\text{B}/\text{mol.f.u.}$ This observed moment is between the value of spin $\frac{1}{2}$ ($1.73 \mu\text{B}$) and spin 1 ($2.83 \mu\text{B}$) per trimer, and cannot

therefore be due to free-ion-like localized magnetic moments. The Curie-Weiss temperature is relatively large and negative, indicating the presence of strong antiferromagnetic interactions between the Ru ions. A freezing temperature to a glassy state was observed at around 4 K. The corresponding frustration index is calculated to be larger than 30, implying that $\text{Ba}_4\text{NbRu}_3\text{O}_{12}$ is a strongly frustrated magnet. A recent neutron study employing both elastic and inelastic neutron scattering (in preparation by T. Halloran et. al) shows that only 1/3 of the spins freeze below 4 K, with the remaining spins still fluctuating. Hence, $\text{Ba}_4\text{NbRu}_3\text{O}_{12}$ is proposed to be a spin liquid or even a quantum spin liquid candidate. As shown in **Figure 12**, both the trimer energy level diagram, 1, and the molecular orbital diagram, 2, result in the overall spin $\frac{1}{2}$ in each Ru_3O_{12} trimer.

Spin-orbit coupling is the interaction of a non-zero electron spin with its orbital motion. This is a relativistic effect, and is proportional to the fourth power of the atomic number $Z^{132,133}$. Thus, it has the strongest effect in $5d$ transition metals (e.g. Ir) compared to $3d$ ions (e.g. Mn) and $4d$ ions (e.g. Ru). $\text{Ba}_4\text{BiIr}_3\text{O}_{12}$, which crystallizes in the distorted monoclinic space group $C2/c$, has Ir_3O_{12} trimers bridged by corner-sharing BiO_6 octahedra^{95,134}. It contains an unusual Bi^{4+} formal oxidation state, but actually has charge disproportionation of the Bi^{4+} into Bi^{3+} and Bi^{5+} . This material shows an anomaly at $T^* = 215$ K. This transition is not seen at the spin gap opening temperature, as is seen in $\text{Ba}_3\text{BiRu}_2\text{O}_9$ or $\text{Ba}_3\text{BiIr}_2\text{O}_9$. The Curie-Weiss temperature is found to be -15 K and the effective moment is $0.22 \mu\text{B}/\text{Ir}$. The relatively low effective moment comes from strong spin orbit coupling for the $5d$ Ir transition metal. Antiferromagnetic interactions within the Ir_3O_{12} trimer are claimed to lead to the formation of an $S = \frac{1}{2}$ doublet. The change in the magnetic state at T^* is claimed to result in a structural distortion to balance the amount of energy for the formation of the $S = \frac{1}{2}$ doublet. The Ir-Ir distance within the trimers is relatively short, 2.6 Å, implying the possibility of direct metal-metal bonding^{40,96,135,136}.

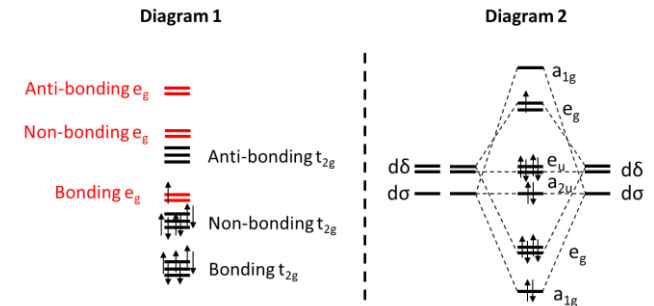


Figure 12. 1 The possible energy level diagram of a trimer¹³⁷ and 2 the alternative molecular orbital diagram⁴⁷. The electron counting shown is taken from the example of $\text{Ba}_4\text{NbRu}_3\text{O}_{12}$, which has a total of 13 electrons in each Ru_3O_{12} trimer. Diagrams are redrawn from the references.

While $\text{Ba}_4\text{RERu}_3\text{O}_{12}$ (RE^{3+}) compounds show magnetic ordering at low temperatures, $\text{Ba}_4\text{REIr}_3\text{O}_{12}$ compounds frequently remain paramagnetic down to 1.8 K. The exception is the case where the RE is Ce^{4+} . $\text{Ba}_4\text{CeIr}_3\text{O}_{12}$ magnetically orders at 10.5 K, while $\text{Ba}_4\text{CeRu}_3\text{O}_{12}$ is paramagnetic down to 1.8 K^{131,138,139}. The ordering temperature and effective magnetic moments of the two trimer-based series, $\text{Ba}_4\text{RERu}_3\text{O}_{12}$ and $\text{Ba}_4\text{REIr}_3\text{O}_{12}$ (RE^{3+}), are summarized in **Table 2**.

3.3. A structure based on both trimers and dimers

There is one example that we can find of a material that has both trimers and dimers in its hexagonal oxide perovskite structure. This material is 10H- $\text{Ba}_5\text{Fe}_4\text{NiO}_{13.5}$, synthesized by the decomposition of nitrate salts, which crystallizes in the hexagonal space group $P6_3/mmc$ with lattice parameters $a = 5.771 \text{ \AA}$ and $c = 24.581 \text{ \AA}$. The crystal structure consists of the stacking of clusters of three face-sharing octahedra (trimers) corner-sharing with clusters of two face-sharing octahedra (dimers). Structural refinement shows that the Ni ions (in gray in **Figure 13**) preferentially occupy the central octahedron of the trimer and Fe ions (in brown in **Figure 13**) occupy the other sites. Fitting of the temperature-dependent magnetic susceptibility results in a Curie-Weiss temperature of -255 K and an effective moment of $5.45 \mu\text{B}$ per formula unit. It is not known how the magnetic moments are distributed. The ordering of the Ni and Fe in different octahedral sites implies that new phases with this kind of unusual stacking might be stabilized for other transition metal combinations as well¹⁴⁰. We note that if the oxygen content of this material is really 13.5 per formula unit then it is quite oxygen deficient. The missing oxygen, which is on the order of 10% of the total, is either missing randomly in the structure, or the coordination in one or more of the layers of ions is not actually octahedral, which is definitely a possibility for Fe^{3+} . More on this concept can be found in subsequent sections of this summary.

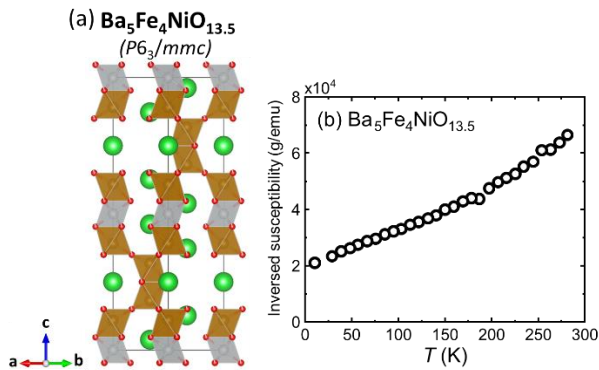


Figure 13. (a) The crystal structure of 10H- $\text{Ba}_5\text{Fe}_4\text{NiO}_{13.5}$, (b) Inverse magnetic susceptibility of $\text{Ba}_5\text{Fe}_4\text{NiO}_{13.5}$ under the applied magnetic field of 1 kOe¹⁴⁰.

3.4. 12R structures based on trimers

An example of this kind of structure is $\text{Ba}_4\text{Fe}_3\text{NiO}_{12}$. In this material the transition metals are ordered and there does not appear to be an issue with the oxygen content. While the two end members BaNiO_3 and BaFeO_3 crystallize in the 2H and 6H hexagonal perovskite structures, a composition in between, $\text{Ba}_4\text{Fe}_3\text{NiO}_{12}$, adopts the 12R hexagonal structure, space group $R-3m$ with lattice parameters $a = 5.66564(7) \text{ \AA}$ and $c = 27.8416(3) \text{ \AA}$ ¹⁴¹. Similar to other trimers discussed above, the crystal structure of $\text{Ba}_4\text{Fe}_3\text{NiO}_{12}$ consists of three face-sharing octahedra (the trimers) separated by a layer of single FeO_6 octahedra, as shown in **Figure 14a**. A combination of synchrotron and neutron diffraction data refinements shows that the Fe^{3+} ions (in brown) occupy the layer of corner-sharing octahedra while Fe^{4+} (again in brown) and Ni^{4+} (in gray) occupy the face-sharing octahedra. The Ni occupy the octahedron in the middle

of the trimer. A small amount of oxygen vacancies ($\sim 5\%$) were found at the intersections of the corner-sharing octahedra only. The magnetic susceptibility is claimed to show a weak ferro/ferrimagnetic transition that couples Fe^{3+} and Fe^{4+} at around 200 K , confirmed by magnetic hysteresis loops, as shown in **Figures 14b-c**.

Similar to $\text{Ba}_4\text{Fe}_3\text{NiO}_{12}$, $\text{Ba}_4\text{Ni}_2\text{Ir}_2\text{O}_{12}$ also crystallizes in a hexagonal 12R perovskite structure, space group $R-3m$, with the lattice parameters $a = 5.7309(2) \text{ \AA}$ and $c = 28.6318(12) \text{ \AA}$, as shown in **Figure 15a**. The crystal structure consists of face-sharing $\text{Ir}_2\text{NiO}_{12}$ trimers and layers of single NiO_6 octahedra. This material is claimed to have the unusual mix of Ni^{2+} and Ni^{4+} in its structure, according to XANES measurements¹⁴² (**Figure 15b**). Fitting of the magnetic susceptibility data yields a Curie-Weiss temperature of -33 K and the effective moment of $4.40 \mu\text{B}/\text{f.u.}$, with data as shown in **Figure 15c**. This observed magnetic moment is consistent with the oxidation states of Ni seen in the XANES measurements, namely that the Ni^{2+} ions occupy the sites within the layer of single NiO_6 octahedra while the $\text{Ir}_2\text{NiO}_{12}$ trimers consist of an alternating face-sharing $\text{Ir}^{5+}\text{O}_6\text{-Ni}^{4+}\text{O}_6\text{-Ir}^{5+}\text{O}_6$ arrangement. Thus, the magnetism has been attributed to the contributions of both the $\text{Ir}_2\text{NiO}_{12}$ trimer and the two unpaired electrons from the Ni^{2+} ions.

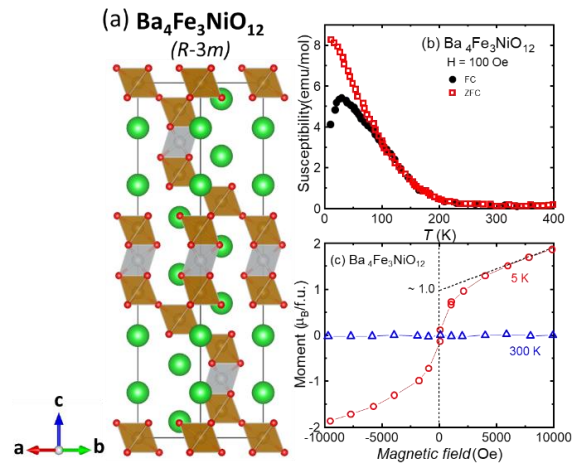


Figure 14. (a) The crystal structure of 12R- $\text{Ba}_4\text{Fe}_3\text{NiO}_{12}$, (b) Temperature-dependent FC/ZFC magnetic susceptibility of $\text{Ba}_4\text{Fe}_3\text{NiO}_{12}$ under the applied magnetic field of 100 Oe, and (c) The field-dependent magnetic hysteresis loops of $\text{Ba}_4\text{Fe}_3\text{NiO}_{12}$ at 300 K and 5 K¹⁴¹.

A polycrystalline sample of $\text{Ba}_4\text{NbIr}_3\text{O}_{12}$ has been synthesized by the solid state method. The material also has a 12R-type structure. It crystallizes in the rhombohedral space group $R-3m$, with lattice parameters $a = 5.7827(2) \text{ \AA}$ and $c = 28.7725(9) \text{ \AA}$. The structure of $\text{Ba}_4\text{NbIr}_3\text{O}_{12}$ is based on a triangular planar geometry of Ir_3O_{12} trimers. The material displays a very low effective moment of $0.80 \mu\text{B}/\text{f.u.}$, reported to be due to the strong spin-orbit coupling effect of the $5d$ Ir-ions. The Curie-Weiss temperature is -13 K , taken to indicate antiferromagnetic interactions between Ir ions. However, there is no magnetic ordering down to 0.35 K , confirmed by heat capacity measurements. The heat capacity of $\text{Ba}_4\text{NbIr}_3\text{O}_{12}$ shows a linear upturn in Cp/T below 2 K under applied magnetic fields of 0 and 1 T. The upturn is suppressed under 2 and 3 T, as previously observed in the reported spin liquid material

$\text{H}_3\text{LiIr}_2\text{O}_6$ ¹⁴³. The heat capacity data for $\text{Ba}_4\text{NbIr}_3\text{O}_{12}$ below 2 K fits the power law $C_p(T) = kT^\alpha$, where $k = 0.1$ and $\alpha \approx 3/4$. The power being smaller than 1 is taken to suggest a possible spin liquid state in this material¹⁴³. The crystal growth of this material with slight off-stoichiometry and disorder has been reported^{144,145}. As shown in **Figure 16**, $\text{Ba}_4\text{Nb}_{0.8}\text{Ir}_{3.2}\text{O}_{12}$ experiences site disorder between Nb and Ir in the isolated octahedra only. A recently reported crystal growth method produces large 3mm size crystals. Magnetic measurements on these single crystals has been found to be consistent with a possible spin liquid state, and is also consistent with the report on the stoichiometric polycrystalline samples. With the availability of large crystals, the potential quantum spin liquid state in this material can be studied by thermal conductivity, μSR , inelastic neutron scattering and heat capacity down to 50 mK.

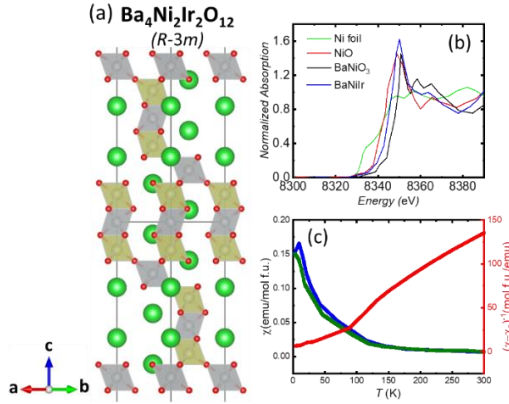


Figure 15. (a) The crystal structure of 12R- $\text{Ba}_4\text{Ni}_2\text{Ir}_2\text{O}_{12}$, (b) XANES characterization of $\text{Ba}_4\text{Ni}_2\text{Ir}_2\text{O}_{12}$ and other standards, Ni, NiO, BaNiO_3 employed to confirm the coexistence of Ni^{2+} and Ni^{4+} in this material. (c) Temperature-dependent FC/ZFC magnetic susceptibility of $\text{Ba}_4\text{Fe}_3\text{NiO}_{12}$ under the applied magnetic field of 1 T¹⁴².

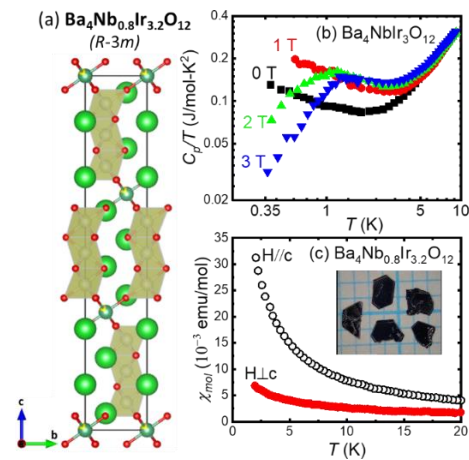


Figure 16. (a) The rhombohedral crystal structure of $\text{Ba}_4\text{Nb}_{0.8}\text{Ir}_{3.2}\text{O}_{12}$ ¹⁴⁴. Ba are light green and oxygens are red. The brown trimers contain only Ir and the isolated octahedra contain disordered mixtures of Nb and Ir. (b) Heat capacity data in $\text{Ba}_6\text{Y}_2\text{Rh}_2\text{Ti}_2\text{O}_{17}$ under different magnetic fields. (c) Temperature-dependent magnetic susceptibility of $\text{Ba}_4\text{Nb}_{0.8}\text{Mn}_{3.2}\text{O}_{12}$ crystals. The inset shows the large size crystals up to 3mm.

3.5. $A_{4-n}A'_n\text{MM}'_2\text{O}_{12}$: Missing an octahedron in a trimer

This is a derivative of the $\text{Ba}_4\text{MRu}_3\text{O}_{12}$ family. The crystal structure is very similar to the 12L- $\text{Ba}_4\text{NbRu}_3\text{O}_{12}$ hexagonal perovskite, except that there is a missing $\text{M}'\text{O}_6$ octahedron in the middle of the trimers. The crystal structure of $\text{Sr}_4\text{CoRe}_2\text{O}_{12}$, an example of a material in this $A_{4-n}A'_n\text{MM}'_2\text{O}_{12}$ family,^{146,147} is shown in **Figure 17a**. (n can range from 0 to 2, with the different A site ions chosen to accommodate the charge on the M, M' sublattice.) The inverse DC magnetic susceptibility and the AC susceptibility for $\text{Sr}_4\text{CoRe}_2\text{O}_{12}$ are displayed in **Figures 17b-c**. The magnetic ordering temperature, Curie-Weiss temperature and effective moment of a few compounds in this series are known; they are summarized in **Table 3**. Two general observations can be made about such phases: (1) the missing octahedron results in a material that has only corner shared octahedra and thus can also be considered as a layered oxide perovskite based on (111) cubic rather than (100) cubic layers, and (2) if the magnetism is really acting as described in the publication, then the Co^{2+} present is undergoing a spin state transition on cooling and in addition the magnetic ordering is not frustrated (T_M and Θ_{CW} are nearly equal).

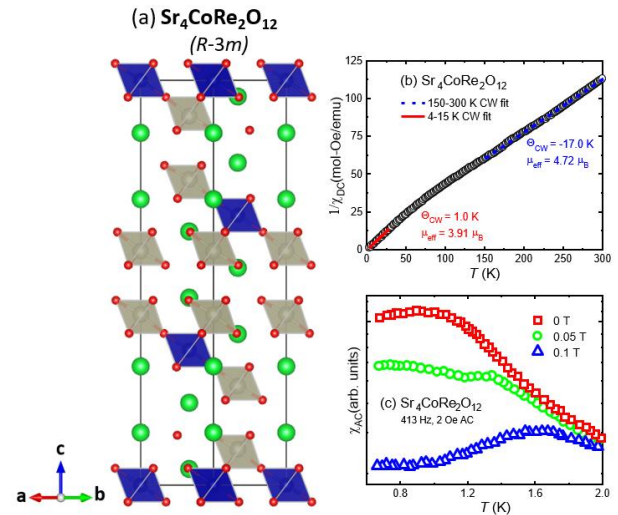


Figure 17. (a) The crystal structure of $\text{Sr}_4\text{CoRe}_2\text{O}_{12}$, (b) Inverse DC magnetic susceptibility of $\text{Sr}_4\text{CoRe}_2\text{O}_{12}$ under the applied field of 5 kOe, and (c) AC susceptibility of $\text{Sr}_4\text{CoRe}_2\text{O}_{12}$ under the 2 Oe-excitation field¹⁴⁶

Table 3. The magnetic ordering temperatures, Curie-Weiss temperature and effective magnetic moment per formula unit for some examples of materials in the $A_{4-n}A'_n\text{MM}'_2\text{O}_{12}$ series.

Compounds	T_M (K)	Θ_{CW} (K)	μ_{eff} (μ_B)
$\text{Sr}_4\text{CoRe}_2\text{O}_{12}$	1.0	1.0	3.91
$\text{Sr}_2\text{La}_2\text{CoW}_2\text{O}_{12}$	1.26	1.5	3.95
$\text{Ba}_2\text{La}_2\text{CoW}_2\text{O}_{12}$	1.28	1.6	4.01
$\text{Ba}_3\text{LaCoReWO}_{12}$	0.83	0.78	3.89
$\text{Ba}_4\text{CoRe}_2\text{O}_{12}$	0.87	0.61	3.87
$\text{Ba}_2\text{La}_2\text{NiW}_2\text{O}_{12}$	6.2	25.5	3.19
$\text{Ba}_2\text{La}_2\text{MnW}_2\text{O}_{12}$	1.7	-10.7	5.73

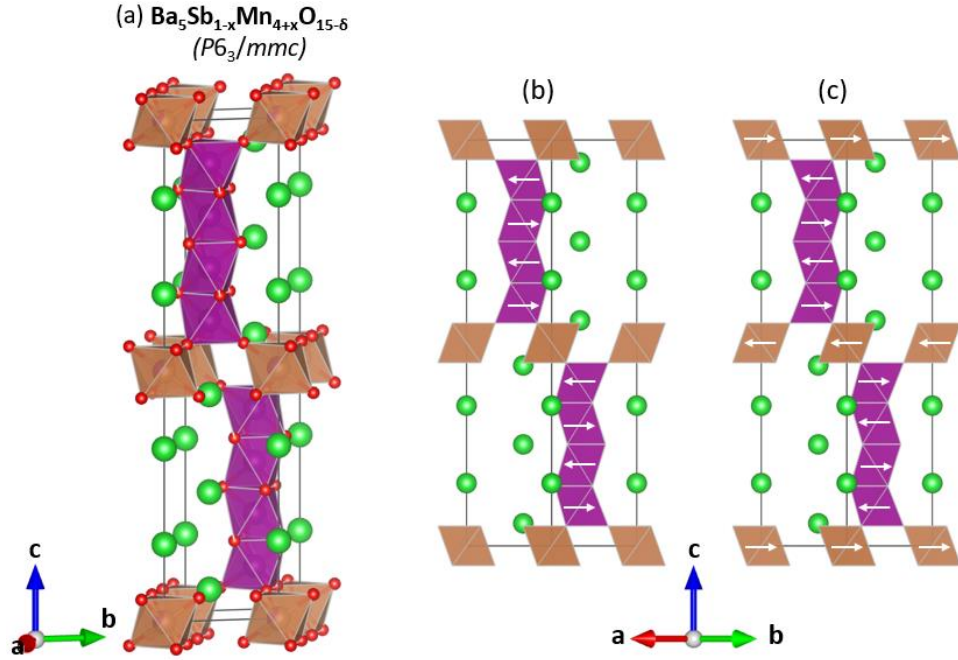


Figure 18. (a) The crystal structure of 10H- $\text{Ba}_5\text{Sb}_{1-x}\text{Mn}_{4+x}\text{O}_{15-\delta}$, (b) and (c) Two proposed magnetic structures for $\text{Ba}_5\text{Sb}_{1-x}\text{Mn}_{4+x}\text{O}_{15-\delta}$ ¹⁴⁸.

3.6. Tetramers

Very few tetramer-based materials are known; we describe one here and another in a later section where we consider the presence of tetrahedral in the crystal structures. The return of Sb^{5+} to our systems allows for the formation of $\text{Ba}_5\text{Sb}_{1-x}\text{Mn}_{4+x}\text{O}_{15-\delta}$, which is a 10 layer, 10H-hexagonal perovskite based on tetramers. It crystallizes in the space group $P6_3/mmc$ with lattice parameters $a = 5.7095(1) \text{ \AA}$, and $c = 23.4866(3) \text{ \AA}$. It has different stacking from $\text{Ba}_5\text{Fe}_4\text{NiO}_{13.5}$. The crystal structure of $\text{Ba}_5\text{Sb}_{1-x}\text{Mn}_{4+x}\text{O}_{15-\delta}$ consists of four face-sharing MnO_6 octahedra (tetramers) and a layer of corner-sharing disordered $(\text{Sb}/\text{Mn})\text{O}_6$ octahedra, as shown in **Figure 18**. The magnetic properties of $\text{Ba}_5\text{Sb}_{1-x}\text{Mn}_{4+x}\text{O}_{15-\delta}$ ($0.24 \leq x \leq 0.36$) solid solutions show two distinct magnetic transitions. For example, when $x = 0.24$, the upper transition at 129 K corresponds to the formation of ferro/ferrimagnetic interactions within the tetramers, and the lower transition at 13 K is the freezing temperature of a glassy state, this latter transition evidenced by the bifurcation of FC/ZFC magnetic susceptibility at low applied magnetic field. This material has an antiferromagnetic Curie-Weiss temperature of -133 K and an effective moment of $3.55 \mu\text{B}/\text{f.u.}$ ¹⁴⁸.

4. Materials with MO_4 tetrahedra in the framework

The crystal structure of $\text{Ba}_5\text{AlIr}_2\text{O}_{11}$ was first reported in 1989, but its quantum magnetism has only recently been investigated. $\text{Ba}_5\text{AlIr}_2\text{O}_{11}$ crystallizes in the orthorhombic space group $Pnma$, with the lattice parameters $a = 18.8360 \text{ \AA}$, $b = 5.7887 \text{ \AA}$ and $c = 11.1030 \text{ \AA}$, it is a distorted version of a hexagonal perovskite. The crystal structure consists of two face-sharing IrO_6 octahedra (Ir_2O_9 dimers), corner-sharing with AlO_4 tetrahedra. However, within the Ir_2O_9 dimers, there are two inequivalent Ir sites, as shown in **Figure 19a**, one that could

contain Ir^{4+} ($5d^5$) and the other one containing Ir^{5+} ($5d^4$). In contrast to this local charge picture, the formation of Ir_2O_9 dimer orbitals in this material has been detected by Resonant Inelastic x-ray scattering (RIXS). Sharp excitations of electrons within the dimer orbitals were observed by this method, and analyzed by using Density Functional Theory (DFT) and theoretical simulations. The spin-orbit coupling present for the Ir-5d transition metal is said to play an important role in the competing interaction between intra-atomic exchange and covalent bonding in this material. The researchers involved argue that Ir-Ir metal-metal bonds are present, causing a substantial reduction of the magnetic moment. This material undergoes a structural phase transition at 210 K, which is supported by temperature-dependent electrical resistivity measurements (**Figure 19b**). The material is *very* highly resistive, so it is basically an insulator. A clear magnetic transition is at 4.5 K, observed in the magnetic susceptibility, where a clear field dependence to the susceptibility even above the ordering temperature is seen. (**Figure 19c**)¹⁴⁹⁻¹⁵³.

The 10L- $\text{Ba}_5\text{In}_2\text{Al}_2\text{ZrO}_{13}$ hexagonal perovskite is another example of a material with MO_4 tetrahedra in the structural framework. The crystal structure is shown in **Figure 20**. It adopts the space group $P6_3/mmc$ with lattice parameters $a = 5.8707(7) \text{ \AA}$ and $c = 24.445(3) \text{ \AA}$. In this case the hexagonal symmetry is maintained. A special feature in the crystal structure of this material is where AlO_4 tetrahedra share corners with InO_6 octahedra, separated by a triangular layer of ZrO_6 octahedra. This remarkable crystal structure is the result of the intergrowth along the c -axis of $\text{Ba}_2\text{InAlO}_5$ and BaZrO_3 blocks.^{154,155} For this material, ALL ions are in their usually highest formal oxidation states and no unpaired d electrons are present, it is thus non-magnetic and therefore no quantum properties are expected.

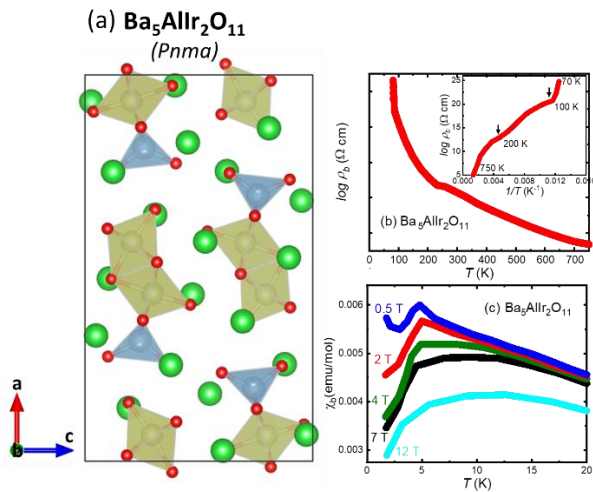


Figure 19. (a) The crystal structure of $\text{Ba}_5\text{AlIr}_2\text{O}_{11}$, with the Ir_2O_9 dimers and AlO_4 tetrahedra (blue polyhedra); (b) Resistivity measurement to show a subtle structural transition at 210 K, and (c) Temperature dependent magnetic susceptibility showing the magnetic transition at 4.5 K. The symmetry of the crystal structure is low compared to standard hexagonal perovskites¹⁴⁹.

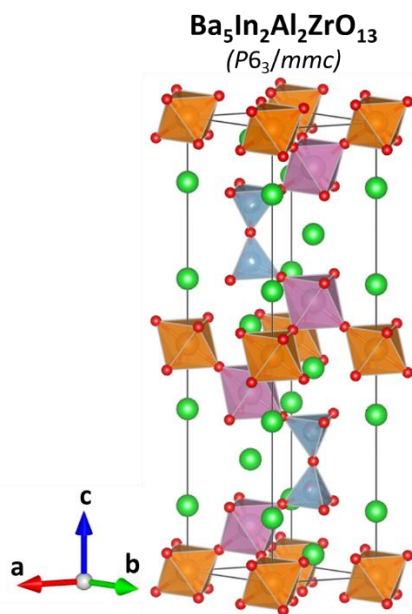


Figure 20. The crystal structure of $\text{Ba}_5\text{In}_2\text{Al}_2\text{ZrO}_{13}$. Ba ions are green, oxygens are red, Al^{3+}O_4 tetrahedra are shown in blue, In^{3+} octahedra as purple and Zr^{4+} octahedra as orange.

In another structure type consisting of octahedra plus tetrahedra of M ions, 12H- $\text{Ba}_6\text{Na}_2\text{Ru}_2\text{V}_2\text{O}_{17}$ crystallizes in a hexagonal structure, space group $P6_3/mmc$, with the lattice parameters $a = 5.8506(1)$ Å and $c = 29.6241(4)$ Å. This crystal structure contains a Ru_2O_9 dimer, which is corner-sharing with layers of NaO_6 octahedra, separated by double sheets of VO_4 tetrahedra (Figure 21). This nominally complex $\text{Ba}_6\text{Na}_2\text{M}_2\text{X}_2\text{O}_{17}$ structure type can be stabilized for many possible cation combinations, for example for $M = \text{Ru}, \text{Nb}, \text{Ta}$ and Sb and $X = \text{V}, \text{Cr}, \text{Mn}, \text{P}$, and

V ¹⁵⁶. The magnetic properties of many of these materials remain unreported.

Recently, two additional compounds with this crystal structure have reported, with formulas $\text{Ba}_6\text{R}_2\text{Ti}_4\text{O}_{17}$ ($R = \text{Nd}$ and Y)¹⁵⁷. In these materials, the triangular layers of NaO_6 octahedra are replaced by octahedra of rare earth ions (Nd or Y). Furthermore, the Ti cations occupy both the TiO_4 tetrahedra and the face-sharing Ti_2O_9 dimers. This is one of the very rare oxides where Ti cations adopt both tetrahedral and octahedral sites in the same structure.

In this complex yet somehow flexible structure, we successfully synthesized the new compound $\text{Ba}_6\text{Y}_2\text{Rh}_2\text{Ti}_2\text{O}_{17}$. In this material, the only magnetic ion is Rh^{4+} ($4d^5$) in the Rh_2O_9 dimers, which helps simplify a potentially complex magnetic picture (Figure 22a). Preliminary magnetic analysis shows that the material displays a small effective magnetic moment, which must arise from the Rh ions present, and a negative Curie-Weiss temperature. The transport band gap and optical band gaps are very similar, at 0.16(1) eV, and thus $\text{Ba}_6\text{Y}_2\text{Rh}_2\text{Ti}_2\text{O}_{17}$ is a small band gap semiconductor. As shown in Figure 22, a large upturn in the heat capacity at temperatures below 1 K, suppressed by magnetic fields larger than 2 Tesla, is observed. A very large Sommerfeld-like T-linear term in the specific heat ($\gamma = 166$ mJ/mol f.u.-K²), as is often observed for Heavy Fermion metals, is seen although the material is highly insulating at low temperatures¹⁵⁸. These results suggest the possibility that a spin liquid state exists at low temperatures in $\text{Ba}_6\text{Y}_2\text{Rh}_2\text{Ti}_2\text{O}_{17}$.

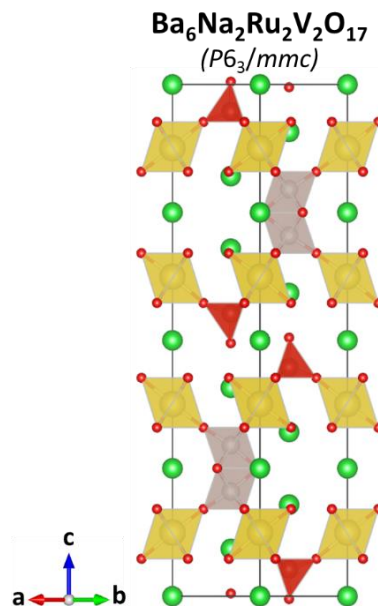


Figure 21. The crystal structure of $\text{Ba}_6\text{Na}_2\text{Ru}_2\text{V}_2\text{O}_{17}$. Ba = green spheres, oxygen = red spheres, AlO_4 tetrahedra depicted in red, Ru_2O_9 dimers in brown and individual layers of NaO_6 octahedra in yellow.

For another example of a material with mixed tetrahedra and octahedra, 21R- $\text{Ba}_7\text{Mn}_5\text{Cr}_2\text{O}_{20}$ crystallizes in a rhombohedral structure, space group $R\bar{3}m$, with the lattice parameters $a = 5.7401(1)$ Å and $c = 50.597(1)$ Å. The c axis is large for this

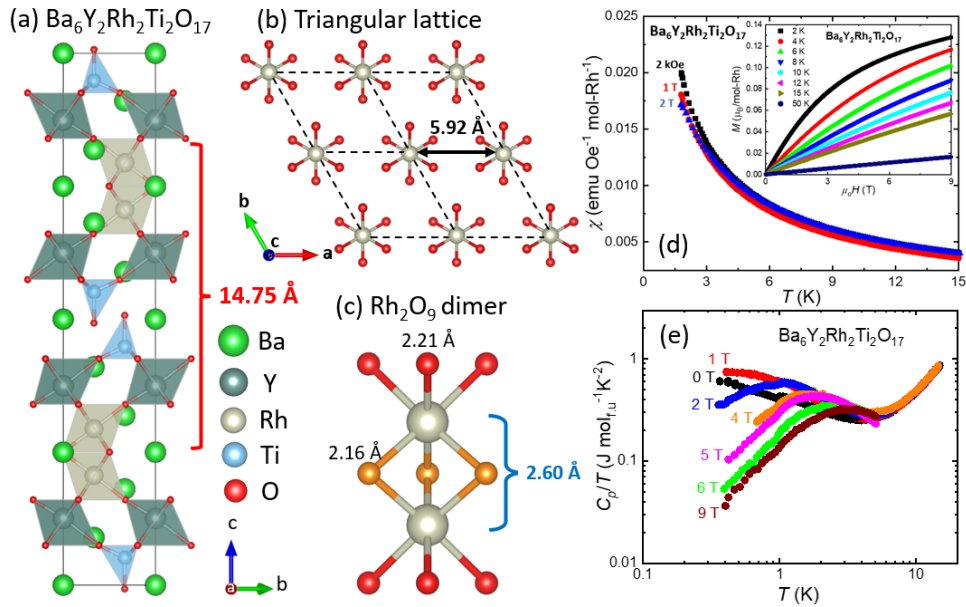


Figure 22. (a) The crystal structure of $\text{Ba}_6\text{Y}_2\text{Rh}_2\text{Ti}_2\text{O}_{17}$, (b) Triangular layer of $\text{Rh}^{4+}(d^5)$ along the c -axis, (c) The Rh-O, and Rh-Rh distances within the Rh_2O_9 dimer, (d) Temperature dependent magnetic susceptibility of $\text{Ba}_6\text{Y}_2\text{Rh}_2\text{Ti}_2\text{O}_{17}$ under different applied magnetic fields, and (e) Heat capacity data in $\text{Ba}_6\text{Y}_2\text{Rh}_2\text{Ti}_2\text{O}_{17}$ under different magnetic fields¹⁵⁸.

structure, which consists of three shifted structural blocks. In **Figure 23a**, the crystal structure is shown. It consists of an ordered array of CrO_4 tetrahedra (when Cr is formally highly charged, then its radius is small), MnO_6 octahedra and face-sharing Mn_3O_{12} trimers. Below 50 K, the material undergoes 2D magnetic ordering, attributed to ferromagnetic super-exchange between the “isolated” MnO_6 octahedra and the Mn_3O_{12} trimers^{159–161}. Under moderate applied magnetic fields, the material converts to 3D magnetic ordering. Magnetic susceptibility measurements reveal a Curie-Weiss temperature of 38 K and an effective moment of $9.69 \mu\text{B}/\text{f.u.}$, as shown in **Figure 23b**. The presence of ferromagnetism at 5 K is confirmed by the presence of a magnetic hysteresis loop, seen in **Figure 23c**. However, the magnetic behavior in this material is quite complex since it contains different magnetic ions with different oxidation states, such as Cr^{5+} , Mn^{2+} and Mn^{4+} .

Finally, we end this section of this summary by describing one more multi-layered structure in the hexagonal perovskite family is $16\text{L-Ba}_4\text{Ca}_{1-x}\text{Mn}_{3+x}\text{O}_{12-8}$ (**Figure 24a**). This material crystallizes in the hexagonal space group $P-6m2$ with the lattice parameters $a = 5.8003(3) \text{ \AA}$ and $c = 38.958(1) \text{ \AA}$, with the large c axis arising because there are 8 layers in each of two building blocks. It is one of the very first hexagonal perovskites known that contains Mn in tetrahedral sites, with Mn charge disproportionation. The crystal structure consists of Mn-tetramers (a cluster of four face-sharing MnO_6 octahedra), corner-sharing with MnO_6 octahedra and MnO_4 tetrahedra. Infrared spectroscopy study of $\text{Ba}_4\text{Ca}_{1-x}\text{Mn}_{3+x}\text{O}_{12-8}$, comparing the results with KMnO_4 and BaMnO_4 standards, has been said to confirm the possible coexistence of Mn^{6+} and Mn^{7+} ions in the structure, as shown **Figure 24b**. Temperature-dependent magnetic susceptibility measurements do not show any magnetic ordering down to 10 K, and high temperature inverse magnetic susceptibility fitting results in a Curie-Weiss temperature of -288 K and an effective moment of $6.7 \mu\text{B}/\text{f.u.}$ (**Figure 24c**). The large

negative Curie-Weiss temperature indicates the presence of strong antiferromagnetic interactions; however, the determination of Mn oxidation states and the magnetic configuration requires careful XANES and neutron diffraction study¹⁶².

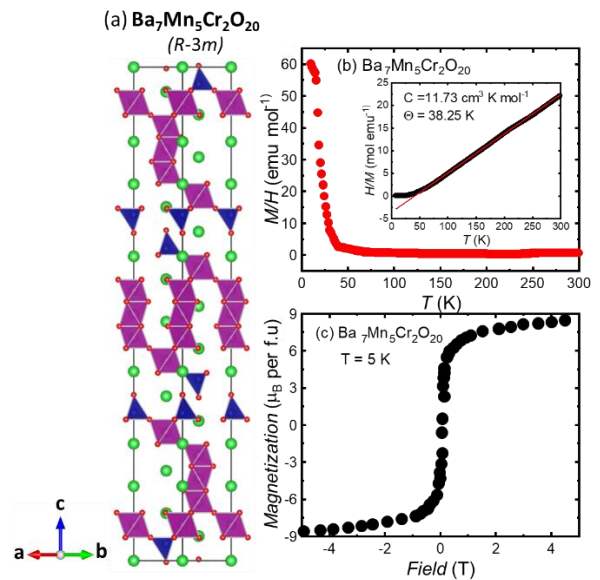


Figure 23. (a) The crystal structure of $21\text{R-Ba}_7\text{Mn}_5\text{Cr}_2\text{O}_{20}$, (b) Temperature dependent FC/ZFC magnetic susceptibility of $\text{Ba}_7\text{Mn}_5\text{Cr}_2\text{O}_{20}$ and (c) Magnetic hysteresis loop at 5 K in $\text{Ba}_7\text{Mn}_5\text{Cr}_2\text{O}_{20}$ ¹⁵⁹.

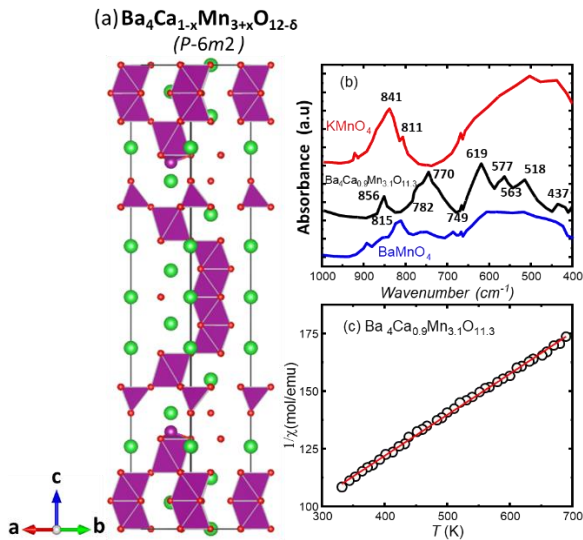


Figure 24. (a) The crystal structure of $16L\text{-Ba}_4\text{Ca}_{1-x}\text{Mn}_{3+x}\text{O}_{12-\delta}$, (b) FTIR spectrum of $\text{Ba}_4\text{Ca}_{1-x}\text{Mn}_{3+x}\text{O}_{12-\delta}$ and the standards, KMnO_4 and BaMnO_4 . (c) The inverse magnetic susceptibility of $\text{Ba}_4\text{Ca}_{1-x}\text{Mn}_{3+x}\text{O}_{12-\delta}$ under the applied magnetic field of 3 kOe ¹⁶².

5. Oxygen deficiency: vacancies both random and ordered

Nominally simple hexagonal oxide perovskites that actually have oxygen deficiency can form complex structures when the vacancies are ordered, especially for multi-valent transition $3d$ metal cations such as Mn, Fe and Co. Even randomly distributed vacancies can lead to a wide variety of structures, presumably to accommodate the different oxidation states if the M site

metals. BaMnO_{3-x} , for example, can adopt different types of structures depending on the fraction of oxygen vacancies present. The published structures have randomly distributed oxygen vacancies, although structural probes that are sensitive to the local structures of the ions may eventually reveal that the structures are more complex. A similar phenomenon is also observed in BaFeO_{3-x} and BaCoO_{3-x} systems. In some cases, for example for the Cobalt compound $\text{BaCoO}_{2.6}$, the oxygens appear to be largely missing in an ordered fashion, resulting in the presence of CoO_4 tetrahedra. This is also seen for some materials in the BaFeO_{3-x} system.

Different polytypes can be stabilized by the ionic size of the central atom and its valence state. Without the oxygen vacancy, BaCoO_3 , with a typical hexagonal perovskite formula, displays infinite linear chains of face-sharing CoO_6 in the ideal hexagonal space group $P6_3/mmc$, with the lattice parameters $a = 5.645(3) \text{ \AA}$ and $c = 4.752(3) \text{ \AA}$ ¹⁶³. When the oxygen content is less than 3 in a formula unit, a variety of octahedral stackings occur, and the crystal structures adopt different space groups as shown in **Figure 25** ¹⁶⁴⁻¹⁶⁹. In the $12H\text{-BaCoO}_{2.6}$ structure, the tetramers consisting of four face-sharing CoO_6 octahedra are bridged by two layers of CoO_4 tetrahedra. The presence of tetrahedral Co in the structure may come from the small ionic size of Co ions in the tetrahedra compared to those in the octahedra. Curiously, it is reported that structures based on hexagonal perovskites convert to an ideal cubic perovskite for the very oxygen deficient material $\text{BaCoO}_{2.23}$. The most reduced form of this structure type results in another hexagonal compound, BaCoO_2 , a material where all the Co is in the formal $2+$ state. However, the crystal structure of BaCoO_2 consists of corner-sharing CoO_4 tetrahedra instead of the CoO_6 octahedra commonly found in the perovskite structures. Cobalt-oxide based perovskites have been intensively studied for many decades, by many different methods, and the issue of whether and how high-spin, intermediate-spin and low-spin in Co^{3+} ions

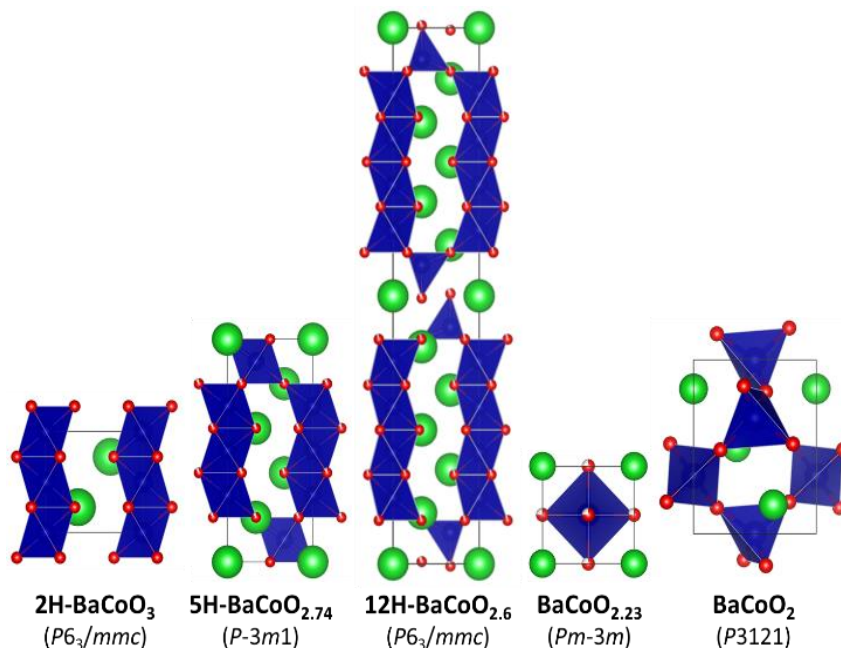


Figure 25. Different types of BaCoO_{3-x} polymorphs, containing CoO_6 octahedra and CoO_4 tetrahedra. The materials with oxygen contents between those of BaCoO_3 and BaCoO_2 as a rule display randomly distributed oxygen vacancies, even in the case where the oxygen efficiency compared to the ideal BaCoO_3 formula is largely accommodated by CoO_4 octahedra.

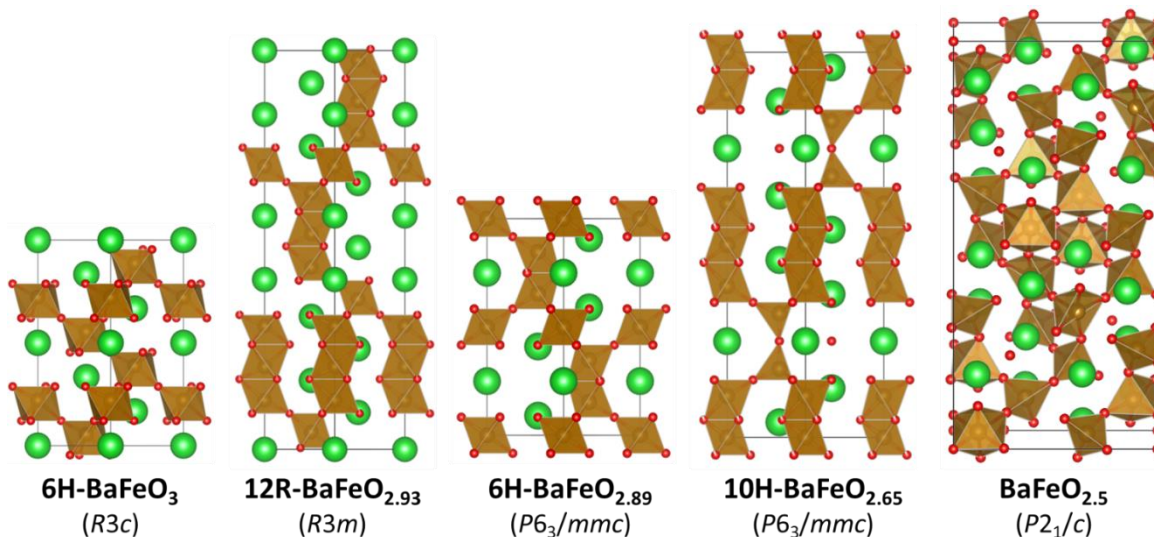


Figure 26. Different types of BaFeO_{3-x} structures.

exist in the “simple” LaCoO₃ perovskite as a function of temperature is still controversial¹⁷⁰⁻¹⁷⁴. Similarly the spin state of Co²⁺ in oxides can also be enigmatic.

Similarly, BaFeO_{3-x} also adopts different structures at different oxygen contents. This family of materials displayed in **Figure 26**. Although similar globally to the Co based materials, some interesting differences are reported. In 10H-BaFeO_{2.65}, the appearance of FeO₄ tetrahedra is similar to the case of 12H-BaCoO_{2.6}. Moreover, a further reduced form of BaFeO_{3-x} leads to the transformation to the monoclinic structure BaFeO_{2.5}, space group *P2₁/c*. In BaFeO_{2.5}, the coordination of Fe ions ranges from 4 to 6, and the crystal structure is very highly distorted. A unique feature of this structure is that within an individual layer, both octahedra and tetrahedra are found.

For the BaMnO_{3-x} system, there is a systematic trend in the number of face-sharing MnO₆ octahedra in the chains. The system goes from an infinite chain of MnO₆ octahedra in 2H-BaMnO₃ to a dimer consisting of two face-sharing MnO₆ octahedra in 4H-BaMnO_{2.59} as seen in **Figure 27**¹⁷⁵⁻¹⁷⁸. The crystal structure and the oxygen vacancies in BaMnO_{3-x} are closely related to interesting properties in manganates, such as metal-insulator transitions and colossal magnetoresistance¹⁷⁹⁻¹⁸². Although there are a larger number of structures observed in this manganite system over a smaller range of oxygen deficiency than is seen in the Co and Fe - based oxygen deficient double perovskite, in a sense their structures appear to be simpler, and thus potentially easier to understand. To the senior author of this manuscript the oxygen deficient hexagonal perovskites for the transition metals Co, Fe and Mn literally scream

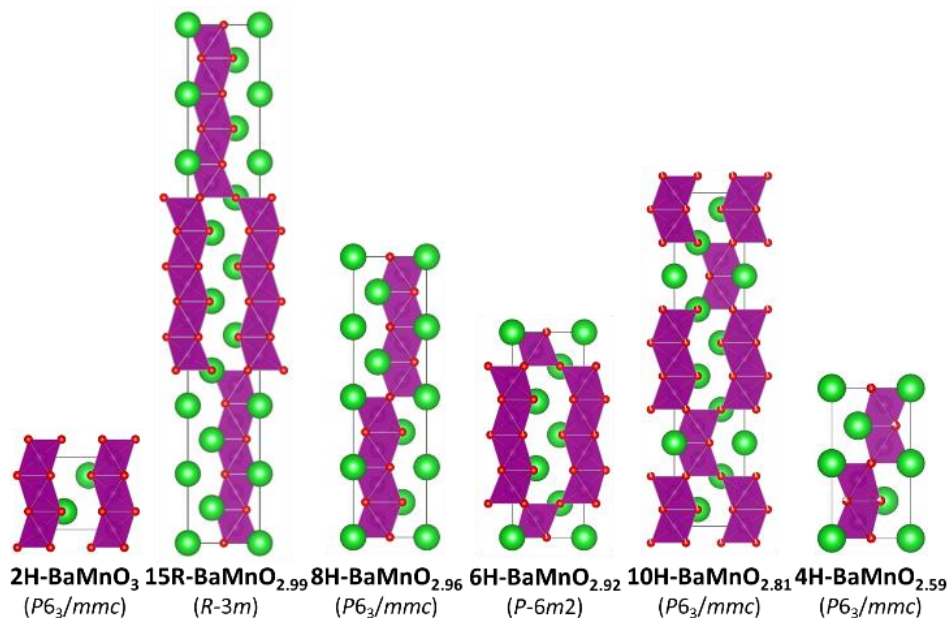


Figure 27. Different types of BaMnO_{3-x} structures.

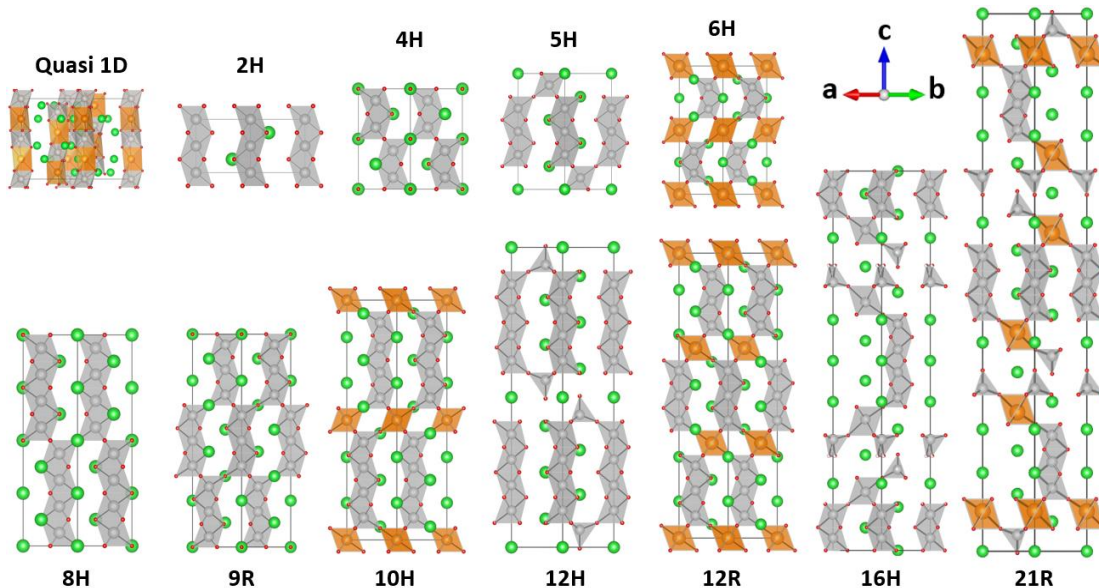


Figure 28. Schematic representation of some of the crystal structures of materials with complex stacking in hexagonal perovskites.

for analysis through local structural methods. It does not seem to be something for impatient people to tackle.

6. Polymorphism

We briefly specifically point out that hexagonal perovskites, even at a fixed AMO_3 formula, are not free from the kind of polymorphism that is seen in many other kinds of materials systems. Although this has been described previously in the case of BaRuO_3 , it is seen in other hexagonal perovskites as well. A nice example is shown in **Figure 28**, which shows two different polymorphs of BaFeO_3 . The first of these is a 3R 111-type rhombohedral distortion of a classical cubic perovskite, while the second is a 6H hexagonal perovskite with Fe_2O_9 dimers and layers of isolated FeO_6 octahedra. In the other way of looking at these materials, the first is a $(\text{ccc})_2$ type and the second is a $(\text{cch})_2$ type. Pressure is a typical way of generating different polytypes, and the same is the case for hexagonal perovskites.

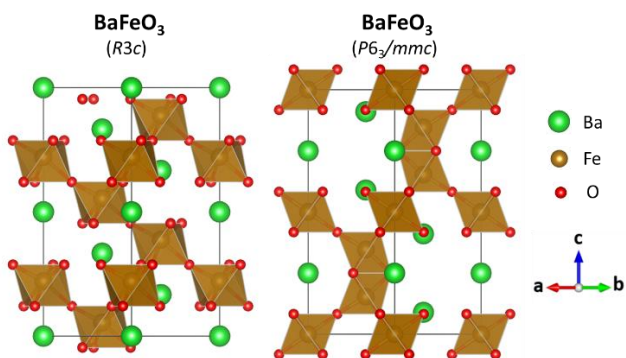


Figure 29. Two different polymorphs of BaFeO_3 .

7. Summary of some of the complex variations in stacking

Figure 29 displays, in the form of a summary image, of some of the complex stacking sequences possible in hexagonal perovskites. In most structures, the sequences of face-sharing octahedra share corners with each other (4H, 8H and 9R) or are bridged by layers of single octahedra (5H, 6H, 10H, 12R and 21R). Moreover, layers of tetrahedra in between the face-sharing octahedral blocks are found in 12H, 16H and 21R structures. Although both form 12-layer structures, the 12H structure includes tetrahedra while the 12R structure only contains octahedra. The 21R structure is an interesting and complicated structure type that has both tetrahedral and octahedral layers in between trimer building blocks. There are many materials with chains of face sharing octahedra or octahedra and triangular prisms. They are described briefly in a later section of this review.

8. Hexagonal Perovskites with Ba-Cl or Ba-Br layers in addition to Ba-O layers

Oxyhalide perovskites have sometimes been found as new phases in the crystal growth of oxide perovskites in a halide flux. In these materials, in addition to the Ba-O layers, Ba-X (X = F, Cl, Br, I) layers can also be stabilized between the face-sharing magnetic building blocks. Oxichlorides are the most frequently reported of this group. As shown in **Figure 30**, the crystal structure of $\text{Ba}_6\text{Ru}_2\text{Pt}_{12}\text{Cl}_2$ contains Ba-Cl layers sandwiched between $(\text{Ru}_2\text{Pt})\text{O}_{12}$ trimers. With both suitable electronegativities and ionic radii, oxichloride and oxybromide perovskites are commonly reported. The space groups and lattice parameters of some selected materials in this family are summarized in

Table 4. Their magnetic properties have not yet been thoroughly studied, although they are likely to be as interesting as

those of the purely oxide hexagonal perovskites. Their potential applications as photocatalysts and cathode materials have, however, recently been investigated¹⁸³⁻¹⁸⁸. When materials physicists figure out that some of them can be grown as nice single crystals, then more detailed studies can be expected.

Table 4. Summary of the space groups and lattice parameters of some of the hexagonal perovskites with Ba-Cl layers in addition to Ba-O layers.

Compounds	Space group	Lattice parameters	Reference
Ba ₂ Co ₄ O ₇ Cl	<i>R-3m</i>	$a = 5.716 \text{ \AA}$ $c = 45.010 \text{ \AA}$	189
Ba ₆ Ru ₂ PtO ₁₂ Cl ₂	<i>P-3m1</i>	$a = 5.805 \text{ \AA}$ $c = 15.006 \text{ \AA}$	190
Ba ₆ Ru ₃ O ₁₂ Cl ₂	<i>P-3m1</i>	$a = 5.815 \text{ \AA}$ $c = 14.915 \text{ \AA}$	191
Ba ₆ Co ₆ O _{15.5} Cl	<i>P-6m2</i>	$a = 5.6738 \text{ \AA}$ $c = 14.5237 \text{ \AA}$	192
Ba ₇ Ru ₄ O ₁₅ Cl ₂ (and Br analog)	<i>R-3m</i>	$a = 5.7785 \text{ \AA}$ $c = 51.6730 \text{ \AA}$	193
Ba ₅ Ru ₂ O ₉ Cl ₂ (and Br analog)	<i>Pnma</i>	$a = 15.310 \text{ \AA}$ $b = 5.945 \text{ \AA}$ $c = 14.197 \text{ \AA}$	194
Ba ₅ Co ₅ O ₁₃ Cl	<i>P6₃/mmc</i>	$a = 5.669 \text{ \AA}$ $c = 24.304 \text{ \AA}$	195
Ba ₅ (MnO ₄) ₃ Cl	<i>P6₃/m</i>	$a = 10.469 \text{ \AA}$ $c = 7.760 \text{ \AA}$	196
KBa ₂ V ₂ O ₇ Cl	<i>P6₃/mmc</i>	$a = 5.7688 \text{ \AA}$ $c = 15.0762 \text{ \AA}$	197
BaZn ₂ (SeO ₃) ₂ Cl ₂	<i>R-3m</i>	$a = 5.5156 \text{ \AA}$ $c = 24.5840 \text{ \AA}$	198
Ba ₈ Co ₂ Mn ₆ O ₂₂ Cl	<i>P-6m2</i>	$a = 5.7207 \text{ \AA}$ $c = 19.4099 \text{ \AA}$	199
Ba ₈ Ru _{3.33} Ta _{1.67} O ₁₈ Cl ₂	<i>R-3m</i>	$a = 5.947 \text{ \AA}$ $c = 59.760 \text{ \AA}$	200
Ba ₁₀ Fe ₈ Pt ₂ Cl ₂ O ₂₅	<i>P6₃/mmc</i>	$a = 5.8034 \text{ \AA}$ $c = 24.9970 \text{ \AA}$	201

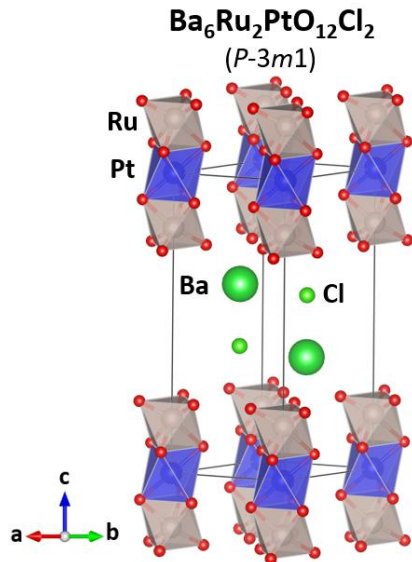


Figure 30. The crystal structure of Ba₆(Ru₂PtO₁₂)Cl₂¹⁹⁰.

9. Chains

One of the very nice structural aspects of hexagonal perovskites is that chain fragments of different lengths can be formed from face centered transition metal octahedra. These chains can be interrupted by face sharing with triangular prisms, which have some leeway along their prismatic lengths to shrink or stretch to accommodate ions of different preferred M-O bond lengths. This leads to some very interesting compounds. In a hexagonal perovskite structure type, materials of the type Sr₄MO₆ (M = Pt, Rh, and Ir), for example, crystallize in a rhombohedral structure, space group *R-3c*, as shown in **Figure 31**. Along the *c*-axis, the magnetic MO₆ octahedra are linked by non-magnetic SrO₆ trigonal prisms to form 1D-chains, where the magnetic octahedra and non-magnetic triangular prisms alternate. In some of these materials, the Sr₄MO₆^{202,203} formula (Sr₄MO₆ = Sr₃(SrM)O₆), because it results in a non- 1:1 A site to Chain site ratio, can lead to incommensurability of the chain periodicity and the A site periodicity.

From the quantum materials perspective, a few materials of this type have been studied. The analysis of magnetic susceptibility in Sr₄RhO₆²⁰⁴ results in an effective moment of 2.03 μB/f.u and a Curie-Weiss temperature of -10 K. The authors of that study argue that Sr₄RhO₆ is the first clear example of a magnetically ordered Rh⁴⁺ compound. The antiferromagnetic ordering temperatures of Sr₄RhO₆ and the related Sr₄IrO₆ chain compounds are 7 K and 12 K, respectively, which has been interpreted as reflecting a greater degree of covalency in the Ir5*d*-O than the Rh 4*d*-O system^{204,205}. Although in this review we have encountered several compounds in which "Rh4+" displays a magnetic moment, that is by far not the usual case in oxides, which, when based on the 4*d* transition metal Rh, are generally non-magnetic.

In this K₄CdCl₆-type structure, a series of 2H-related perovskites (A_{3-x}Na_x)NaBO₆ (A = La, Pr, Nd; B = Rh, Pt) has also been reported, made through synthesis by carbonate and hydroxide flux techniques. These materials are different in that the ions on the A site are mixed to yield charge neutrality. All of the materials crystallize in the rhombohedral space group *R-3c*. The temperature dependent magnetic susceptibility of a selected material in this family, (Nd₂Na)NaPtO₆ shows no magnetic ordering down to 2 K. The observed effective moment is found to be 5.06 μB/f.u, which agrees well with the expected moment of non-interacting Nd³⁺ ions, 5.12 μB/f.u.²⁰⁶. In fact many rare earth oxides do not magnetically order above 2K, and thus with Pt⁴⁺ and Na⁺ being non-magnetic ions, these hexagonal perovskite materials can be considered as rare-earth-based paramagnets. Further study may or may not reveal magnetic ordering of the rare earth moments in these materials at lower temperatures.

In the same A_{3n+3m}A'_nB_{3m+n}O_{9m+6n} family, the compound Sr₆Rh₅O₁₅²⁰⁷ with m = 1 and n = 1, grown by a molten K₂CO₃ flux technique, has been reported. It crystallizes in the hexagonal space group *R32*, with the lattice parameters a = 9.6517(5) Å and c = 13.0480(5) Å. The crystal structure consists of 1D-chains parallel to the *c*-axis of four face-sharing RhO₆ octahedra a single RhO₆ trigonal prism. This material differs from the ones we have described so far because the atom in the triangular prism is the same as the atom in the octahedra. Magnetic susceptibility measurements shows an antiferromagnetic

transition at 11 K, and thus that this material is another example of a magnetic Rh-based hexagonal oxide perovskite. The material is reported to have a large magnetic anisotropy, with the magnetic susceptibility when the applied field is parallel to the crystal's c -axis being many orders of magnitude larger than the case when the applied field is perpendicular to the crystal's c -axis.

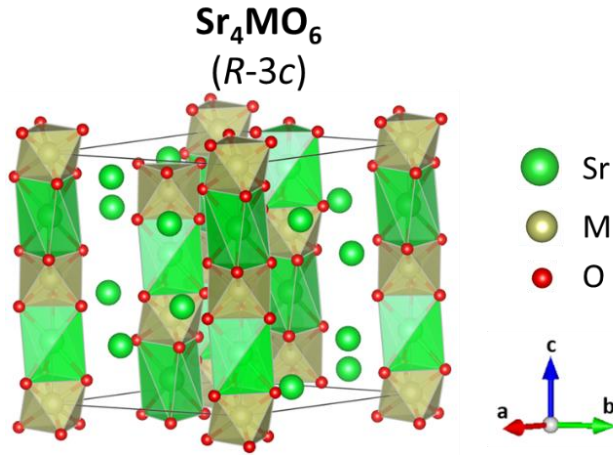


Figure 31. The crystal structure of Sr₄MO₆ (M = Pt, Rh, Ir).

Another example of a chain-structure variation is found for Sr₄CuIr₂O₉, whose crystal structure consists of Ir₂O₉ dimers face-sharing with CuO₆ trigonal prisms, to form 1 D chains along the c -axis (**Figure 32**). An alternative view is that the continuous chains are made of IrO₆ octahedra interrupted after only two share faces by sharing faces with a Cu triangular prism or a vacant prism. The crystal structure of this material, which has Cu/Ir ordering in the M site chains, is very sensitive to the conditions of synthesis: prolonged heating of a commensurately ordered trigonal material leads to the transformation to an incommensurate structure, which can be described as a mixture of two substructures with the same lattice parameter a , but with different lattice parameters c_1 and c_2 ($c \sim 2c_1 \sim 3c_2$)²⁰⁸. The incommensurability, as is seen in this type of compound and for other materials in the hexagonal perovskite family, comes from the difference in periodicities of the A-site and M-site chains, from which one can infer that the atoms in the chains are more strongly interacting along their lengths than with other chains. In contrast, in the Ba₆CuIr₄O₁₅ crystal structure, a disordered distribution of Cu and Ir, rather than an ordered distribution, is seen in both the trigonal prismatic and the octahedral sites. The incommensurate structure of this material can be considered as a combination of trigonal and rhombohedral substructures, similarly to the incommensurate hexagonal perovskites SrMn_{1-x}Co_xO_{3-y}^{209,210}.

Along the same line of study is a material where Cu and Ir are mixed in triangular prisms but there are three octahedra before the chains are interrupted by a triangular prism. The crystal structure of Ba₅CuIr₃O₁₂ was determined by a combination of both X-ray and neutron diffraction in 1999²¹¹. As shown in **Figure 33**, its structure consists of three face-sharing IrO₆ octahedra forming a quasi 1D chain along the c -axis. DFT calculations for this material show that the localized $j = \frac{1}{2}$ picture cannot fully explain the electronic and magnetic properties of Ba₅CuIr₃O₁₂, attributed by the authors of that study to strong

covalency among the atoms that is not captured by the calculations. In other words, the very short Ir-Ir distance present within the Ir₃O₁₂ trimers results in strong uncaptured metal-metal interactions that may lead to the formation of molecular orbitals²¹². Recently, a spin liquid ground state in Ba₅CuIr₃O₁₂ has been tested by thermodynamic and high magnetic field measurements. Although weak antiferromagnetic interactions were seen in the magnetic susceptibility and heat capacity measurements, the magnetization did not saturate, even up to a 59 T applied magnetic field. This implies the existence of a random single state, which can fully explain the experimental data²¹³.

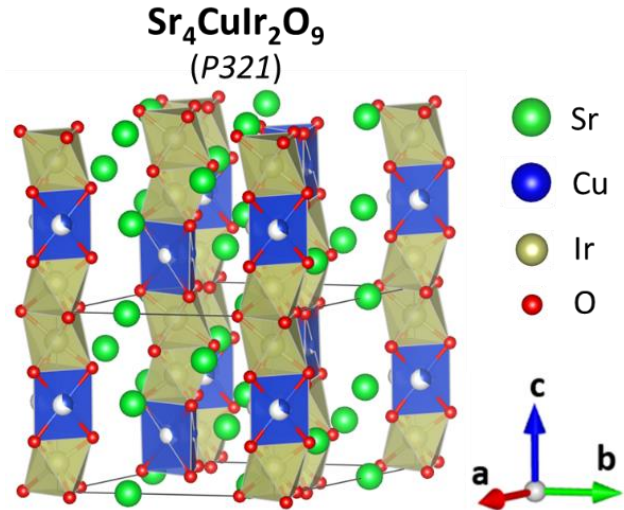


Figure 32. The crystal structure of Sr₄CuIr₂O₉.

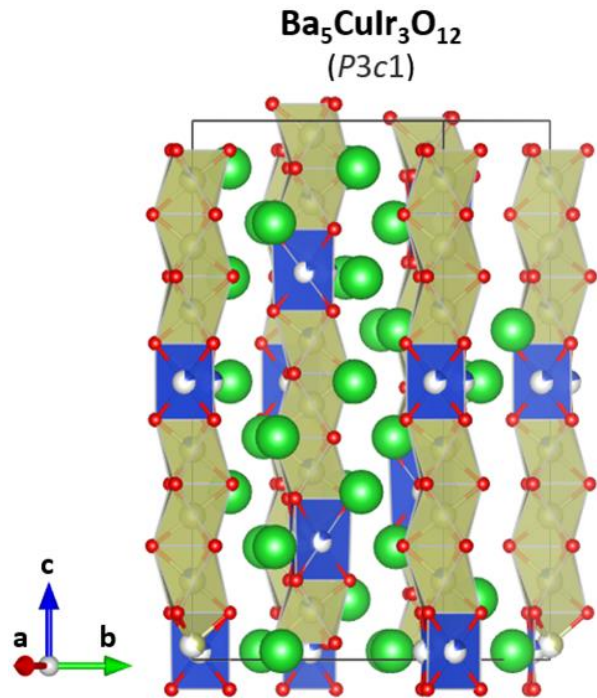


Figure 33. The crystal structure of Ba₅CuIr₃O₁₂.

In contrast to the other materials described here, the crystal structure of Ca_2IrO_4 ²¹⁴ displays a pure 1D chain of edge-sharing (not face-sharing) IrO_6 octahedra, but nonetheless has hexagonal symmetry, as shown in **Figure 34**. DFT calculations have been performed for this material and they argue that the material should be an antiferromagnetic insulator with a band gap of 0.64 eV and an effective moment of 0.68 $\mu\text{B}/\text{f.u.}$ The band gap has been attributed to the long range antiferromagnetic interactions of Ir^{4+} spins. Moreover, attributed to the inherent, strong spin orbit coupling present for the 5d Ir transition metal, large magnetic anisotropy has been observed in this system. The crystal structure of a more traditional hexagonal perovskite based on chains, 2H BaCoO_3 , is shown in the figure for comparison. The Co-Co bond length in 2H- BaCoO_3 is even shorter than that in the metal; the distances being 2.38 Å and 2.50 Å along the chain, respectively¹⁷⁰.

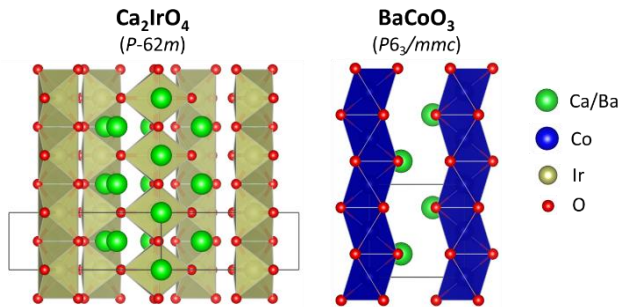


Figure 34. The crystal structure of Ca_2IrO_4 and 2H- BaCoO_3 .

Sticking with continuous chains of octahedra for the moment, a continuous 1D chain of face-sharing IrO_6 octahedra has been observed recently reported material, $\text{K}_3\text{Ir}_2\text{O}_6$ ²¹⁵. This material is an electrical insulator, but DFT calculations show no band gap near the Fermi level. This has been interpreted to indicate that $\text{K}_3\text{Ir}_2\text{O}_6$ is a Mott insulator. More interestingly, “flat bands” (that is, electronic bands that show no dispersion of electron energy versus electron wave vector) along the Γ -F direction in the Brillouin zone in the electronic band structure suggest that the electrons are localized along certain momentum vectors in the unit cell. This material may also prove to be of interest from the quantum materials perspective on further study.

A few more crystal structures of materials with 1D chains are outlined in **Figure 35**. They are obviously complex structures, because the chain fragments are quite long and have different lengths. RhO_6 octahedra seem to be a fertile constituent of such systems. $\text{Ba}_9\text{Rh}_8\text{O}_{24}$ ²¹⁶ crystallizes in the hexagonal space group $R\text{-}3c$ with the lattice parameters $a = 10.0899(4)$ Å, and $c = 41.462(2)$ Å. A chain of seven face-sharing RhO_6 octahedra is sandwiched by RhO_6 trigonal prisms in this material. The directional magnetic susceptibility shows divergence below 100 K, implying the onset of the magnetic anisotropy in this material. Its high temperature magnetic susceptibility does not follow the Curie-Weiss law, and it is too complex to allow the assignment of the oxidation states of Rh ions along the chain. The next two materials, $\text{Ba}_{11}\text{Rh}_{10}\text{O}_{30}$ and $\text{Ba}_{32}\text{Rh}_{29}\text{O}_{87}$ ²¹⁷, both crystallize in the hexagonal space group $R\text{-}3m$. $\text{Ba}_{11}\text{Rh}_{10}\text{O}_{30}$ contains chains of nine face-sharing RhO_6 octahedra while $\text{Ba}_{32}\text{Rh}_{29}\text{O}_{87}$ has eight repeated face-sharing RhO_6 octahedra followed by a RhO_6 trigonal prism. The longest chain of face-

sharing octahedra is seen in $12\text{R-Ba}_{12}\text{Rh}_{9.25}\text{Ir}_{1.75}\text{O}_{33}$ ²¹⁸, for which Ir is mixed with the Rh in a disordered fashion. The chain consists of ten face-sharing $(\text{Rh}/\text{Ir})\text{O}_6$ octahedra, connected to single $(\text{Rh}/\text{Ir})\text{O}_6$ trigonal prism. This material adopts a hexagonal structure, space group $R32$, with lattice parameters $a = 10.0492(2)$ Å and $c = 28.386(3)$ Å. Magnetic susceptibility measurements yield a Curie-Weiss temperature of -1 K, and a very low effective moment of 1.08 $\mu\text{B}/\text{f.u.}$ This very low observed effective moment has been attributed to a strong spin orbit coupling effect in both the Rh and Ir ions and strong metal-metal interactions along the chains. The continuous sequence of face-sharing octahedra displays very short metal-metal bond lengths (2.5-2.6 Å) in this material, which indicates the presence of direct metal-metal bonding along the 1D chain. This apparent bonding would not lead to a preference of one type of magnetic model over any other. If these compounds could be made in quantities sufficient for detailed study, or as large enough single crystals, then they would certainly challenge theorist’s understanding of quantum materials

10. Some unusual derivatives of hexagonal perovskites

But the crystal structures can sometimes be even more complex than these. $\text{Pb}_3\text{Rh}_7\text{O}_{15}$ ²¹⁹ for example crystallizes in a hexagonal structure, space group $P6_3/mmc$ with lattice parameters $a = 10.3537(2)$ Å and $c = 13.2837(5)$ Å. The crystal structure of $\text{Pb}_3\text{Rh}_7\text{O}_{15}$ is shown in **Figure 36a**. It is a variant of a “dimer” type hexagonal perovskite. The electrical resistivity is low and isotropic, about 1 mΩcm at room temperature. As seen in **Figures 36b-c**, there exists a clear transition at 185 K in both magnetic susceptibility and heat capacity measurements. This comes from a structural phase transition at 185 K that has been attributed to the charge modulation of Rh^{3+} and Rh^{4+} . The substitution of Bi for Pb leads to the disappearance of the structural transition at 185 K, which the authors argue confirms that the transition in $\text{Pb}_3\text{Rh}_7\text{O}_{15}$ is due to Rh^{3+} - Rh^{4+} charge modulation.

The crystal structure of a recently described rhodate $\text{Bi}_{1.4}\text{CuORh}_5\text{O}_{10}$ ²²⁰ is shown in **Figure 37**. This material crystallizes in a monoclinic space group, $C2/m$, with the lattice parameters $a = 17.310(3)$ Å, $b = 3.0775(9)$ Å, $c = 16.009(3)$ Å and $\beta = 95.903(15)$, with a more severe distortion of a hexagonal perovskite structure than the Pb rhodate described above. The crystal structure contains undulating layers of both edge-sharing and corner-sharing RhO_6 octahedra, with Cu ions occupying square planar coordinate sites. This type of octahedral framework with channels is commonly known in rhodates, such as rutile RhO_2 , hollandite $\text{Ba}_{1.72}\text{Rh}_8\text{O}_{16}$, and todorokite $\text{Bi}_6\text{Rh}_{12}\text{O}_{29}$.

As shown in **Figure 38**, $\text{Sr}_7\text{Mn}_4\text{O}_{15}$ ²²¹ is a distorted dimer-based perovskite. Studied by neutron diffraction, this material crystallizes in the monoclinic space group, $P2_1/c$, with the lattice parameters $a = 6.81825(9)$ Å, $b = 9.6228(1)$ Å, $c = 10.3801(1)$ Å, and $\beta = 91.8771(9)$. The crystal structure consists of dimers of face-sharing MnO_6 octahedra that are then corner shared with other dimers, but the crystal structure is highly distorted, with an unusual ratio of seven Sr^{2+} ions to four Mn ions, which in the end remarkably yields a uniform formal charge state of Mn^{4+} , a $3d^3$ electron configuration to accompany the highly distorted crystal structure that accommodates the 7:4 metal ion ratio. Magnetic susceptibility measurements

show the presence of three different magnetically ordered states in this material as a function of temperature at ambient temperature and below. Above 150 K, intradimer ordering is observed. 2D-magnetic clusters are formed in the temperature range of 150-75 K, and finally, full 3D antiferromagnetic ordering among the Mn^{4+} spins is established below 75 K. The magnetic structure of $Sr_7Mn_4O_{15}$, determined by using neutron diffraction, was interpreted as showing the presence of those three different magnetic phases. Mn seems to be highest among royalty in its ability to couple lattice and electronic and magnetic states in oxides.

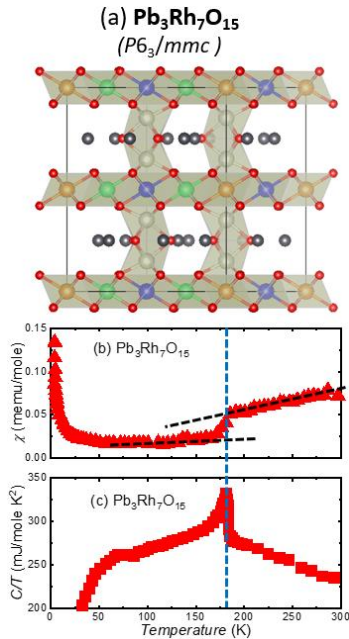


Figure 36. (a) The crystal structure of $Pb_3Rh_7O_{15}$, (b) Temperature dependent magnetic susceptibility and (c) Heat capacity of $Pb_3Rh_7O_{15}$ ²¹⁹.

The ternary Ba-Ru-O and Ba-Ir-O hexagonal perovskite chemical systems display many unusual derivatives, largely based on different Ba:M ratios, with interesting quantum properties. First of all, $Ba_5Ru_2O_{10}$ ²²² crystallizes in the hexagonal space group $P6_3/mmc$, and its crystal structure shown in **Figure 39** consists of two face-sharing RuO_6 octahedra forming Ru_2O_9 dimers. The Ru-Ru distance in the dimer is 2.071 Å, and the Ru in this material has a formal charge of 5+. The magnetic susceptibility of $Ba_5Ru_2O_{10}$ has a large maximum at around 280 K, which has been ascribed to the antiferromagnetic interactions of the Ru moments within the Ru_2O_9 dimers, and the coupling exchange is calculated to be -116 K. With the same synthesis conditions in an O_2 rich environment, $Ba_5Ru_2O_{11}$ is formed instead. The only difference in the crystal structures between $Ba_5Ru_2O_{10}$ and $Ba_5Ru_2O_{11}$ is that peroxide groups O_2^{2-} are stabilized in the Ba_2O_2 layers in $Ba_5Ru_2O_{11}$ while only isolated oxygen ions are found in the unit cell in $Ba_5Ru_2O_{10}$. The high stability of the peroxide O_2^{2-} group has been said to limit reversible electrochemical reactions of the O_2^{2-}/O_2^- redox couples used in oxygen evolution reaction catalysts and Li-ion battery materials ²²³. In the mind of the senior author of this manuscript, the fact that peroxide ions are actually observed in the crystal structure of $Ba_5Ru_2O_{11}$ really raises the question of how to think about the distribution of electrons in materials like these that have high ratios of electropositive ions (i.e. Ba^{2+}) to highly oxidized transition elements (i.e. Ru); he realizes of course that people who do DFT calculations will say that they know where the charges are, but for his generation at least, proposed charge distributions are best determined experimentally not through DFT calculations. A famous case of this is found in cuprate superconductors such as $La_{2-x}Sr_xCuO_4$. As Sr is substituted for La, do the electrons come out of Cu orbitals, making the actual number of electrons that can be associated with the Cu go down, or is the charge actually removed from oxygen p states? Much of the observed phenomenology is not sensitive to this. $Ba_5Ru_2O_{10}$ by the way appears to be a simple example of relatively isolated Ru_2O_9 dimers on a layered hexagonal lattice.

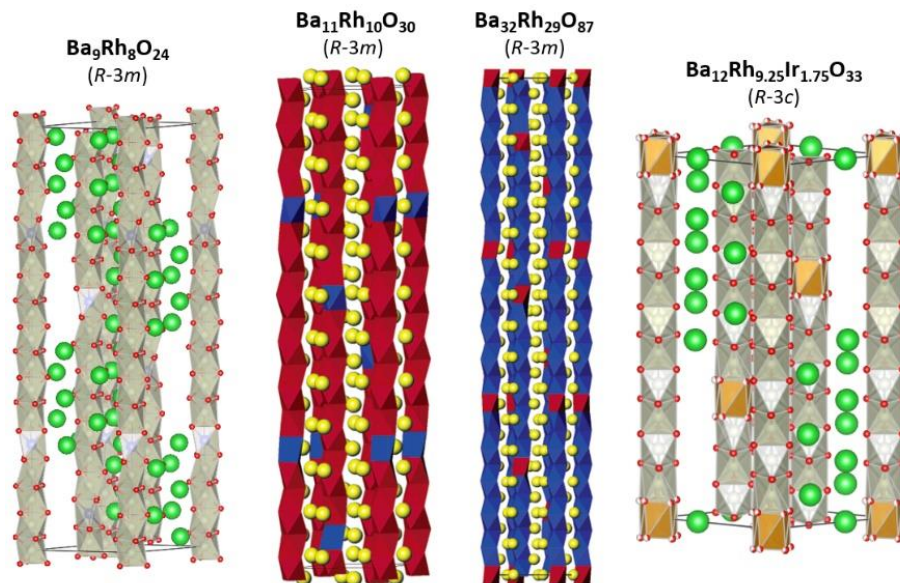


Figure 35. The crystal structures of $Ba_9Rh_8O_{24}$, $Ba_{11}Rh_{10}O_{30}$, $Ba_{32}Rh_{29}O_{87}$ and $Ba_{12}Rh_{9.25}Ir_{1.75}O_{33}$.

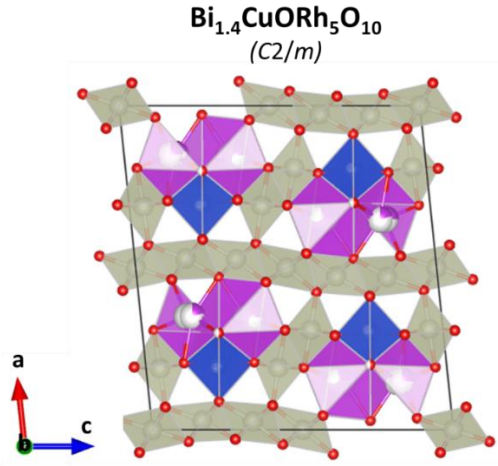


Figure 37. The crystal structure of Bi_{1.4}CuORh₅O₁₀.

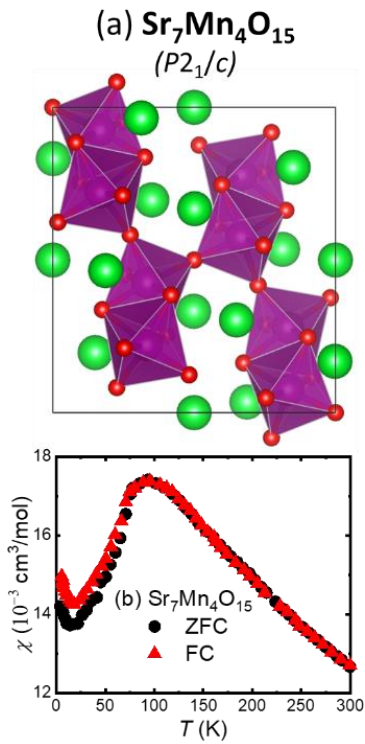


Figure 38. (a) The crystal structure of Sr₇Mn₄O₁₅, (b) FC/ZFC magnetic susceptibility of Sr₇Mn₄O₁₅ under the applied magnetic field of 100 Oe²²¹.

Ba₄Ru₃O₁₀²²⁴ is a distorted monoclinic material based on the 9R-BaRuO₃ hexagonal perovskite. It crystallizes in the space group $P2_1/a$ with the lattice parameters $a = 5.776 \text{ \AA}$, $b = 13.076 \text{ \AA}$, $c = 7.234 \text{ \AA}$, and $\beta = 113.53^\circ$. Its crystal structure, as shown in **Figure 40**, consists of three face-sharing RuO₆ octahedra making Ru₃O₁₂ trimers, corner-sharing with each other to form zig-zag layers parallel to the (001) plane. The crystal structure is skewed away from simple hexagonal symmetry by the presence of the 4:3 Ba to Ru ratio and the trimer formation. The intra-atomic Ru-Ru distance within a trimer is shorter than that in Ru metal, 2.57 \AA compared to 2.65 \AA , which the authors

interpret as implying the presence of strong metal-metal bonds, as commonly seen in face-sharing octahedra. The temperature dependent magnetic susceptibility of Ba₄Ru₃O₁₀ displays a broad peak at 200 K, taken by the authors to be characteristic of a 2D-antiferromagnetic transition. Further, the effective moment was calculated to be 3.0 $\mu\text{B}/\text{f.u.}$, which would yield an $S = 1$ for every Ru⁴⁺-based trimer in Ba₄Ru₃O₁₀. The DFT-based calculations that the authors performed on Ba₄Ru₃O₁₀ were interpreted as indicating the presence of a nonmagnetic ground state for one-third of the Ru⁴⁺ ions and a different charge distribution between different Ru sites in the trimer and molecular orbital formation in the trimer.²²⁵ Readers interested in the question of “where’s the charge” in this and other materials in the hexagonal perovskite family are referred to the theoretical contribution in this issue by Streltsov and Khomskii.

Continuing along this line of structural complexity, Ba₅Ru₃O₁₂²²⁶ adopts the orthorhombic space group $Pnma$ with lattice parameters $a = 10.862 \text{ \AA}$, $b = 5.893 \text{ \AA}$, and $c = 19.790 \text{ \AA}$. As shown in **Figure 39**, the crystal structure also contains the Ru₃O₁₂ trimers, similar to the case of Ba₄Ru₃O₁₀. However, for this material, the trimers are isolated from each other and separated by Ba atoms. In Ba₅Ru₃O₁₂, there exists a formal mix of Ru⁴⁺ and Ru⁵⁺ in a 1 to 2 ratio. The material displays antiferromagnetic ordering at 60 K. Fitting of the high temperature magnetic susceptibility results in a Curie-Weiss temperature of -320 K, indicating a relatively strong antiferromagnetic interaction between Ru ions.

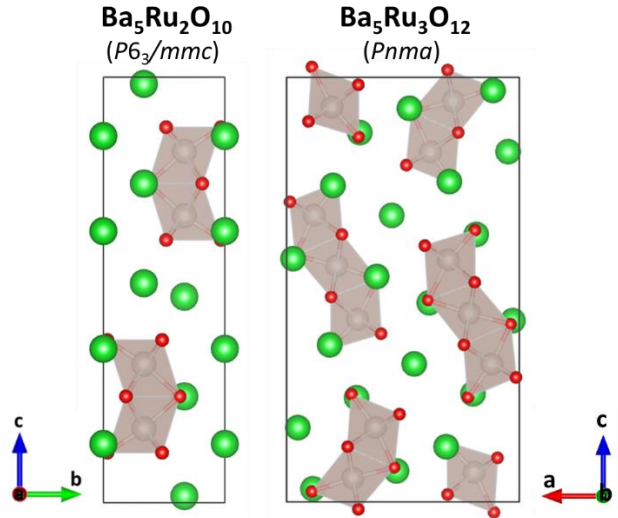


Figure 39. The crystal structures of Ba₅Ru₂O₁₀ and Ba₅Ru₃O₁₂.

We move on now to barium iridates. Quantum spin liquids are often found in strongly frustrated magnetic systems. Typically, the magnetic ions are arranged in simple triangular, honeycomb, and kagome lattices. Ba₄Ir₃O₁₀ is proposed to be a quantum spin liquid candidate, but has the Ir ions arranged in a nominally unfrustrated lattice due to its structural complexity, which is based on zig-zag corner-sharing of Ru₃O₁₂ trimers **Figure 40**. The temperature-dependent magnetic susceptibility has been interpreted as yielding a very large negative Curie-Weiss temperature of -766 K, which would indicate the presence of very strong antiferromagnetic interactions in this

material. The authors report that no magnetic ordering is observed down to 0.2 K in this material, interpreted as meaning that a quantum spin liquid state exists down to that temperature. The authors further report that only 2% doping of Sr on the Ba sites kills the QSL state and uncovers antiferromagnetic ordering at 130 K. Further, although there is strong intra-trimer magnetic exchange present due to short the Ir-Ir distances present, inter-trimer coupling also plays an important role in fully explaining the low temperature magnetic properties in this quantum magnet.

$\text{Ba}_7\text{Ir}_6\text{O}_{19}$ ²²⁷ adopts a distorted monoclinic structure in space group $C2/m$ with the lattice parameters $a = 14.913 \text{ \AA}$, $b = 5.778 \text{ \AA}$, $c = 10.979 \text{ \AA}$ and $\beta = 99.58$. As shown in **Figure 40**, the crystal structure consists of three-face-sharing IrO_6 octahedra, forming Ir_3O_{12} trimers, corner-shared to each other. Its magnetic properties have not yet been investigated.

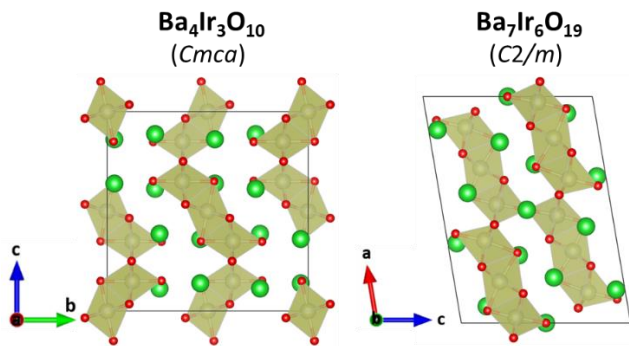


Figure 40. The crystal structures of $\text{Ba}_4\text{Ir}_3\text{O}_{10}$ (left) and $\text{Ba}_7\text{Ir}_6\text{O}_{19}$ (right).

11. Conclusions

In a way, the hexagonal oxide perovskites and their distorted derivatives are much richer materials than the cubic perovskites and their derivatives because the crystal structures are more widely varied. Their properties are not studied as much because the hexagonal perovskites are not as jaw-dropping when considered as quantum materials as the classical perovskites are. There are no known superconductors in this family for example. Growing crystals by the optical floating zone method for the simple ones is not often done, presumably due to the volatility of the constituents and relatively little motivation by the physical properties. However, the study of quantum spin liquids is a topic of considerable interest nowadays, especially in the neutron scattering community, and thus single crystals of some of the dimer-based materials have been studied extensively. Quite a few hexagonal-perovskite-based materials have been identified as potential candidates for the quantum spin liquid state at low temperatures (i.e. $\text{Ba}_3\text{CuSb}_2\text{O}_9$, $\text{Ba}_3\text{CoSb}_2\text{O}_9$, $\text{Ba}_3\text{InIr}_2\text{O}_9$, $\text{Ba}_3\text{IrTi}_2\text{O}_9$, $\text{Ba}_4\text{NbIr}_3\text{O}_{12}$, $\text{Ba}_4\text{Ir}_3\text{O}_{10}$ and $\text{Ba}_2\text{Y}_2\text{Rh}_2\text{Ti}_2\text{O}_{17}$), but so far the field remains “dynamic”; and at the time of this writing there appears to be no community-wide accepted hexagonal perovskite quantum spin liquid, although as described above there are many candidates. Perhaps the problem is that there are too many contenders and different researchers have different favorites among them. Several ferromagnetic hexagonal perovskites have recently been reported, such as $\text{Ba}_4\text{NdRu}_3\text{O}_{12}$ ordering at 11.5 K or $\text{Ba}_4\text{NbMn}_3\text{O}_{12}$ ordering at 42 K. There may be worth further study.

Most of the hexagonal perovskite derivatives are materials in the $\text{Ba}_3\text{MM}'_2\text{O}_9$ family (based on dimers) and next the $\text{Ba}_4\text{MM}'_3\text{O}_{12}$ family (based on trimers). The ferroelectric and dielectric properties of these materials have not generally been reported, though $\text{Ba}_6\text{Nd}_2\text{Ti}_4\text{O}_{17}$, a material that includes layers of both tetrahedra and octahedra, is a well-known dielectric. In the near future, in our view, comprehensive studies will reveal more interesting quantum properties in the hexagonal oxide perovskite family. The family does seem to have an excellent chance for hosting the exotic quantum spin liquid state, and that may turn out after several more years of study, to be its primary “claim to fame”.

12. Acknowledgments

The authors’ research on hexagonal oxide perovskites and geometric magnetic frustration has been supported by the Gordon and Betty Moore Foundation, grant GBMF-4412, and by the Basic Energy Sciences Division of the Department of Energy, grant number DE-FG02-08ER46544 to the Institute of Quantum Matter, which continues as an Energy Frontier Research Center funded by the U.S. Department of Energy, Office of Science, Basic Energy Sciences under Award No. DE-SC0019331. The magnetic data presented in this review has been extracted and plotted through use of the program *Origin*. Similarly, the crystal structures presented have been imaged through use of the program *Vesta*, using information available on the International Crystal Structure Database or in the published literature.

13. Author contributions

This review article was written through equal contributions of both authors, Loi Nguyen and Robert Cava.

14. Notes

The authors declare no competing financial interest.

15. Biographies

Loi T. Nguyen graduated from the California State University, Fullerton (CSUF) in 2017, where his solid state chemistry research was on unconventional oxide perovskites. He is currently a third year graduate student in the Department of Chemistry at Princeton University. His research focuses on the synthesis and magnetic properties of hexagonal perovskites. He has discovered several new face-sharing hexagonal perovskites, several of which potentially host a quantum spin liquid state.

Robert J. Cava is the Russell Wellman Moore Professor and former chair of the Chemistry Department at Princeton University. He received his Ph.D. in Ceramics from MIT in 1978, after which he was an NRC Postdoctoral Fellow at the National Bureau of Standards. He then eventually became a Distinguished Member of Technical Staff at Bell Laboratories, where he worked for 17 years. He is a member of the US National Academy of Sciences and a Foreign Member of the Royal Society of London.

16. References

- (1) Elbaz, G. A.; Straus, D. B.; Semonin, O. E.; Hull, T. D.;

- Paley, D. W.; Kim, P.; Owen, J. S.; Kagan, C. R.; Roy, X. Unbalanced Hole and Electron Diffusion in Lead Bromide Perovskites. *Nano Lett* **2017**, *17* DOI: 10.1021/acs.nanolett.6b05022.
- (2) Dong, Q.; Fang, Y.; Shao, Y.; Mulligan, P.; Qiu, J.; Cao, L.; Huang, J. Electron-Hole Diffusion Lengths > 175 nm in Solution-Grown CH₃NH₃PbI₃ Single Crystals. *Science* (80-.). **2015**, *347* (6225), 967–970 DOI: 10.1126/science.aaa5760.
- (3) Shi, D.; Adinolfi, V.; Comin, R.; Yuan, M.; Alarousu, E.; Buin, A.; Chen, Y.; Hoogland, S.; Rothenberger, A.; Katsiev, K.; Losovyj, Y.; Zhang, X.; Dowben, P. A.; Mohammed, O. F.; Sargent, E. H.; Bakr, O. M. Low Trap-State Density and Long Carrier Diffusion in Organolead Trihalide Perovskite Single Crystals. *Science* (80-.). **2015**, *347* (6221), 519–522 DOI: 10.1126/science.aaa2725.
- (4) Bi, Y.; Hutter, E. M.; Fang, Y.; Dong, Q.; Huang, J.; Savenije, T. J. Charge Carrier Lifetimes Exceeding 15 ns in Methylammonium Lead Iodide Single Crystals. *J. Phys. Chem. Lett* **2016**, *7*, 16 DOI: 10.1021/acs.jpcclett.6b00269.
- (5) Straus, D. B.; Guo, S.; Cava, R. J. Kinetically Stable Single Crystals of Perovskite-Phase CsPbI₃. **2019** DOI: 10.1021/jacs.9b06055.
- (6) Linaburg, M. R.; McClure, E. T.; Majher, J. D.; Woodward, P. M. Cs_{1-x}Rb_xPbCl₃ and Cs_{1-x}Rb_xPbBr₃ Solid Solutions: Understanding Octahedral Tilting in Lead Halide Perovskites. *Chem. Mater.* **2017**, *29* (8), 3507–3514 DOI: 10.1021/acs.chemmater.6b05372.
- (7) McClure, E. T.; Ball, M. R.; Windl, W.; Woodward, P. M. Cs₂AgBiX₆ (X = Br, Cl): New Visible Light Absorbing, Lead-Free Halide Perovskite Semiconductors. *Chem. Mater.* **2016**, *28* (5), 1348–1354 DOI: 10.1021/acs.chemmater.5b04231.
- (8) Majher, J. D.; Gray, M. B.; Strom, T. A.; Woodward, P. M. Cs₂NaBiCl₆:Mn²⁺ - A New Orange-Red Halide Double Perovskite Phosphor. *Chem. Mater.* **2019**, *31* (5), 1738–1744 DOI: 10.1021/acs.chemmater.8b05280.
- (9) Fabiani, D. H.; Hogan, T.; Evans, H. A.; Stoumpos, C. C.; Kanatzidis, M. G.; Seshadri, R. Dielectric and Thermodynamic Signatures of Low-Temperature Glassy Dynamics in the Hybrid Perovskites CH₃NH₃PbI₃ and HC(NH₂)₂PbI₃. *J. Phys. Chem. Lett.* **2016**, *7* (3), 376–381 DOI: 10.1021/acs.jpcclett.5b02821.
- (10) Green, M. A.; Ho-Baillie, A. Perovskite Solar Cells: The Birth of a New Era in Photovoltaics. *ACS Energy Lett.* **2017**, *2* (4), 822–830 DOI: 10.1021/acsenergylett.7b00137.
- (11) Galasso, F. S. (2013). Structure, properties and preparation of perovskite-type compounds: international series of monographs in solid state physics (Vol. 5). Elsevier.
- (12) Mitchell, R. H. (2002). Perovskites: Modern and Ancient (Vol. 7). Thunder Bay: Almaz Press.
- (13) Tilley, R. J. (2016). Perovskites: structure-property relationships. John Wiley & Sons.
- (14) Kerman, K.; Ramanathan, S.; Baniecki, J. D.; Ishii, M.; Kotaka, Y.; Aso, H.; Kurihara, K.; Schafrank, R.; Vailionis, A. Thermopower in Quantum Confined La-Doped SrTiO₃ Epitaxial Heterostructures. *Appl. Phys. Lett.* **2013**, *103* (17), 173904 DOI: 10.1063/1.4826098.
- (15) Takada, Y. Theory of Superconductivity in Polar Semiconductors and Its Application to N-Type Semiconducting SrTiO₃. *J. Phys. Soc. Japan* **1980**, *49* (4), 1267–1275 DOI: 10.1143/JPSJ.49.1267.
- (16) Luo, W.; Duan, W.; Louie, S. G.; Cohen, M. L. Structural and Electronic Properties of N-Doped and p-Doped SrTiO₃. *Phys. Rev. B - Condens. Matter Mater. Phys.* **2004**, *70* (21), 1–8 DOI: 10.1103/PhysRevB.70.214109.
- (17) Dai, P.; Hu, J.; Dagotto, E. Magnetism and Its Microscopic Origin in Iron-Based High-Temperature Superconductors. *Nat. Phys.* **2012** DOI: 10.1038/NPHYS2438.
- (18) Keimer, B.; Kivelson, S. A.; Norman, M. R.; Uchida, S.; Zaanen, J. From Quantum Matter to High-Temperature Superconductivity in Copper Oxides. *Nature* **2014**, *518* DOI: 10.1038/nature14165.
- (19) Coronado, E.; Martí-Gastaldo, C.; Navarro-Moratalla, E.; Ribera, A.; Blundell, S. J.; Baker, P. J. Coexistence of Superconductivity and Magnetism by Chemical Design. **2010** DOI: 10.1038/NCHEM.898.
- (20) Slavney, A. H.; Hu, T.; Lindenberg, A. M.; Karunadasa, H. I. A Bismuth-Halide Double Perovskite with Long Carrier Recombination Lifetime for Photovoltaic Applications. *J. Am. Chem. Soc.* **2016**, *138* (7), 2138–2141 DOI: 10.1021/jacs.5b13294.
- (21) Connor, B. A.; Leppert, L.; Smith, M. D.; Neaton, J. B.; Karunadasa, H. I. Layered Halide Double Perovskites: Dimensional Reduction of Cs₂AgBiBr₆. *J. Am. Chem. Soc.* **2018**, *140* (15), 5235–5240 DOI: 10.1021/jacs.8b01543.
- (22) Majher, J. D.; Gray, M. B.; Strom, T. A.; Woodward, P. M. Cs₂NaBiCl₆:Mn²⁺ - A New Orange-Red Halide Double Perovskite Phosphor. *Chem. Mater.* **2019**, *31* (5), 1738–1744 DOI: 10.1021/acs.chemmater.8b05280.
- (23) Tran, T. T.; Panella, J. R.; Chamorro, J. R.; Morey, J. R.; McQueen, T. M. Designing Indirect-Direct Bandgap Transitions in Double Perovskites. *Mater. Horizons* **2017**, *4* (4), 688–693 DOI: 10.1039/c7mh00239d.

- (24) Smith, A. E.; Sleight, A. W.; Subramanian, M. A. Electrical and Magnetic Properties of New Rhodium Perovskites: La₂MRhO₆, M = Cr, Fe, Cu. *Mater. Res. Bull.* **2010**, *45* (4), 460–463 DOI: 10.1016/j.materresbull.2009.11.008.
- (25) Mao, L.; Teicher, S. M. L.; Stoumpos, C. C.; Kennard, R. M.; Decrescent, R. A.; Wu, G.; Schuller, J. A.; Chabiny, M. L.; Cheetham, A. K.; Seshadri, R. Chemical and Structural Diversity of Hybrid Layered Double Perovskite Halides. *J. Am. Chem. Soc.* **2019**, *141* (48), 19099–19109 DOI: 10.1021/jacs.9b09945.
- (26) Vishnoi, P.; Zuo, J. L.; Strom, T. A.; Wu, G.; Wilson, S. D.; Seshadri, R.; Cheetham, A. K. Structural Diversity and Magnetic Properties of Hybrid Ruthenium Halide Perovskites and Related Compounds. *Angew. Chemie* **2020**, ange.202003095 DOI: 10.1002/ange.202003095.
- (27) Khomskii, D. I.; Sawatzky, G. A. Interplay between Spin, Charge and Orbital Degrees of Freedom in Magnetic Oxides. *Solid State Commun.* **1997**, *102* (2–3), 87–99 DOI: 10.1016/S0038-1098(96)00717-X.
- (28) Khomskii, D. (2014). *Transition Metal Compounds*. Cambridge University Press.
- (29) Khomskii, D. I. (2010). *Basic Aspects of the Quantum Theory of Solids: Order and Elementary Excitations*. Cambridge University Press.
- (30) Jin, C.-Q. Q.; Zhou, J.-S. S.; Goodenough, J. B.; Liu, Q. Q.; Zhao, J. G.; Yang, L. X.; Yu, Y.; Yu, R. C.; Katsura, T.; Shatskiy, A.; Ito, E. High-Pressure Synthesis of the Cubic Perovskite BaRuO₃ and Evolution of Ferromagnetism in ARuO₃ (A = Ca, Sr, Ba) Ruthenates. *Proc. Natl. Acad. Sci. U. S. A.* **2008**, *105* (20), 7115–7119 DOI: 10.1073/pnas.0710928105.
- (31) Itoh, S.; Endoh, Y.; Yokoo, T.; Ibuka, S.; Park, J. G.; Kaneko, Y.; Takahashi, K. S.; Tokura, Y.; Nagaosa, N. Weyl Fermions and Spin Dynamics of Metallic Ferromagnet SrRuO₃. *Nat. Commun.* **2016**, *7*, 1–8 DOI: 10.1038/ncomms11788.
- (32) Zhao, J. G.; Yang, L.; Yu, Y.; Li, F.; Yu, R.; Jin, C. Q. Structural and Electrical Properties Evolution in Ba_{1-x}Sr_xRuO₃ Synthesized under High Pressure. *J. Solid State Chem.* **2009**, *182* (6), 1524–1528 DOI: 10.1016/j.jssc.2009.03.007.
- (33) Donohue, P. C.; Katz, L.; Ward, R. The Modification of Structures of Ternary Oxides by Cation Substitution. I. Substitution of Strontium for Barium in Barium Ruthenium Oxide and in Barium Iridium Oxide. *Inorg. Chem.* **1966**, *5* (3), 335–338 DOI: 10.1021/ic50037a001.
- (34) Santoro, A.; Sora, I. N.; Huang, Q. Bond-Valence Analysis of the Structure of (Ba_{0.875}Sr_{0.125})RuO₃. *J. Solid State Chem.* **1999**, *143* (1), 69–73 DOI: 10.1006/jssc.1998.8080.
- (35) Ying, Y. A.; Liu, Y.; He, T.; Cava, R. J. Magnetotransport Properties of BaRuO₃: Observation of Two Scattering Rates. *Phys. Rev. B* **2011**, *84* (4), 233104–233105 DOI: 10.1103/PhysRevB.84.233104.
- (36) Vojta, T. Strong-Disorder Magnetic Quantum Phase Transitions: Status and New Developments. *J. Phys. Conf. Ser.* **2014**, *529* (1), 012016 DOI: 10.1088/1742-6596/529/1/012016.
- (37) Gat-Malureanu, I. M.; Carlo, J. P.; Goko, T.; Fukaya, A.; Ito, T.; Kyriakou, P. P.; Larkin, M. I.; Luke, G. M.; Russo, P. L.; Savici, A. T.; Wiebe, C. R.; Yoshimura, K.; Uemura, Y. J. Muon Spin Relaxation and Susceptibility Measurements of an Itinerant-Electron System Sr_{1-x}Ca_xRuO₃: Quantum Evolution from Ferromagnet to Paramagnet. *Phys. Rev. B - Condens. Matter Mater. Phys.* **2011**, *84* (22), 224415 DOI: 10.1103/PhysRevB.84.224415.
- (38) Zarzycki, A.; Rams, M.; Goerlich, E. A.; Tomala, K. Investigation of Anomalous Thermodynamic and Transport Properties of Sr_{1-x}Ca_xRuO₃ (x ≥ 0.8). **2018**.
- (39) Longo, J. M.; Kafalas, J. A.; Arnott, R. J. Structure and Properties of the High and Low Pressure Forms of SrIrO₃. *J. Solid State Chem.* **1971**, *3* (2), 174–179 DOI: 10.1016/0022-4596(71)90022-3.
- (40) Cheng, J. G.; Alonso, J. A.; Suard, E.; Zhou, J. S.; Goodenough, J. B. A New Perovskite Polytype in the High-Pressure Sequence of BaIrO₃. *J. Am. Chem. Soc.* **2009**, *131* (21), 7461–7469 DOI: 10.1021/ja901829e.
- (41) Nguyen, L. T.; Cava, R. J. Trimer-Based Spin Liquid Candidate B A₄NbI₃R₃O₁₂. *Phys. Rev. Mater.* **2019**, *3* (1) DOI: 10.1103/PhysRevMaterials.3.014412.
- (42) Phelan, B. F.; Krizan, J.; Xie, W.; Gibson, Q.; Cava, R. J. New Material for Probing Spin-Orbit Coupling in Iridates. *Phys. Rev. B - Condens. Matter Mater. Phys.* **2015**, *91* (15), 1–29 DOI: 10.1103/PhysRevB.91.155117.
- (43) Jackeli, G.; Khaliullin, G. Mott Insulators in the Strong Spin-Orbit Coupling Limit: From Heisenberg to a Quantum Compass and Kitaev Models. *Phys. Rev. Lett.* **2009**, *102* (1) DOI: 10.1103/PhysRevLett.102.017205.
- (44) Kim, B. J.; Jin, H.; Moon, S. J.; Kim, J. Y.; Park, B. G.; Leem, C. S.; Yu, J.; Noh, T. W.; Kim, C.; Oh, S. J.; Park, J. H.; Durairaj, V.; Cao, G.; Rotenberg, E. Novel Jeff=1/2 Mott State Induced by Relativistic Spin-Orbit Coupling in Sr₂IrO₄. *Phys. Rev. Lett.* **2008**, *101* (7) DOI: 10.1103/PhysRevLett.101.076402.
- (45) Pesin, D.; Balents, L. Mott Physics and Band Topology in Materials with Strong Spin-Orbit Interaction. *Nat. Phys.* **2010**, *6* (5), 376–381 DOI: 10.1038/nphys1606.
- (46) Kim, J.; Said, A. H.; Casa, D.; Upton, M. H.; Gog, T.; Daghofer, M.; Jackeli, G.; Van Den Brink, J.; Khaliullin, G.; Kim, B. J.; Brink, J. Van Den; Khaliullin, G.; Kim, B. J.;

- Van Den Brink, J.; Khaliullin, G.; Kim, B. J. Large Spin-Wave Energy Gap in the Bilayer Iridate Sr₃Ir₂O₇: Evidence for Enhanced Dipolar Interactions Near the Mott Metal-Insulator Transition. *Phys. Rev. Lett.* **2012**, *157402* (October), 1–5 DOI: 10.1103/PhysRevLett.109.157402.
- (47) Hinatsu, Y. Diverse Structures of Mixed-Metal Oxides Containing Rare Earths and Their Magnetic Properties. *Nippon Seramikkusu Kyokai Gakujutsu Ronbunshi/Journal Ceram. Soc. Japan* **2015**, *123* (1441), 845–852 DOI: 10.2109/jcersj2.123.845.
- (48) Singh, V.; Pulikkotil, J. J. Theoretical Study of Coulomb Correlations and Spin-Orbit Coupling in SrIrO₃. In *AIP Conference Proceedings*; American Institute of Physics Inc., 2015; Vol. 1665, p 090034.
- (49) Zhao, J.; Yang, L.; Yu, Y.; Li, F.; Yu, R.; Jin, C. Structural and Physical Properties of the 6M BaIrO₃: A New Metallic Iridate Synthesized under High Pressure. *Inorg. Chem.* **2009**, *48* (10), 4290–4294 DOI: 10.1021/ic801707m.
- (50) Bremholm, M.; Yim, C. K.; Hirai, D.; Climent-Pascual, E.; Xu, Q.; Zandbergen, H. W.; Ali, M. N.; Cava, R. J. Destabilization of the 6H-SrIrO₃ Polymorph through Partial Substitution of Zinc and Lithium. *J. Mater. Chem.* **2012**, *22* (32), 16431–16436 DOI: 10.1039/c2jm32558f.
- (51) Okuda, T.; Kobayashi, K. I.; Tomioka, Y.; Tokura, Y. Anomalous Low-Temperature Specific Heat around the Metal-Insulator Transition in Ordered Double-Perovskite Alloys Sr₂Fe(Mo₁-YW_y)O₆ (0 < y < 1). *Phys. Rev. B - Condens. Matter Mater. Phys.* **2003**, *68* (14), 144407 DOI: 10.1103/PhysRevB.68.144407.
- (52) King, G.; Abakumov, A. M.; Hadermann, J.; Alekseeva, A. M.; Rozova, M. G.; Perikis, T.; Woodward, P. M.; Van Tendeloo, G.; Antipov, E. V. Crystal Structure and Phase Transitions in Sr₃WO₆. *Inorg. Chem.* **2010**, *49* (13), 6058–6065 DOI: 10.1021/ic100598v.
- (53) Sinha, M.; Pearson, T. J.; Reeder, T. R.; Vivanco, H. K.; Freedman, D. E.; Phelan, W. A.; McQueen, T. M. Introduction of Spin Centers in Single Crystals of Ba₂CaW_{0.6}Os_{0.4}. *Phys. Rev. Mater.* **2019**, *3* (12), 125002 DOI: 10.1103/PhysRevMaterials.3.125002.
- (54) Barnes, P. W.; Lufaso, M. W.; Woodward, P. M. Structure Determination of A₂M₃+TaO₆ and A₂M₃+NbO₆ Ordered Perovskites: Octahedral Tilting and Pseudosymmetry. *Acta Crystallogr. Sect. B Struct. Sci.* **2006**, *62* (3), 384–396 DOI: 10.1107/S0108768106002448.
- (55) Yamamura, K.; Wakeshima, M.; Hinatsu, Y. Structural Phase Transition and Magnetic Properties of Double Perovskites Ba₂CaMO₆ (M=W, Re, Os). *J. Solid State Chem.* **2006**, *179* (3), 605–612 DOI: 10.1016/j.jssc.2005.10.003.
- (56) Nguyen, L. T.; Cava, R. J.; Fry-Petit, A. M. Low Temperature Structural Phase Transition in the Ba₂CaMoO₆ Perovskite. *J. Solid State Chem.* **2019**, *277* (June), 415–421 DOI: 10.1016/j.jssc.2019.06.037.
- (57) Morrow, R.; McGuire, M. A.; Yan, J.; Woodward, P. M. The Crystal Structure and Magnetic Behavior of Quinary Osmate and Ruthenate Double Perovskites La₃AB₂B'Os₂O₁₂ (A = Ca, Sr; B = Co, Ni; B' = Ru, Os). *Inorg. Chem.* **2018**, *57* (6), 2989–3001 DOI: 10.1021/acs.inorgchem.7b02282.
- (58) Yan, B.; Jansen, M.; Felser, C. A Large-Energy-Gap Oxide Topological Insulator Based on the Superconductor BaBiO₃. *Nat. Phys.* **2013**, *9* (11), 709–711 DOI: 10.1038/nphys2762.
- (59) Schoop, L. M.; Muehler, L.; Felser, C.; Cava, R. J. Lone Pair Effect, Structural Distortions, and Potential for Superconductivity in Tl Perovskites. *Inorg. Chem.* **2013**, *52* (9), 5479–5483 DOI: 10.1021/ic400381g.
- (60) Levin, I.; Chan, J. Y.; Geyer, R. G.; Maslar, J. E.; Vanderah, T. A. Cation Ordering Types and Dielectric Properties in the Complex Perovskite Ca(Ca_{1/3}Nb_{2/3})O₃. *J. Solid State Chem.* **2001**, *156* (1), 122–134 DOI: 10.1006/jssc.2000.8971.
- (61) Levin, I.; Bendersky, L. A.; Cline, J. P.; Roth, R. S.; Vanderah, T. A. Octahedral Tilting and Cation Ordering in Perovskite-Like Ca₄Nb₂O₉=3•Ca(Ca_{1/3}Nb_{2/3})O₃ Polymorphs. *J. Solid State Chem.* **2000**, *150* (1), 43–61 DOI: 10.1006/jssc.1999.8547.
- (62) Fry, A. M.; Woodward, P. M. Structures of α-K₃MoO₃F₃ and α-Rb₃MoO₃F₃: Ferroelectricity from Anion Ordering and Noncooperative Octahedral Tilting. *Cryst. Growth Des.* **2013**, *13* (12), 5404–5410 DOI: 10.1021/cg401342q.
- (63) Arevalo-Lopez, A. M.; Senn, M. S.; Skedd, L.; Attfield, J. P. High Pressure Synthesis of the Cation-Ordered Perovskite 3Ca₁-2-Ba₃NaRu₂O₉. *Zeitschrift für Anorg. und Allg. Chemie* **2014**, *640* (6), 1164–1167 DOI: 10.1002/zaac.201300549.
- (64) Stitzer, K. E.; Smith, M. D.; Gemmill, W. R.; Zur Loye, H. C. Novel Mixed-Valent (V/VI) Triple Perovskite Ruthenates: Observation of a Complex Low-Temperature Structural and Magnetic Transition. *J. Am. Chem. Soc.* **2002**, *124* (46), 13877–13885 DOI: 10.1021/ja0271781.
- (65) Samata, H.; Kai, M.; Uchida, T.; Ohtsuka, M.; Tanaka, G.; Sawada, S.; Taniguchi, T.; Nagata, Y. Synthesis and Properties of Ba₃NaRu₂O₉-δ and Ba₃(Na, R)Ru₂O₉-δ (R=rare Earth) Crystals. *J. Alloys Compd.* **2003**, *350* (1–2), 77–85 DOI: 10.1016/S0925-8388(02)00990-8.
- (66) Køuhl, P. Die Kristallstruktur Der Hexagonalen Verbindungen Ba₃IIIMe₂Sb₂V₂O₉. II. Ba₃CuSb₂O₉. *Zeitschrift für Anorg. und Allg. Chemie* **1978**, *442* (1), 280–288 DOI: 10.1002/zaac.19784420136.
- (67) Anderson, P. W. Resonating Valence Bonds: A New

- Kind of Insulator? *Mater. Res. Bull.* **1973**, *8* (2), 153–160 DOI: 10.1016/0025-5408(73)90167-0.
- (68) Anderson, P. W.; Baskaran, G.; Zou, Z.; Hsu, T. Resonating Valence-Bond Theory of Phase Transitions and Superconductivity in La₂CuO₄-Based Compounds. *Phys. Rev. Lett.* **1987**, *58* (26), 2790–2793 DOI: 10.1103/PhysRevLett.58.2790.
- (69) Baskaran, G.; Zou, Z.; Anderson, P. W. The Resonating Valence Bond State and High-T_c Superconductivity - A Mean Field Theory. *Solid State Commun.* **1987**, *63* (11), 973–976 DOI: 10.1016/0038-1098(87)90642-9.
- (70) Zhou, H. D.; Choi, E. S.; Li, G.; Balicas, L.; Wiebe, C. R.; Qiu, Y.; Copley, J. R. D.; Gardner, J. S. Spin Liquid State in the S=1/2 Triangular Lattice Ba₃CuSb₂O₉. *Phys. Rev. Lett.* **2011**, *106* (14) DOI: 10.1103/PhysRevLett.106.147204.
- (71) Katayama, N.; Kimura, K.; Han, Y.; Nasu, J.; Drichko, N.; Nakanishi, Y.; Halim, M.; Ishiguro, Y.; Satake, R.; Nishibori, E.; Yoshizawa, M.; Nakano, T.; Nozue, Y.; Wakabayashi, Y.; Ishihara, S.; Hagiwara, M.; Sawa, H.; Nakatsuji, S. Absence of Jahn–Teller Transition in the Hexagonal Ba₃CuSb₂O₉ Single Crystal. *Proc. Natl. Acad. Sci.* **2015**, *112* (30), 9305–9309 DOI: 10.1073/pnas.1508941112.
- (72) Chen, J.; Feng, H. L.; Matsushita, Y.; Belik, A. A.; Tsujimoto, Y.; Katsuya, Y.; Tanaka, M.; Wu, M.; Li, M. R.; Zhou, R.; Zhou, W.; Liang, H.; Zheng, L.; Jansen, M.; Yamaura, K. High-Pressure Synthesis, Crystal Structure, and Magnetic Properties of Hexagonal Ba₃CuOs₂O₉. *J. Solid State Chem.* **2019**, *272* (January), 182–188 DOI: 10.1016/j.jssc.2019.02.003.
- (73) Prabhakaran, D.; Boothroyd, A. T. Crystal Growth of the Triangular-Lattice Antiferromagnet Ba₃CoSb₂O₉. *J. Cryst. Growth* **2017**, *468*, 345–348 DOI: 10.1016/j.jcrysgro.2016.10.075.
- (74) Koutroulakis, G.; Zhou, T.; Kamiya, Y.; Thompson, J. D.; Zhou, H. D.; Batista, C. D.; Brown, S. E. Quantum Phase Diagram of the S = 1/2 Triangular-Lattice Antiferromagnet Ba₃CoSb₂O₉. *Phys. Rev. B* **2015**, *91*, 24410 DOI: 10.1103/PhysRevB.91.024410.
- (75) Ghioldi, E. A.; Mezio, A.; Manuel, L. O.; Singh, R. R. P.; Oitmaa, J.; Trumper, A. E. Magnons and Excitation Continuum in XXZ Triangular Antiferromagnetic Model: Application to Ba₃CoSb₂O₉. *Phys. Rev. B* **2015**, *91*, 134423 DOI: 10.1103/PhysRevB.91.134423.
- (76) Quirion, G.; Lapointe-Major, M.; Poirier, M.; Quilliam, J. A.; Dun, Z. L.; Zhou, H. D. Magnetic Phase Diagram of Ba₃CoSb₂O₉ as Determined by Ultrasound Velocity Measurements. *Phys. Rev. B* **2015**, *92*, 14414 DOI: 10.1103/PhysRevB.92.014414.
- (77) Antiferromagnet Ba₃H; Susuki, T.; Kurita, N.; Tanaka, T.; Nojiri, H.; Matsuo, A.; Kindo, K.; Tanaka, H. Magnetization Process and Collective Excitations in the S = 1/2 Triangular-Lattice. **2013** DOI: 10.1103/PhysRevLett.110.267201.
- (78) Li, M.; Zelenskiy, A.; Quilliam, J. A.; Dun, Z. L.; Zhou, H. D.; Plumer, M. L.; Quirion, G. Magnetoelastic Coupling and the Magnetization Plateau in Ba₃CoSb₂O₉. *Phys. Rev. B* **2019**, *99* DOI: 10.1103/PhysRevB.99.094408.
- (79) Sera, A.; Kousaka, Y.; Akimitsu, J.; Sera, M.; Kawamata, T.; Koike, Y.; Inoue, K. S = 1/2 Triangular-Lattice Antiferromagnets Ba₃CoSb₂O₉ and CsCuCl₃: Role of Spin-Orbit Coupling, Crystalline Electric Field Effect, and Dzyaloshinskii-Moriya Interaction. *Phys. Rev. B* **2016**, *94*, 214408 DOI: 10.1103/PhysRevB.94.214408.
- (80) Ba, A.; Ma, J.; Kamiya, Y.; Hong, T.; Cao, H. B.; Ehlers, G.; Tian, W.; Batista, C. D.; Dun, Z. L.; Zhou, H. D.; Matsuda, M. Static and Dynamical Properties of the Spin-1=2 Equilateral Triangular-Lattice. **2016** DOI: 10.1103/PhysRevLett.116.087201.
- (81) Clauss, C.; Dressel, M.; Scheffler, M. Thermal Conductivity in the Triangular-Lattice Antiferromagnet Ba₃CoSb₂O₉. *J. Phys. Conf. Ser.* **2014**, *568*, 42014 DOI: 10.1088/1742-6596/568/4/042014.
- (82) Zhou, H. D.; Xu, C.; Hallas, A. M.; Silverstein, H. J.; Wiebe, C. R.; Umegaki, I.; Yan, J. Q.; Murphy, T. P.; Park, J. H.; Qiu, Y.; Copley, J. R. D.; Gardner, J. S.; Takano, Y. Successive Phase Transitions and Extended Spin-Excitation Continuum in the S=12 Triangular-Lattice Antiferromagnet Ba₃CoSb₂O₉. *Phys. Rev. Lett.* **2012**, *109* (26) DOI: 10.1103/PhysRevLett.109.267206.
- (83) Shikano, M.; Ishiyama, O.; Inaguma, Y.; Nakamura, T.; Itoh, M. Structure and Magnetic Properties of 6-Layered Hexagonal Oxides Ba₃Cr₂MO₉ (M = Mo and W). *J. Solid State Chem.* **1995**, *120* (2), 238–243 DOI: 10.1006/jssc.1995.1404.
- (84) Rijssenbeek, J. T.; Huang, Q.; Erwin, R. W.; Zandbergen, H. W.; Cava, R. J. The Crystal Structure of Ba₃CuRu₂O₉ and Comparison to Ba₃MRu₂O₉ (M=In, Co, Ni, and Fe). *J. Solid State Chem.* **1999**, *146* (1), 65–72 DOI: 10.1006/jssc.1999.8309.
- (85) Wilkens, J.; Müller-Buschbaum, H. Einkristalluntersuchung an Ba₃CaRu₂O₉. *J. Alloys Compd.* **1991**, *177* (2), L31–L33 DOI: 10.1016/0925-8388(91)90071-3.
- (86) Beran, P.; Ivanov, S. A.; Nordblad, P.; Middey, S.; Nag, A.; Sarma, D. D.; Ray, S.; Mathieu, R. Neutron Powder Diffraction Study of Ba₃ZnRu₂X₁rxO₉ (x = 0, 1, 2) with 6H-Type Perovskite Structure. *Solid State Sci.* **2015**, *50*, 58–64 DOI: 10.1016/j.solidstatesciences.2015.10.011.
- (87) Treiber, U.; Kemmler-Sack, S.; Ehmann, A. Edelmetallhaltige Sauerstoffperovskite Vom Typ Ba₃BM₂O₉ Mit B=Mg, Fe, Co, Ni, Zn, Cd; M=Ru, Ir. *Zeitschrift für Anorg. und Allg. Chemie* **1982**, *487* (1), 189–198 DOI: 10.1002/zaac.19824870117.
- (88) Lightfoot, P.; Battle, P. D. The Crystal and Magnetic

- Structures of Ba₃NiRu₂O₉, Ba₃CoRu₂O₉, and Ba₃ZnRu₂O₉. *J. Solid State Chem.* **1990**, *89* (1), 174–183 DOI: 10.1016/0022-4596(90)90309-L.
- (89) Zandbergen, H. W.; Ijdo, D. J. W. Tribarium Strontium Diruthenate(V), Ba₃SrRu₂O₉, a Rietveld Refinement of Neutron Powder Diffraction Data. *Acta Crystallogr. Sect. C Cryst. Struct. Commun.* **1984**, *40* (6), 919–922 DOI: 10.1107/S0108270184006272.
- (90) Shlyk, L.; Kryukov, S.; Durairaj, V.; Parkin, S.; Cao, G.; De Long, L. E. Magnetic, and Electronic Properties of a Ba₃InRu₂O₉ Single Crystal. *J. Magn. Magn. Mater.* **2007**, *319* (1–2), 64–68 DOI: 10.1016/j.jmmm.2007.04.033.
- (91) Ziat, D.; Aczel, A. A.; Sinclair, R.; Chen, Q.; Zhou, H. D.; Williams, T. J.; Stone, M. B.; Verrier, A.; Quilliam, J. A. Frustrated Spin-1/2 Molecular Magnetism in the Mixed-Valence Antiferromagnets Ba₃MRu₂O₉ (M = In, Y, Lu). *Phys. Rev. B* **2017**, *95*, 184424 DOI: 10.1103/PhysRevB.95.184424.
- (92) Schaller, H.-U.; Kemmler-sack, S. Über Ruthenium-Perovskite Vom Typ Ba₃BRu₂O₉ Und Ba₃BRu₂O₉, Mit B = Indium, Rhodium. *Zeitschrift für Anorg. und Allg. Chemie* **1981**, *473* (2), 178–188 DOI: 10.1002/zaac.19814730220.
- (93) Huang, Z.; Avdeev, M.; Kennedy, B. J.; Knight, K. S.; Zhou, Q.; Ling, C. D. Tuning the Giant Magnetoelastic Transition in Ba₃BiRu₂O₉ and Ba₃BiRu₂O₉. *J. Phys. Condens. Matter* **2014**, *26* (27), 276003 DOI: 10.1088/0953-8984/26/27/276003.
- (94) Müller, W.; Avdeev, M.; Zhou, Q.; Studer, A. J.; Kennedy, B. J.; Kearley, G. J.; Ling, C. D. Spin-Gap Opening Accompanied by a Strong Magnetoelastic Response in the S=1 Magnetic Dimer System Ba₃BiRu₂O₉. *Phys. Rev. B - Condens. Matter Mater. Phys.* **2011**, *84* (22), 4–7 DOI: 10.1103/PhysRevB.84.220406.
- (95) Blanchard, P. E. R.; Chapman, K. W.; Heald, S. M.; Zbiri, M.; Johnson, M. R.; Kennedy, B. J.; Ling, C. D. Direct Observation of Pressure-Driven Valence Electron Transfer in Ba₃BiRu₂O₉, Ba₃BiIr₂O₉, and Ba₄BiIr₃O₁₂. *Inorg. Chem.* **2016**, *55* (11), 5649–5654 DOI: 10.1021/acs.inorgchem.6b00718.
- (96) Blanchard, P. E. R.; Huang, Z.; Kennedy, B. J.; Liu, S.; Müller, W.; Reynolds, E.; Zhou, Q.; Avdeev, M.; Zhang, Z.; Aitken, J. B.; Cowie, B. C. C.; Jang, L. Y.; Tan, T. T.; Li, S.; Ling, C. D. Key Role of Bismuth in the Magnetoelastic Transitions of Ba₃BiRu₂O₉ and Ba₃BiIr₂O₉ as Revealed by Chemical Doping. *Inorg. Chem.* **2014**, *53* (2), 952–960 DOI: 10.1021/ic4023745.
- (97) Verdoes, D.; Zandbergen, H. W.; Ijdo, D. J. W. Tribarium Titanium(IV) Diruthenate(IV), Ba₃TiRu₂O₉, a Rietveld Refinement of Neutron Powder Diffraction Data. *Acta Crystallogr. Sect. C Cryst. Struct. Commun.* **1985**, *41* (2), 170–173 DOI: 10.1107/S0108270185003201.
- (98) Nguyen, L. T.; Cava, R. J. A Spin Glass State in Ba₃TiRu₂O₉. *J. Magn. Magn. Mater.* **2019**, *476* (December 2018), 334–336 DOI: 10.1016/j.jmmm.2018.12.087.
- (99) Gönen, Z. S.; Gopalakrishnan, J.; Eichhorn, B. W.; Greene, R. L. Structurally Modulated Magnetic Properties in the A₃MnRu₂O₉ Phases (A = Ba, Ca): The Role of Metal-Metal Bonding in Perovskite-Related Oxides. *Inorg. Chem.* **2001**, *40* (19), 4996–5000 DOI: 10.1021/ic0013431.
- (100) Rijssenbeek, J. T.; Malo, S.; Caignaert, V.; Poeppelmeier, K. R. Site and Oxidation-State Specificity Yielding Dimensional Control in Perovskite Ruthenates. *J. Am. Chem. Soc.* **2002**, *124* (10), 2090–2091 DOI: 10.1021/ja017586p.
- (101) Wallace, D. C.; McQueen, T. M. New Honeycomb Iridium(v) Oxides: NaIrO₃ and Sr₃CaIr₂O₉. *Dalt. Trans.* **2015**, *44* (47), 20344–20351 DOI: 10.1039/c5dt03188e.
- (102) Sakamoto, T.; Doi, Y.; Hinatsu, Y. Crystal Structures and Magnetic Properties of 6H-Perovskite-Type Oxides Ba₃M₂Ir₂O₉ (M=Mg, Ca, Sc, Ti, Zn, Sr, Zr, Cd and In). *J. Solid State Chem.* **2006**, *179* (8), 2595–2601 DOI: 10.1016/j.jssc.2006.04.055.
- (103) Doi, Y.; Hinatsu, Y. The Structural and Magnetic Characterization of 6H-Perovskite-Type Oxides Ba₃LnIr₂O₉ (Ln = Y, Lanthanides). *J. Phys. Condens. Matter* **2004**, *16* (16), 2849–2860 DOI: 10.1088/0953-8984/16/16/009.
- (104) Dey, T.; Majumder, M.; Orain, J. C.; Senyshyn, A.; Prinz-Zwick, M.; Bachus, S.; Tokiwa, Y.; Bert, F.; Khuntia, P.; Büttgen, N.; Tsirlin, A. A.; Gegenwart, P. Persistent Low-Temperature Spin Dynamics in the Mixed-Valence Iridate Ba₃InIr₂O₉. *Phys. Rev. B* **2017**, *96*, 174411 DOI: 10.1103/PhysRevB.96.174411.
- (105) Kumar, R.; Sheptyakov, D.; Khuntia, P.; Rolfs, K.; Freeman, P. G.; Rønnow, H. M.; Dey, T.; Baenitz, M.; Mahajan, A. V. Ba₃M_xTi_{3-x}O₉ (M = Ir, Rh): A Family of 5d/4d-Based Diluted Quantum Spin Liquids. *Phys. Rev. B* **2016**, *94*, 174410 DOI: 10.1103/PhysRevB.94.174410.
- (106) Catuneanu, A.; Rau, J. G.; Kim, H.-S.; Kee, H.-Y. Magnetic Orders Proximal to the Kitaev Limit in Frustrated Triangular Systems: Application to Ba₃IrTi₂O₉. *Phys. Rev. B* **2015**, *92*, 165108 DOI: 10.1103/PhysRevB.92.165108.
- (107) Becker, M.; Hermanns, M.; Bauer, B.; Garst, M.; Trebst, S. Spin-Orbit Physics of J= 12 Mott Insulators on the Triangular Lattice. *Phys. Rev. B - Condens. Matter Mater. Phys.* **2015**, *91*, 155135 DOI: 10.1103/PhysRevB.91.155135.
- (108) Bhowal, S.; Ganguly, S.; Dasgupta, I. Spin-Orbit Coupling Driven Novel Magnetism in d⁵ 6H-Perovskite Iridates Ba₃IrTi₂O₉ and Ba₃TiIr₂O₉. *J. Phys. Condens. Matter* **2019**, *31* (18), 185802 DOI:

- (109) Byrne, R. C.; Moeller, C. W. Magnetic Interactions of Ruthenium, Rhodium, and Iridium in the Hexagonal Barium Titanate Structure. *J. Solid State Chem.* **1970**, *2* (2), 228–235 DOI: 10.1016/0022-4596(70)90075-7.
- (110) Dey, T.; Mahajan, A. V.; Khuntia, P.; Baenitz, M.; Koteswararao, B.; Chou, F. C. Spin-Liquid Behavior in J Eff = 1 2 Triangular Lattice Compound $Ba_3IrTi_2O_9$. *RAPID Commun. Phys. Rev. B* **2012**, *86*, 140405 DOI: 10.1103/PhysRevB.86.140405.
- (111) Lee, W.-J.; Do, S.-H.; Yoon, S.; Lee, S.; Choi, Y. S.; Jang, D. J.; Brando, M.; Lee, M.; Choi, E. S.; Ji, S.; Jang, Z. H.; Suh, B. J.; Choi, K.-Y. Putative Spin Liquid in the Triangle-Based Iridate $Ba_3IrTi_2O_9$. *Phys. Rev. B* **2017**, *96*, 14432 DOI: 10.1103/PhysRevB.96.014432.
- (112) Bhowal, S.; Satpathy, S. Dirac Nodal Lines and Large Spin Hall Effect in the 6H-Perovskite Iridate $Ba_3TiIr_2O_9$. *Phys. Rev. B* **2019**, *100* (11), 115101 DOI: 10.1103/PhysRevB.100.115101.
- (113) Paddison, J. A. M.; Daum, M.; Dun, Z.; Ehlers, G.; Liu, Y.; Stone, M. B.; Zhou, H.; Mourigal, M. Continuous Excitations of the Triangular-Lattice Quantum Spin Liquid $YbMgGaO_4$. *Nat. Phys.* **2017**, *13* (2), 117–122 DOI: 10.1038/nphys3971.
- (114) Zhang, X.; Mahmood, F.; Daum, M.; Dun, Z.; Paddison, J. A. M.; Laurita, N. J.; Hong, T.; Zhou, H.; Armitage, N. P.; Mourigal, M. Hierarchy of Exchange Interactions in the Triangular-Lattice Spin Liquid $YbMgGaO_4$. *Phys. Rev. X* **2018**, *8* (3), 031001 DOI: 10.1103/PhysRevX.8.031001.
- (115) Zhu, Z.; Maksimov, P. A.; White, S. R.; Chernyshev, A. L. Disorder-Induced Mimicry of a Spin Liquid in $YbMgGaO_4$. *Phys. Rev. Lett.* **2017**, *119* (15), 157201 DOI: 10.1103/PhysRevLett.119.157201.
- (116) Ferreira, T.; Carone, D.; Huon, A.; Herklotz, A.; Stoian, S. A.; Heald, S. M.; Morrison, G.; Smith, M. D.; Loye, H. C. Zur. $Ba_3Fe_{1.56}Ir_{1.44}O_9$: A Polar Semiconducting Triple Perovskite with Near Room Temperature Magnetic Ordering. *Inorg. Chem.* **2018**, *57* (12), 7362–7371 DOI: 10.1021/acs.inorgchem.8b01015.
- (117) Doi, Y.; Matsuhira, K.; Hinatsu, Y. Crystal Structures and Magnetic Properties of 6H-Perovskites $Ba_3MRu_2O_9$ ($M = Y, In, La, Sm, Eu, \text{ and } Lu$). *J. Solid State Chem.* **2002**, *165* (2), 317–323 DOI: 10.1006/jssc.2002.9538.
- (118) Doi, Y.; Wakeshima, M.; Hinatsu, Y.; Tobo, A.; Ohoyama, K.; Yamaguchi, Y. Magnetic and Calorimetric Studies on 6H-Perovskite $Ba_3TbRu_2O_9$. *J. Alloys Compd.* **2002**, *344* (1–2), 166–169 DOI: 10.1016/S0925-8388(02)00333-X.
- (119) Chen, Q.; Fan, S.; Taddei, K. M.; Stone, M. B.; Kolesnikov, A. I.; Cheng, J.; Musfeldt, J. L.; Zhou, H.; Aczel, A. A. Large Positive Zero-Field Splitting in the Cluster Magnet $Ba_3CeRu_2O_9$. *J. Am. Chem. Soc.* **2019**, *141* (25), 9928–
- (120) Hinatsu, Y.; Oyama, S.; Doi, Y. The Magnetic Susceptibilities and Electron Paramagnetic Resonance Spectra of 6H-Perovskites $Ba_3PrM_2O_9$ ($M = Ir, Ru$). *Bull. Chem. Soc. Jpn.* **2004**, *77* (8), 1479–1483 DOI: 10.1246/bcsj.77.1479.
- (121) Doi, Y.; Wakeshima, M.; Hinatsu, Y.; Tobo, A.; Ohoyama, K.; Yamaguchi, Y. Crystal Structures and Magnetic Properties of the 6H-Perovskites $Ba_3LnRu_2O_9$ ($Ln = Ce, Pr \text{ and } Tb$). *J. Mater. Chem.* **2001**, *11* (12), 3135–3140 DOI: 10.1039/b105134m.
- (122) Chemie, A. Weitere Verbindungen Mit Verwandtschaft Zum α - Ba_2ScAlO_5 -Typ: $Ba_6Rh_2,33Yb_2Al_{1,67}O_{15}$, $Ba_5,5Ca_0,5Rh_2Y_2Al_2O_{15}$ Und $Ba_6Rh_4Al_2O_{15}$. *J. Alloys Compd.* **1993**, *197*, 51–55.
- (123) Revelli, A.; Moretti Sala, M.; Monaco, G.; Becker, P.; Bohatý, L.; Hermanns, M.; Koethe, T. C.; Fröhlich, T.; Warzanowski, P.; Lorenz, T.; Streltsov, S. V.; van Loosdrecht, P. H. M.; Khomskii, D. I.; van den Brink, J.; Grüninger, M. Resonant Inelastic X-Ray Incarnation of Young's Double-Slit Experiment. *Sci. Adv.* **2019**, *5* (1), eaav4020 DOI: 10.1126/sciadv.aav4020.
- (124) Mukhin, A. A.; Ivanov, V. Y.; Travkin, V. D.; Balbashov, A. M. Magnetic Anisotropy and Ground State of the Rare-Earth Ions in $PrMnO_3$ and $NdMnO_3$. *J. Magn. Mater.* **2001**, *226–230* (PART II), 1139 DOI: 10.1016/S0304-8853(00)00710-1.
- (125) Lufaso, M. W.; Zur Loye, H. C. Crystal Structures and Magnetic Properties of Mixed Iridium-Ruthenium Triple Perovskites. 1. $Ba_3MRuIrO_9$ ($M = \text{Lanthanide}, Y$). *Inorg. Chem.* **2005**, *44* (25), 9143–9153 DOI: 10.1021/ic051344z.
- (126) Nguyen, L. T.; Kong, T.; Cava, R. J. Trimers of MnO_6 Octahedra and Magnetic Ordering in $Ba_4NbMn_3O_{12}$. **2019**, 1–18.
- (127) Nguyen, L. T.; Halloran, T.; Xie, W.; Kong, T.; Broholm, C. L.; Cava, R. J. Geometrically Frustrated Trimer-Based Mott Insulator. *Phys. Rev. Mater.* **2018**, *2* (5), 054414 DOI: 10.1103/PhysRevMaterials.2.054414.
- (128) Drillon, M.; Darriet, J.; Hagenmuller, P.; Georges, R. Etude d'un Groupement $(Ru_3O_{12})_{13}$ – En Presence de Degenerescence Orbitale et de Couplage Spin-Orbite. *J. Phys. Chem. Solids* **1980**, *41* (5), 507–515 DOI: 10.1016/0022-3697(80)90182-1.
- (129) Shimoda, Y.; Doi, Y.; Hinatsu, Y.; Ohoyama, K. Synthesis, Crystal Structures, and Magnetic Properties of New 12L-Perovskites $Ba_4LnRu_3O_{12}$ ($Ln = \text{Lanthanides}$). *Chem. Mater.* **2008**, *20* (13), 4512–4518 DOI: 10.1021/cm800708g.
- (130) Shimoda, Y.; Doi, Y.; Wakeshima, M.; Hinatsu, Y. Magnetic Properties of Quadruple Perovskites $Ba_4LnRu_3O_{12}$ ($Ln = La, Nd, Sm-Gd, Dy-Lu$). *J. Solid State Chem.* **2010**, *183* (1), 33–40 DOI:

10.1016/j.jssc.2009.10.007.

- (131) Shimoda, Y.; Doi, Y.; Wakeshima, M.; Hinatsu, Y. Synthesis and Magnetic Properties of 12L-Perovskites Ba₄LnIr₃O₁₂ (Ln=lanthanides). *J. Solid State Chem.* **2009**, *182* (10), 2873–2879 DOI: 10.1016/j.jssc.2009.07.056.
- (132) Landau, L. D., & Lifshitz, E. M. (2013). Quantum mechanics: non-relativistic theory (Vol. 3). Elsevier.
- (133) Rashba, E. I. Spin–Orbit Coupling Goes Global. *J. Phys. Condens. Matter* **2016**, *28* (42), 421004 DOI: 10.1088/0953-8984/28/42/421004.
- (134) Müller, W.; Dunstan, M. T.; Huang, Z.; Mohamed, Z.; Kennedy, B. J.; Avdeev, M.; Ling, C. D. Complex 5d Magnetism in a Novel S = 1/2 Trimer System, the 12L Hexagonal Perovskite Ba₄BiIr₃O₁₂. *Inorg. Chem.* **2013**, *52* (21), 12461–12467 DOI: 10.1021/ic4014619.
- (135) Müller, W.; Avdeev, M.; Zhou, Q.; Kennedy, B. J.; Sharma, N.; Kutteh, R.; Kearley, G. J.; Schmid, S.; Knight, K. S.; Blanchard, P. E. R.; Ling, C. D. Giant Magnetoelastic Effect at the Opening of a Spin-Gap in Ba₃BiIr₂O₉. *J. Am. Chem. Soc.* **2012**, *134* (6), 3265–3270 DOI: 10.1021/ja211517h.
- (136) Colabello, D. M.; Sobalvarro, E. M.; Sheckelton, J. P.; Neufeind, J. C.; Mcqueen, T. M.; Khalifah, P. G. Observation of Vacancies, Faults, and Superstructures in Ln₅Mo₂O₁₂ (Ln = La, Y, and Lu) Compounds with Direct Mo–Mo Bonding. *Inorg. Chem.* **2017**, *56*, 12866–12880 DOI: 10.1021/acs.inorgchem.6b02531.
- (137) Streltsov, S. V.; Khomskii, D. I. Cluster Magnetism of Ba₄NbMn₃O₁₂: Localized Electrons or Molecular Orbitals? 1. *JETP Lett.* **2018**, *108* (10), 686–690 DOI: 10.1134/S0021364018220071.
- (138) Shimoda, Y.; Doi, Y.; Wakeshima, M.; Hinatsu, Y. Magnetic and Electrical Properties of Quadruple Perovskites with 12 Layer Structures Ba₄LnM₃O₁₂ (Ln=rare Earths; M=Ru, Ir): The Role of Metal–Metal Bonding in Perovskite-Related Oxides. *J. Solid State Chem.* **2010**, *183* (9), 1962–1969 DOI: 10.1016/j.jssc.2010.06.023.
- (139) Shimoda, Y.; Doi, Y.; Wakeshima, M.; Hinatsu, Y. Crystal Structures and Characterizations of Mixed Valence 12 L-Perovskites Ba₄EuM₃O₁₂ (M = Ru and Ir). *Inorg. Chem.* **2009**, *48* (20), 9952–9957 DOI: 10.1021/ic9009652.
- (140) Takizawa, H.; Steinfink, H. Preparation and the Crystal Structure of Ten-Layer Ba₅Fe₄NiO_{13.5}. *J. Solid State Chem.* **1996**, *121* (1), 133–137 DOI: 10.1006/jssc.1996.0019.
- (141) Tan, Z.; Saito, T.; Denis Romero, F.; Amano Patino, M.; Goto, M.; Chen, W. T.; Chuang, Y. C.; Sheu, H. S.; Shimakawa, Y. Hexagonal Perovskite Ba₄Fe₃NiO₁₂ Containing Tetravalent Fe and Ni Ions. *Inorg. Chem.* **2018**, *57* (16), 10410–10415 DOI: 10.1021/acs.inorgchem.8b01618.
- (142) Ferreira, T.; Heald, S. M.; Smith, M. D.; zur Loye, H.-C. C. Unusual Coexistence of Nickel(II) and Nickel(IV) in the Quadruple Perovskite Ba₄Ni₂Ir₂O₁₂ Containing Ir₂NiO₁₂ Mixed-Metal-Cation Trimers. *Inorg. Chem.* **2018**, *57* (6), 2973–2976 DOI: 10.1021/acs.inorgchem.8b00249.
- (143) Kitagawa, K.; Takayama, T.; Matsumoto, Y.; Kato, A.; Takano, R.; Kishimoto, Y.; Bette, S.; Dinnebier, R.; Jackeli, G.; Takagi, H. A Spin-Orbital-Entangled Quantum Liquid on a Honeycomb Lattice. *Nature* **2018**, *554* (7692), 341–345 DOI: 10.1038/nature25482.
- (144) Wilkens, J.; Müller-Buschbaum, H. Ba₁₂Ir₁₂-XNb_xO₃₆ (x = 2,4) - Eine Neue Verbindung Mit 12R-Perowskit-Stapelvariante. *J. Alloys Compd.* **1991**, *176* (1), 141–146 DOI: 10.1016/0925-8388(91)90019-R.
- (145) Thakur, G. S.; Chattopadhyay, S.; Doert, T.; Herrmannsdörfer, T.; Felser, C. Crystal Growth of Spin-Frustrated Ba₄Nb_{0.8}Ir_{3.2}O₁₂: A Possible Spin Liquid Material. *Cryst. Growth Des.* **2020** DOI: 10.1021/acs.cgd.0c00262.
- (146) Rawl, R.; Lee, M.; Choi, E. S.; Li, G.; Chen, K. W.; Baumbach, R.; Dela Cruz, C. R.; Ma, J.; Zhou, H. D. Magnetic Properties of the Triangular Lattice Magnets A₄B'B₂O₁₂ (A=Ba, Sr, La; B'=Co, Ni, Mn; B= W, Re). *Phys. Rev. B* **2017**, *95* (17) DOI: 10.1103/PhysRevB.95.174438.
- (147) Doi, Y.; Wakeshima, M.; Tezuka, K.; Shan, Y. J.; Ohoyama, K.; Lee, S.; Torii, S.; Kamiyama, T.; Hinatsu, Y. Crystal Structures, Magnetic Properties, and DFT Calculation of B-Site Defected 12L-Perovskites Ba₂La₂MW₂O₁₂ (M = Mn, Co, Ni, Zn). *J. Phys. Condens. Matter* **2017**, *29* (36), 365802 DOI: 10.1088/1361-648X/aa7c9b.
- (148) Yin, C.; Li, G.; Kockelmann, W. A.; Liao, F.; Atfield, J. P.; Lin, J. Frustrated and Unfrustrated Magnetic Orders in the 10H Perovskite Ba₅Sb_{1-x}Mn_{4+x}O_{15-δ}. *Chem. Mater.* **2010**, *22* (10), 3269–3276 DOI: 10.1021/cm100578u.
- (149) Terzic, J.; Wang, J. C.; Ye, F.; Song, W. H.; Yuan, S. J.; Aswartham, S.; DeLong, L. E.; Streltsov, S. V.; Khomskii, D. I.; Cao, G. Coexisting Charge and Magnetic Orders in the Dimer-Chain Iridate B_{A5}AlI_{R2}O₁₁. *Phys. Rev. B - Condens. Matter Mater. Phys.* **2015**, *91* (23), 6–11 DOI: 10.1103/PhysRevB.91.235147.
- (150) Streltsov, S. V.; Khomskii, D. I. Covalent Bonds against Magnetism in Transition Metal Compounds. *Proc. Natl. Acad. Sci. U. S. A.* **2016**, *113* (38), 10491–10496 DOI: 10.1073/pnas.1606367113.
- (151) Streltsov, S. V.; Cao, G.; Khomskii, D. I. Suppression of Magnetism in Ba₅Allr₂O₁₁: Interplay of Hund's Coupling, Molecular Orbitals, and Spin-Orbit

- Interaction. *Phys. Rev. B* **2017**, 96 (1), 014434 DOI: 10.1103/PhysRevB.96.014434.
- (152) Wang, Y.; Wang, R.; Kim, J.; Upton, M. H.; Casa, D.; Gog, T.; Cao, G.; Kotliar, G.; Dean, M. P. M.; Liu, X. Direct Detection of Dimer Orbitals in Ba₅Allr₂O₁₁. **2019** DOI: 10.1103/PhysRevLett.122.106401.
- (153) Muller-Buschbaum, H.; Lang, C. Ba₅Allr₂O₁₁: Eine Neue Verbindung Mit Iridium(IV, V). *Zeitschrift für Anorg. und Allg. Chemie* **1989**, 568 (1), 29–34 DOI: 10.1002/zaac.19895680105.
- (154) Shpanchenko, R. V.; Abakumov, A. M.; Antipov, E. V.; Kovba, L. M. Crystal Structure of Ba₅In₂Al₂ZrO₁₃. *J. Alloys Compd.* **1994**, 206 (2), 185–188 DOI: 10.1016/0925-8388(94)90033-7.
- (155) Shpanchenko, R. V.; Abakumov, A. M.; Antipov, E. V.; Nistor, L.; Van Tendeloo, G.; Amelinckx, S. Structural Study of the New Complex Oxides Ba₅-YSr_yR₂-XAl₂Zr_{1+x}O_{13+x/2} (R = Gd-Lu, Y, Sc). *J. Solid State Chem.* **1995**, 118 (1), 180–192 DOI: 10.1006/jssc.1995.1329.
- (156) Quarez, E.; Abraham, F.; Mentré, O. Synthesis, Crystal Structure and Characterization of New 12H Hexagonal Perovskite-Related Oxides Ba₆M₂Na₂X₂₀₁₇ (M=Ru, Nb, Ta, Sb; X=V, Cr, Mn, P, As). *J. Solid State Chem.* **2003**, 176 (1), 137–150 DOI: 10.1016/S0022-4596(03)00379-7.
- (157) Kuang, X.; Jing, X.; Loong, C. K.; Lachowski, E. E.; Skakle, J. M. S.; West, A. R. A New Hexagonal 12-Layer Perovskite-Related Structure: Ba₆R₂Ti₄O₁₇ (R = Nd and Y). *Chem. Mater.* **2002**, 14 (10), 4359–4363 DOI: 10.1021/cm020374m.
- (158) Nguyen, L. T.; Cava, R. J. Structure and Magnetism of the Ba₆Y₂Rh₂Ti₂O₁₇ Hexagonal Perovskite. *arXiv Prepr. arXivXXXX.YYYYY*.
- (159) Clark, J. H.; Hayward, M. A. Structure, Magnetism, and Substitutional Chemistry of Cation-Ordered (Ba/Sr)_{5+n}Mn_{3+n}Cr₂O_{3n+14} Phases. *Chem. Mater.* **2008**, 20 (14), 4612–4618 DOI: 10.1021/cm8005138.
- (160) Floros, N.; Michel, C.; Hervieu, M.; Raveau, B. The N=2 Member of the New Layered Structural Family Ba_{5+n}Ca₂Mn_{3+n}O_{3n+14} Derived from the Hexagonal Perovskite: Ba₇Ca₂Mn₅O₂₀. *J. Solid State Chem.* **2002**, 168 (1), 11–17 DOI: 10.1006/jssc.2002.9667.
- (161) Kuang, X.; Allix, M.; Ibberson, R. M.; Claridge, J. B.; Niu, H.; Rosseinsky, M. J. Oxygen Vacancy Ordering Phenomena in the Mixed-Conducting Hexagonal Perovskite Ba₇y₂Mn₃Ti₂O₂₀. *Chem. Mater.* **2007**, 19 (11), 2884–2893 DOI: 10.1021/cm0626740.
- (162) Floros, N.; Michel, C.; Hervieu, M.; Raveau, B. A New Hexagonal 16L Perovskite-Related Structure: Ba₄Ca(1-x)Mn(3+x)O(12-δ). *Chem. Mater.* **2000**, 12 (10), 3197–3201 DOI: 10.1021/cm000277y.
- (163) Taguchi, H.; Takeda, Y.; Kanamaru, F.; Shimada, M.; Koizumi, M. *Barium Cobalt Trioxide*; 1977; Vol. 33.
- (164) Parras, M.; Varela, A.; Seehofer, H.; González-Calbet, J. M. HREM Study of the BaCoO_{3-y} System: Evidence for a New 5H Phase. *J. Solid State Chem.* **1995**, 120 (2), 327–331 DOI: 10.1006/jssc.1995.1416.
- (165) von Helmolt, R.; Wecker, J.; Holzapfel, B.; Schultz, L.; Samwer, K. Giant Negative Magnetoresistance in Perovskitelike La₂/3Ba₁/3MnO_x Ferromagnetic Films. *Phys. Rev. Lett.* **1993**, 71 (14), 2331–2333 DOI: 10.1103/PhysRevLett.71.2331.
- (166) Gushee, B. E.; Katz, L.; Ward, R. The Preparation of a Barium Cobalt Oxide and Other Phases with Similar Structures. *J. Am. Chem. Soc.* **1957** DOI: 10.1021/ja01578a004.
- (167) Jacobson, A. J.; Hutchison, J. L. An Investigation of the Structure of 12HBaCoO_{2.6} by Electron Microscopy and Powder Neutron Diffraction. *J. Solid State Chem.* **1980**, 35 (3), 334–340 DOI: 10.1016/0022-4596(80)90530-7.
- (168) Mihaela, I.; Marielle, H.; Renaut, N. BaCoO_{2.22}: The Most Oxygen-Deficient Certified Cubic Perovskite. *Dalt. Trans.* **2015** DOI: 10.1039/c4dt03874f.
- (169) de la Calle, C.; Alonso, J. A.; Fernández-Díaz, M. T. Polymorphism of Ba_{1-x}Sr_xCoO_{3-δ} (0 ≤ x ≤ 1) Perovskites: A Thermal and Structural Study by Neutron Diffraction. *Zeitschrift für Naturforsch. B* **2008**, 63 (6), 647–654 DOI: 10.1515/znbb-2008-0609.
- (170) Felser, C.; Yamaura, K.; Cava, R. J. The Electronic Structure of Hexagonal BaCoO₃. *J. Solid State Chem.* **1999**, 146 (2), 411–417 DOI: 10.1006/jssc.1999.8382.
- (171) Yamaura, K.; Cava, R. J. Magnetic, Electric and Thermoelectric Properties of the Quasi-1D Cobalt Oxides Ba_{1-x}LaxCoO₃ (x = 0, 0.2). *Solid State Commun.* **2000**, 115 (6), 301–305 DOI: 10.1016/S0038-1098(00)00188-5.
- (172) Botta, P. M.; Pardo, V.; de la Calle, C.; Baldomir, D.; Alonso, J. A.; Rivas, J. Ferromagnetic Clusters in Polycrystalline BaCoO₃. *J. Magn. Magn. Mater.* **2007**, 316 (2 SPEC. ISS.), e670–e673 DOI: 10.1016/j.jmmm.2007.03.058.
- (173) Pardo, V.; Rivas, J.; Baldomir, D.; Iglesias, M.; Blaha, P.; Schwarz, K.; Arias, J. E. Evidence for Magnetic Clusters in BaCoO₃. *Phys. Rev. B - Condens. Matter Mater. Phys.* **2004**, 70 (21), 1–4 DOI: 10.1103/PhysRevB.70.212404.
- (174) Pardo, V.; Blaha, P.; Iglesias, M.; Schwarz, K.; Baldomir, D.; Arias, J. E. Magnetic Structure and Orbital Ordering in BaCoO₃ from First-Principles Calculations. *Phys. Rev. B - Condens. Matter Mater. Phys.* **2004**, 70 (14) DOI: 10.1103/PhysRevB.70.144422.
- (175) Adkin, J. J.; Hayward, M. A. BaMnO_{3-x} Revisited: A

- Structural and Magnetic Study. *Chem. Mater.* **2007**, *19* (4), 755–762 DOI: 10.1021/cm062055r.
- (176) Negas, T.; Roth, R. S. Phase Equilibria and Structural Relations in the System BaMnO₃-X. *J. Solid State Chem.* **1971**, *3* (3), 323–339 DOI: 10.1016/0022-4596(71)90068-5.
- (177) Adkin, J. J.; Hayward, M. A. Structure and Magnetism of 4H-BaMnO_{3-x} (0 ≤ x ≤ 0.35) and 4H-Ba_{0.5}Sr_{0.5}MnO_{3-x} (0 ≤ x ≤ 0.21). *J. Solid State Chem.* **2006**, *179* (1), 70–76 DOI: 10.1016/j.jssc.2005.09.046.
- (178) Cussen, E. J.; Battle, P. D. Crystal and Magnetic Structures of 2H BaMnO₃. *Chem. Mater.* **2000**, *12* (3), 831–838 DOI: 10.1021/cm991144j.
- (179) Rusydi, A.; Rauer, R.; Neuber, G.; Bastjan, M.; Mahns, I.; Müller, S.; Saichu, P.; Schulz, B.; Singer, S. G.; Lichtenstein, A. I.; Qi, D.; Gao, X.; Yu, X.; Wee, A. T. S.; Stryganyuk, G.; Dörr, K.; Sawatzky, G. A.; Cooper, S. L.; Rübhausen, M. Metal-Insulator Transition in Manganites: Changes in Optical Conductivity up to 22 eV. *Phys. Rev. B - Condens. Matter Mater. Phys.* **2008**, *78* (12) DOI: 10.1103/PhysRevB.78.125110.
- (180) Von Helmolt, R.; Wecker, J.; Holzapfel, B.; Schultz, L.; Samwer, K. Giant Negative Magnetoresistance in Perovskitelike La_{2/3}Ba_{1/3}MnO_x Ferromagnetic Films. *Phys. Rev. Lett.* **1993**, *71* (14), 2331–2333 DOI: 10.1103/PhysRevLett.71.2331.
- (181) Levy, P. M. Giant Magnetoresistance in Magnetic Layered and Granular Materials. *Science (80-.)* **1992**, *256* (5059), 972–973 DOI: 10.1126/science.256.5059.972.
- (182) Álvarez-Serrano, I.; López, M. L.; Pico, C.; Veiga, M. L. CMR in a Manganite with 50% of Ti in the Mn Sites. *Solid State Sci.* **2006**, *8* (1), 37–43 DOI: 10.1016/j.solidstatesciences.2005.10.015.
- (183) Fujito, H.; Kunioku, H.; Kato, D.; Suzuki, H.; Higashi, M.; Kageyama, H.; Abe, R. Layered Perovskite Oxychloride Bi₄Nb_{0.8}Cl: A Stable Visible Light Responsive Photocatalyst for Water Splitting. *J. Am. Chem. Soc.* **2016**, *138* (7), 2082–2085 DOI: 10.1021/jacs.5b11191.
- (184) Zhang, L.; Yang, S.; Zhang, S. A Novel Perovskite Oxychloride as a High Performance Cathode for Protonic Ceramic Fuel Cells. *J. Power Sources* **2019**, *440*, 227125 DOI: 10.1016/j.jpowsour.2019.227125.
- (185) Zhou, X.; Dong, H. Density Functional Studies on Layered Perovskite Oxyhalide Bi₄MO₈X Photocatalysts (M = Nb and Ta, X = Cl, Br, and I). *J. Phys. Chem. C* **2017**, *121* (38), 20662–20672 DOI: 10.1021/acs.jpcc.7b06576.
- (186) Dixon, E.; Hayward, M. A. The Topotactic Reduction of Sr₃Fe₂O₅Cl₂-Square Planar Fe(II) in an Extended Oxyhalide. *Inorg. Chem.* **2010**, *49* (20), 9649–9654 DOI: 10.1021/ic101371z.
- (187) Fry, A. M.; Seibel, H. A.; Lokuhewa, I. N.; Woodward, P. M. Na_{1.5}Ag_{1.5}MO₃F₃ (M = Mo, W): An Ordered Oxyfluoride Derivative of the LiNbO₃ Structure. *J. Am. Chem. Soc.* **2012**, *134* (5), 2621–2625 DOI: 10.1021/ja208587e.
- (188) Kirsch, J. E.; Izumi, H. K.; Stern, C. L.; Poeppelmeier, K. R. Synthesis and Characterization of the Face-Sharing Biocuboctahedral [Mo₂O₆F₃]³⁻-Anion. **2005** DOI: 10.1021/ic0502877.
- (189) Kauffmann, M.; Tancret, N.; Abraham, F.; Roussel, P. New Cobaltite Materials Containing CdI₂-Type Layers: Synthesis and Structures of Ba₂Co₄ClO₇ and Ba₂Co₄BrO₇. *Solid State Sci.* **2007**, *9* (10), 885–894 DOI: 10.1016/j.solidstatesciences.2007.06.012.
- (190) Neubacher, M.; Müller-Buschbaum, H. Zur Kenntnis von Ba₆Ru₂PtO₁₂Cl₂. *Zeitschrift für Anorg. und Allg. Chemie* **1992**, *609* (3), 59–62 DOI: 10.1002/zaac.19926090311.
- (191) Tancret, N.; Roussel, P.; Abraham, F. Layered Perovskite-Related Ruthenium Oxychlorides: Crystal Structure of Two New Compounds Ba₅Ru₂Cl₂O₉ and Ba₆Ru₃Cl₂O₁₂. *J. Solid State Chem.* **2004**, *177* (3), 806–816 DOI: 10.1016/j.jssc.2003.09.014.
- (192) Kauffmann, M.; Mentré, O.; Legris, A.; Tancret, N.; Abraham, F.; Roussel, P. 3D-Magnetic Ordering of Co³⁺,⁴⁺ Dimers in a New Co³⁺,⁴⁺ Oxychloride: Neutron Diffraction Analysis and DFT Calculations. *Chem. Phys. Lett.* **2006**, *432* (1–3), 88–93 DOI: 10.1016/j.cplett.2006.10.064.
- (193) Wilkens, J.; Müller-Buschbaum, H. Single-Crystal Investigation of a New Ruthenium Chloride Oxide, Ba₇Ru₄O₁₅Cl₂. *Acta Chem. Scand.* **1991**, *45*, 812–815 DOI: 10.3891/acta.chem.scand.45-0812.
- (194) Lang, C.; Müller-Buschbaum, H. Ein Neuer Strukturtyp eines Neuen Ruthenium(V)-Oxidchlorids: Ba₅Ru₂O₉Cl₂. *ZAAC - J. Inorg. Gen. Chem.* **1990**, *587* (1), 39–46 DOI: 10.1002/zaac.19905870106.
- (195) Tancret, N.; Roussel, P.; Abraham, F. New Ba₅M₅-XPt_xClO₁₃ (M=Fe, Co) Oxychlorides with Layered Perovskite-Related Structure. *J. Solid State Chem.* **2004**, *177* (3), 1023–1031 DOI: 10.1016/j.jssc.2003.10.007.
- (196) Reinen, D.; Lachwa, H.; Allmann, R. Farbe und Konstitution bei Mn^{IV} in tetraedrischer Sauerstoffkoordination. I. EPR- und Ligandenfeldspektroskopische Untersuchungen an Mn^{IV}-haltigen Apatiten sowie die Struktur von Ba₅(MnO₄)₃Cl. *ZAAC - J. Inorg. Gen. Chem.* **1986**, *542* (11), 71–88 DOI: 10.1002/zaac.19865421112.
- (197) Martin, F.-D.; Müller-Buschbaum, H. Zur Kenntnis von K₂Ba₂V₂O₇Cl / On K₂Ba₂V₂O₇Cl. *Zeitschrift für Naturforsch. B* **1994**, *49* (8), 1141–1144 DOI: 10.1515/znB-1994-0820.

- (198) Li, Q.; Geng, L.; Lu, H. Y.; Dai, K.; Cheng, W. D. Crystal Structures and Characterizations of Two New Selenite Chlorides: 1D Ba₂Zn(SeO₃)₂Cl₂ and 2D BaZn₂(SeO₃)₂Cl₂. *J. Solid State Chem.* **2018**, *265*, 117–122 DOI: 10.1016/j.jssc.2018.05.035.
- (199) Iorgulescu, M.; Kabbour, H.; Tancret, N.; Mentré, O.; Roussel, P. Ba₈Co₂Mn₆ClO₂₂, a Quasi-1D Hexagonal Perovskite Polytype Containing New 8H-Blocks. *Chem. Commun.* **2010**, *46* (29), 5271–5273 DOI: 10.1039/c0cc00294a.
- (200) Wilkens, J.; Müller-Buschbaum, H. Darstellung Und Strukturaufklärung von Ba₈Ru_{3,33}Ta_{1,67}O₁₈Cl₂. *J. Alloys Compd.* **1992**, *184* (2), 195–201 DOI: 10.1016/0925-8388(92)90493-S.
- (201) Leib, W.; Muller-Buschbaum, H. Zur Kenntnis von Ba₁₀Fe₈Pt₂Cl₂O₂₅. *Zeitschrift für Anorg. und Allg. Chemie* **1987**, *551* (8), 7–12 DOI: 10.1002/zaac.19875510802.
- (202) Randall Jnr, J. J.; Katz, L. The Crystal Structure of Sr₄PtO₆ and Two Related Compounds. *Acta Crystallogr.* **1959**, *12* (7), 519–521 DOI: 10.1107/S0365110X59001566.
- (203) Powell, A. V.; Battle, P. D.; Gore, J. G. Structure of Sr₄IrO₆ by Time-of-Flight Neutron Powder Diffraction. *Acta Crystallogr. Sect. C Cryst. Struct. Commun.* **1993**, *49* (5), 852–854 DOI: 10.1107/S0108270192012721.
- (204) Vente, J. F.; Lear, J. K.; Battle, P. D. Sr_{4-*x*}Ca_{*x*}RhO₆: A Magnetically Ordered Rh IV Compound. *J. Mater. Chem.* **1995**, *5* (11), 1785–1789 DOI: 10.1039/JM9950501785.
- (205) Powell, A. V.; Gore, J. G.; Battle, P. D. The Magnetic Properties of Iridium in Mixed-Metal Oxides. *J. Alloys Compd.* **1993**, *201* (1–2), 73–84 DOI: 10.1016/0925-8388(93)90864-J.
- (206) Macquart, R. B.; Gemmill, W. R.; Davis, M. J.; Smith, M. D.; Zur Loye, H. C. Single-Crystal Structure of the 2H-Related Perovskites (A₃-XNax)NaBO₆ (A = La, Pr, Nd; B = Rh, Pt). *Inorg. Chem.* **2006**, *45* (11), 4391–4395 DOI: 10.1021/ic060105o.
- (207) Stitzer, K. E.; El Abed, A.; Darriet, J.; Zur Loye, H. C. Growth of Sr₆Rh₅O₁₅ Single Crystals from High-Temperature Solutions: Structure Determination Using the Traditional 3-D and the 4-D Superspace Group Methods and Magnetic Measurements on Oriented Single Crystals. *J. Am. Chem. Soc.* **2001**, *123* (36), 8790–8796 DOI: 10.1021/ja011071g.
- (208) Battle, P. D.; Blake, G. R.; Sloan, J.; Vente, J. F. Commensurate and Incommensurate Phases in the System A₄A' Ir₂O₉ (A = Sr, Ba; A' = Cu, Zn). *J. Solid State Chem.* **1998**, *136* (1), 103–114 DOI: 10.1006/jssc.1997.7666.
- (209) Battle, P. D.; Blake, G. R.; Darriet, J.; Gore, J. G.; Weill, F. Modulated Structure of Ba₆ZnIr₄O₁₅; a Comparison with Ba₆CuIr₄O₁₅ and SrMn_{1-x}CoxO_{3-y}. *J. Mater. Chem.* **1997**, *7* (8), 1559–1564 DOI: 10.1039/a700964j.
- (210) Battle, P. D.; Gibb, T. C.; Strange, R. A Study of a New Incommensurate Phase in the System SrMn_{1-x}CoxO_{3-y}. *J. Solid State Chem.* **1989**, *81* (2), 217–229 DOI: 10.1016/0022-4596(89)90009-1.
- (211) Blake, G. R.; Battle, P. D.; Sloan, J.; Vente, J. F.; Darriet, J.; Weill, F. Neutron Diffraction Study of the Structures of Ba₅CuIr₃O₁₂ and Ba₁₆Cu₃Ir₁₀O₃₉. **1999** DOI: 10.1021/cm9807844.
- (212) Ye, M.; Kim, H.-S.; Kim, J.-W.; Won, C.-J.; Haule, K.; Vanderbilt, D.; Cheong, S.-W.; Blumberg, G. Covalency-Driven Collapse of Strong Spin-Orbit Coupling in Face-Sharing Iridium Octahedra. *Phys. Rev. B* **2011**, *98*, 201105 DOI: 10.1103/PhysRevB.98.201105.
- (213) Volkov, P. A.; Won, C.-J.; Gorbunov, D. I.; Kim, J.; Ye, M.; Kim, H.-S.; Pixley, J. H.; Cheong, S.-W.; Blumberg, G. Random Singlet State in Ba₅CuIr₃O₁₂ Single Crystals. *Phys. Rev. B* **2020**, *101* (2), 020406 DOI: 10.1103/PhysRevB.101.020406.
- (214) Babel, D.; Rüdorff, W.; Tschöpp, R. Ternäre Oxide Der Übergangsmetalle. VI. Erdalkaliiridium(IV)-oxide: Struktur von Dicalciumiridium(IV)-oxid, Ca₂IrO₄. *ZAAC - J. Inorg. Gen. Chem.* **1966**, *347* (5–6), 282–288 DOI: 10.1002/zaac.19663470509.
- (215) Guo, S.; Zhong, R.; Wang, W.; Tao, J.; Ni, D.; Cava, R. J. K₃Ir₂O₆ and K₁₆Ir₈O₃₀, Low-Dimensional Iridates with Infinite IrO₆ Chains. *J. Am. Chem. Soc.* **2020**, *142* (11), 5389–5395 DOI: 10.1021/jacs.0c00849.
- (216) Stitzer, K. E.; Smith, M. D.; Darriet, J.; Loye, H. C. zu. Crystal Growth, Structure Determination and Magnetism of a New Hexagonal Rhodate: Ba₉Rh₈O₂₄. *Chem. Commun.* **2001**, *17*, 1680–1681 DOI: 10.1039/b104513j.
- (217) Stitzer, K. E.; El Abed, A.; Darriet, J.; Zur Loye, H. C. Crystal Growth and Structure Determination of Barium Rhodates: Stepping Stones toward 2H-BaRhO₃. *J. Am. Chem. Soc.* **2004**, *126* (3), 856–864 DOI: 10.1021/ja0374271.
- (218) Stitzer, K. E.; El Abed, A.; Darriet, J.; Zur Loye, H. C. Crystal Growth, Structure Determination and Magnetism of a New M=3, N=1 Member of the A_{3n+3}mA'nB_{3m+n}O_{9m+6n} Family of Oxides: 12R-Ba₁₂Rh_{9.25}Ir_{1.75}O₃₃. *J. Solid State Chem.* **2004**, *177* (4–5), 1405–1411 DOI: 10.1016/j.jssc.2003.11.021.
- (219) Mizoguchi, H.; Ramirez, A. P.; Siegrist, T.; Zakharov, L. N.; Sleight, A. W.; Subramanian, M. A. Possible Verwey-Type Transition in Pb₃Rh₇O₁₅. *Chem. Mater.* **2009**, *21* (11), 2300–2305 DOI: 10.1021/cm900697s.
- (220) Mizoguchi, H.; Michiue, Y.; Sleight, A. W.; Subramanian, M. A. Undulating Layers in a New Rhodate Network:

Structure of Bi_{1.4}CuORh₅O₁₀. *Inorg. Chem.* **2011**, *50* (20), 10397–10401 DOI: 10.1021/ic201481d.

- (221) Vente, J. F.; Kamenev, K. V.; Sokolov, D. A. Structural and Magnetic Properties of Layered Sr₇Mn₄O₁₅. *Phys. Rev. B* **2001**, *64* (21), 214403 DOI: 10.1103/PhysRevB.64.214403.
- (222) Grasset, F.; Zakhour, M.; Darriet, J. Synthesis, Crystal Structure and Magnetic Properties of Ba₅Ru₂O₉(O₂), Ba₅Nb₂O₉(O₂) and Ba₅Ru₂O₁₀ Related to the Perovskite-Type Structure, and Structural Relationships with Corresponding Sulfides. *J. Alloys Compd.* **1999** DOI: 10.1016/S0925-8388(99)00036-5.
- (223) Grimaud, A.; Iadecola, A.; Batuk, D.; Saubanè, M.; Abakumov, A. M.; Freeland, J. W.; Cabana, J.; Li, H.; Doublet, M.-L.; Gwenaëlle Rousse, I.; Tarascon, J.-M. Chemical Activity of the Peroxide/Oxide Redox Couple: Case Study of Ba₅Ru₂O₁₁ in Aqueous and Organic Solvents. **2018** DOI: 10.1021/acs.chemmater.8b01372.
- (224) Klein, Y.; Rousse, G.; Damay, F.; Porcher, F.; André, G.; Terasaki, I. Antiferromagnetic Order and Consequences on the Transport Properties of Ba₄Ru₃O₁₀. *Phys. Rev. B* **2011**, *84* (5), 054439 DOI: 10.1103/PhysRevB.84.054439.
- (225) Streltsov, S. V.; Khomskii, D. I. Unconventional Magnetism as a Consequence of the Charge Disproportionation and the Molecular Orbital Formation in Ba₄Ru₃O₁₀. *Phys. Rev. B - Condens. Matter Mater. Phys.* **2012**, *86* (6), 3–7 DOI: 10.1103/PhysRevB.86.064429.
- (226) Dussarrat, C.; Grasset, F.; Bontchev, R.; Darriet, J. Crystal Structures and Magnetic Properties of Ba₄Ru₃O₁₀ and Ba₅Ru₃O₁₂. *J. Alloys Compd.* **1996** DOI: 10.1016/0925-8388(96)80029-6.
- (227) Lang, C.; Müller-Buschbaum, H. Über Ein Neues Oxoiridat(IV): Ba₇Ir₆O₁₉. *Monatshefte für Chemie Chem. Mon.* **1989**, *120* (8–9), 705–710 DOI: 10.1007/BF00809961.